UNIVERSITY OF CALIFORNIA
RIVERSIDE

Magnetically Responsive Photonic Structures

A Dissertation submitted in partial satisfaction
of the requirements for the degree of

Doctor of Philosophy

in

Chemistry

by

Yongxing Hu

August 2011

Dissertation Committee:
Dr. Yadong Yin, Chairperson
Dr. Christopher J. Bardeen
Dr. Chia-En Chang

The Dissertation of Yongxing Hu is approved:

_____

_____

_____

Committee Chairperson

University of California, Riverside

Acknowledgements

First, I would like to take this opportunity to express my deepest gratitude to my mentor, Professor Yadong Yin, for his academic advice and constant encouragement during my five years' Ph. D. study. His endless patience and strong support guide me through all the difficulties in both my scientific research and daily life. His deep insights and valuable discussions help me explore the mystery of nanoworld and ensure my graduate study much more productive. He is my role model and I hope that one day I would become as excellent a scientist as Yadong.

I greatly appreciate my dearest friends, the past and current members and the visiting students in Yin group, for their great help and support: Dr. Jianping Ge, Dr. Tierui Zhang, Dr. Xiaogang Han, Dr. Chuanbo Gao, Dr. Jibong Joo, Qiao Zhang, Zhenda Lu, Le He, James Goebl, Michael Dahl, Sean Quinlivan, Mingsheng Wang, Yiding Liu, Chunguang Li, Yan Wang, Wenshou Wang, Miaomiao Ye, Junxiang Fu and Na Li. I must thank Dr. Krassimir N. Bozhilov and Stephen McDaniel for their kind assistance in using facilities in CFAMM at UCR. I am also thankful to my committee members Professor Christopher J. Bardeen and Professor Chia-en Chang for their valuable comments on my dissertation.

Most importantly, I am extremely grateful to my family because their wholehearted support and unfailing understanding is what makes this Ph. D. degree possible. I would like to express my heart-felt gratitude to my grandparents Shaoheng Yao and Deyu Hu in heaven, who dedicate themselves to give me the best education and life. Same gratefulness goes to my mother Qiuhong Yi and father Zixun Hu for their

attentive care and unreserved love. I am also very grateful to my fiancé Hongping Yan for everything he has done for me. Thank you!

Last but not least, I would like to take the opportunity to thank all persons who have ever helped me at UCR within the five years.

Dedication

To my grandparents Shaoheng Yao and Deyu Hu, my parents Zixun Hu and Qiuhong Yi, and my fiancé Hongping Yan.

ABSTRACT OF THE DISSERTATION

Magnetically Responsive Photonic Structures

by

Yongxing Hu

Doctor of Philosophy, Graduate Program in Chemistry
University of California, Riverside, August 2011
Dr. Yadong Yin, Chairperson

Magnetically responsive photonic crystals (MRPCs), whose colors can be controlled by external magnetic field, have drawn lots of attention during the past two decades. They are highly desirable for the potential applications, such as sensors and tunable color displays. However it remains difficult to fabricate MRPCs with convenient control, fast response, excellent reversibility and easy integration into advanced devices.

In my thesis work, I have focused on the development of novel magnetically responsive photonic structures with rapid and full reversibility. First, superparamagnetic magnetite (Fe_3O_4) colloidal nanocrystal clusters (CNCs) have been synthesized and employed as building blocks to construct colloidal photonic crystals. The one dimensional periodic chainlike structure whose diffraction can be moved across the entire visible spectral region can be achieved by the application of an external magnetic field. The precise control, fast response and the fully reversible optical properties show great potential in applications such as responsive color displays or sensors.

The assembled structures have been studied by using a method that combines magnetic assembly with sol–gel processes to physically fix individual photonic chains. The resulting nanochains exhibit magnetically responsive photonic properties and long-term structural/optical stability. Greatly improved magnetically responsive photonic structures with widely tunable optical properties and long-term stability can be achieved by porous silica coating on the CNCs surface by a novel water based etching method.

A new mechanism of stabilizing the magnetic photonic crystals against packing force while keeping the tunability will be shown in the thesis. By taking advantage of agarose gel as a matrix to prevent the photonic structures inside from aggregation, the system shows remarkable stability against an external magnetic field. Other features such as fast, reversible, and tunable optical response to external magnetic fields are well kept in this system.

In addition, a bistable color-reflective magnetic tunable photonic film with thermally erasable property will be presented. This film exhibits excellent cycling stability and durability over a long period. The simple fabrication process, easy control over the color change, the superior stability over cycling and prolonged field exposure, and the low cost and energy saving properties allow broad potential applications including outdoor displays.

Table of Contents

List of Figures

Figure 2.2 (A) Typical HRTEM image of a 31-nm cluster. (B, C) High magnification TEM images of 93- and 174-nm CNCs. (D) SAED pattern of the cluster in (C).

Figure 2.3 Optical microscope images of a 120 nm Fe_3O_4 CNC solution enclosed in a glass capillary under an increasing (from A to F) magnetic field.

Figure 2.4 (A and B) Optical microscope images showing the assembly of Fe_3O_4 CNCs dispersed in a liquid film encapsulated between two glass slides in a magnetic field parallel to the viewing angle. The field strength increases from (A) to (B). (C) Optical microscope image illustrating the assembly of CNCs into chainlike structures by slight tilting of the magnetic field (~15° from the view angle).

Figure 2.5 (A) Schematic illustration of the structure of Fe_3O_4 colloids self-assembled in the presence of an external magnetic field. (B and C) Digital photos of a CNC solution captured from the direction (B) parallel and (C) perpendicular to the magnetic field.

Figure 2.6 (A) Photographs of colloidal crystals formed in response to an external magnetic field; the magnet–sample distance decreases gradually from right to left. (B) Dependence of the reflection spectra at normal incidence of the colloidal crystals on the distance of the sample from the magnet. Diffraction peaks blue-shift (from right to left) as the distance decreases from 3.7 to 2.0 cm with step size of 0.1 cm. The average diameter of the CNCs in this sample is 120 nm. (C) Spatial distribution of the magnetic field strength and gradient (inset) measured using a Hall probe. (D) Relation between the estimated interparticle spacing along the magnetic field and the strength of the magnetic field.

Figure 2.7 Reflection spectra of a 130 nm CNC solution after additional washing cycles (1-5 for a-e, respectively) with pure DI water. The starting sample was precleaned with a mixture of ethanol and water to remove most of the solvent and extra surfactants. Diffraction peaks blue-shift as the magnet-sample distance decreases from (A) 3.5 to 2.6 cm, (B) 3.1 to 2.2 cm, (C) 2.9 to 2.0 cm, (D) 2.8 to 1.9 cm, and (E) 2.7 to 1.8 cm. Peaks obtained at a specific distance were plotted in the same color.

Figure 2.8 Influence of additional electrolyte NaCl on the (A) wavelength and (B) intensity of the diffraction peaks.

Figure 2.9 Dependence of the tuning range for diffraction on particle size. The average diameter of Fe_3O_4 CNCs in (A-D) is estimated to be 91, 108, 130, 180 nm, respectively, from TEM images. All scale bars correspond to 200

nm. For each sample, the diffraction peak blue-shifts as the magnet-sample distance decreases from (a) 2.6 to 1.2 cm, (b) 3.2 to 1.8 cm, (c) 3.5 to 2.1 cm, and (d) 3.7 to 2.3 cm.

Figure 2.10 Reflection spectra of (A)~75 nm and (B)~116 nm Fe_3O_4 CNCs and (C) their 1:1 (in mass ratio) mixture in response to external magnetic fields. Since (A) and (B) are similar in size, the mixture shows slight broadening of the diffraction tuning range. In all cases, diffraction peaks blue-shift as the magnet-sample distance decreases from 3.3 to 1.9 cm. The scale bars correspond to 200 nm.

Figure 2.11 Influence of CNC concentration on the diffraction tuning range. Diffraction peaks blue-shift as the magnet-sample distance decreases from (A-C) 3.0 to 2.1 cm, (D) 2.9 to 2.0 cm, and (E) 2.8 to 1.9 cm. Peaks obtained at a specific magnet-sample distance were assigned the same color.

Figure 2.12 (A) Modulated diffractions of a 130 nm CNC solution in a 0.5 Hz periodic magnetic field, with a spectra integration time of 200 ms. (B-D) Variation of the diffraction peak intensity at (B) 470 nm, (C) 535 nm, and (D) 654 nm for 70, 130, and 180 nm colloidal photonic crystals in a 1 Hz periodic magnetic field, with a spectra integration time of 100 ms.

Figure 3.1 Schematic illustration of the fabrication process of the fixed 1D nanochains containing periodically arranged Fe_3O_4 particles. The key is to induce chaining of the uniform magnetic particles by a brief magnetic exposure during their silica coating process and then allow additional silica deposition to further stabilize the chain structures.

Figure 3.2 (A,B) SEM and (C) TEM images of typical photonic nanochains. The particles in chains are permanently fixed by silica coating so that they remain stable when dispersed in solution or dried on solid substrates.

Figure 3.3 Dark-field optical microscopy images of magnetic photonic chains with different diffraction colors switched between "off" (A, C, E, without magnetic field) and "on" (B, D, F, with vertical magnetic field) states. These photonic chains diffract at different wavelengths because they were prepared using Fe_3O_4 CNCs of different average sizes: (A, B) 182 nm; (C, D) 160 nm; (E, F) 113 nm. All images are at the same scale.

Figure 3.4 Representative TEM images and corresponding interparticle spacing distributions of photonic chains prepared by changing the timing of magnetic exposure during silica coating. The duration of magnetic exposure is 1 s. All scale bars are 1 μm.

Figure 3.5 (A) Representative TEM images of photonic chains with different interparticle spacing controlled by applying magnetic fields at different times after injecting TEOS (left to right): 6 min; 8 min; 10 min; 11 min; 16 min. All scale bars correspond to 200 nm. (B) The dependence of interparticle spacing on the timing of magnetic exposure. (C) The dependence of diffraction wavelength of the photonic chains on the timing of magnetic exposure. The inset plots the shift in diffraction wavelength against the change in interparticle spacing.

Figure 3.6 Dark-field optical microscopy images of photonic chains with different lengths obtained by applying magnetic field for different duration: (A) 0.5 s; (B) 1 s; (C) 2 s; (D) 4s. The field strength of magnetic exposure is estimated at ~ 570 G and field gradient ~ 197 G/cm. All images are at the same scale.

Figure 3.7 TEM images of photonic chains with silica coating of different thicknesses controlled by using different amounts of TEOS precursor: (A) 100 μL; (B) 140 μL; (C) 180 μL; (D-F) Corresponding TEM images at a higher magnification.

Figure 3.8 (A) Plot of the diffraction peak intensities in response to external magnetic fields: the magnet-sample distance decreases from 170 to 0 mm with 10 mm in each step. Corresponding nano flashlights are prepared with 150 nm Fe_3O_4 CNCs. (B) Plots of reflection intensities by the nano flashlights in a magnetic field with the magnet-sample distance of 70mm over time (Top plot); corresponding diffraction wavelength over time (Bottom plot).

Figure 4.1 (A) Transmittance spectra of SiO_2 spheres (~360 nm in diameter) in ethanol after they are heated in water at 95 ^oC for various periods. (B, C) Digital photos of unetched (B) and etched (C) silica spheres dispersed in ethanol. The etched colloidal SiO_2 spheres become almost transparent due to the close matching of their refractive index with the solvent.

Figure 4.2 (A, C) TEM images of 360 nm colloidal SiO_2 spheres (A) before and (C) after heat treatment in water at 95 ^oC for 8 h; (B, D) High magnification TEM images of the silica spheres (B) before and (D) after heat treatment in water.

Figure 4.3 (A-D) High-magnification TEM images of the Ag@SiO_2 core-shell colloids after heat treatment in water for 0 min, 10 min, 30 min, and 120 min. (E) The corresponding low-magnification TEM survey image for the sample shown in D. (F) UV-Vis absorption spectra of Ag@SiO_2 core-shell colloids in ethanol after heat treatment in water at 95 °C for various times. The scale bars are 20 nm in A to D and 50 nm in E.

Chapter 1

Overview of Responsive Photonic Crystals

1.1 Photonic Crystals

Colors, as one of the most fulfilling elements in our lives, provide significant functions in both recognition and communication, linking interactions between the animate and inanimate world.[1, 2] An important class of material that can produce color is based on photonic crystal structures.[3] Color-generating photonic crystals are periodically structured dielectric or metallo-dielectric materials with a regularly repeated modulation of refractive index on a perticular length scale, which creates a forbidden gap to prevent propagation of certain wavelengths of light in the visible range.[4-6] The light is affected in the same way a semiconductor crystal affects electron motion.[7, 8] Visible diffraction colors are then generated from photonic band gaps (PBGs) in the visible range. Photonic crystals with a complete PBG act like a light trap, in which light with a specific wavelength cannot propagate in any direction. However, it is challenging to obtain materials with a complete PBG in the visible range because of the limited choices in materials with high refractive indices and low absorption of visible light.[9-11] As a result, photonic crystals with incomplete PBGs are usually produced with distinct structural colors varying with the viewing angle, which are commonly exhibited throughout nature on the wings of butterflies, insects, and some marine creatures.[12-15] On the basis of this behavior, photonic crystals with incomplete PBGs become attractive optical materials for controlling and manipulating the flow of light: they can be used for displays as color

units, reflective coatings for optics, waveguides for directing the propagation of light, and many other optical components.[16-19]

Although a number of methods such as electrochemical etching[20, 21] and interference lithography[22-24] have been developed to fabricate photonic crystals with different length scales, it remains a difficult task to produce structures with periodicity on the length scale of half the wavelength of visible light: ~400/2 nm (blue) to 700/2 nm (red) for photonic crystals with visible diffraction. Alternative approaches have been developed for preparation of color-generating photonic structures under the driving force from the fabrication challenge, for example, self-assembly approaches with either monodisperse submicron colloidal particles or block copolymers undergoing phase separation.[25-28] Using self-assembly methods, different dimensional periodic structures can be fabricated at much lower cost while with higher efficiency.[29] It is also more convenient to modify the building blocks before or after the formation of the crystal structures to enable functionalities.[30, 31]

In this chapter, I will to give an overview on self-assembled photonic crystal structures, especially structures with photonic properties that can be tuned by external stimuli. First, the basic physical principles behind photonic crystal structures will be briefly introduced, followed by a summary of the various approaches for fabricating photonic crystal structures through self-assembly processes. Afterwards, an overview of assorted responsive photonic structures classified by corresponding stimulus will be presented. Finally, the objective of this work will be discussed, together with a general description of each chapter.

1.1.1 Physical Principles Behind Photonic Crystals

The diffraction property of periodic arrays can be described by a relation similar to Bragg's law after a good approximation.[32] The frequency and the bandwidth of the corresponding PBG are determined by the refractive index contrast between materials, the structural symmetry and lattice constant, the filling fraction, and the morphology of the photonic structures.[1, 33, 34] In order to ascertain the reason why they are related, the physical principles behind the photonic structures should be understood first. In fact, photonic band structure originates from the interference of lights scattered from the dielectric lattice and reflected at each interface in the photonic structure.[10, 35] The dependence of photonic properties can be modeled considering the conditions for interference. The pathway of lights interacting with two media of different refractive indices is shown in Figure 1.1 and the interference is described by combining the law of reflection with Snell's law: the optical path length difference (L) between ray R_2 and ray R_1 that interact with two media of different refractive indices (n_0 and n_1) can be expressed as following by applying the law of reflection:

$$L = 2n_1 l_2 - n_0 l_1 \qquad \text{(Eq. 1.1)}$$

$$L = 2n_1 \left(\frac{d}{cos\theta_1}\right) - n_0\left[\left(\frac{d}{cos\theta_1}\right)\frac{n_0}{n_1} sin^2\theta_0\right] \qquad \text{(Eq. 1.2)}$$

With Snell's law:

$$n_0 sin\theta_0 = n_1 sin\theta_1 \qquad \text{(Eq. 1.3)}$$

the optical path length difference can be determined:

$$L = 2n_1 d\sqrt{1 - \frac{n_0^2}{n_1^2} sin^2\theta_0} \qquad \text{(Eq. 1.4)}$$

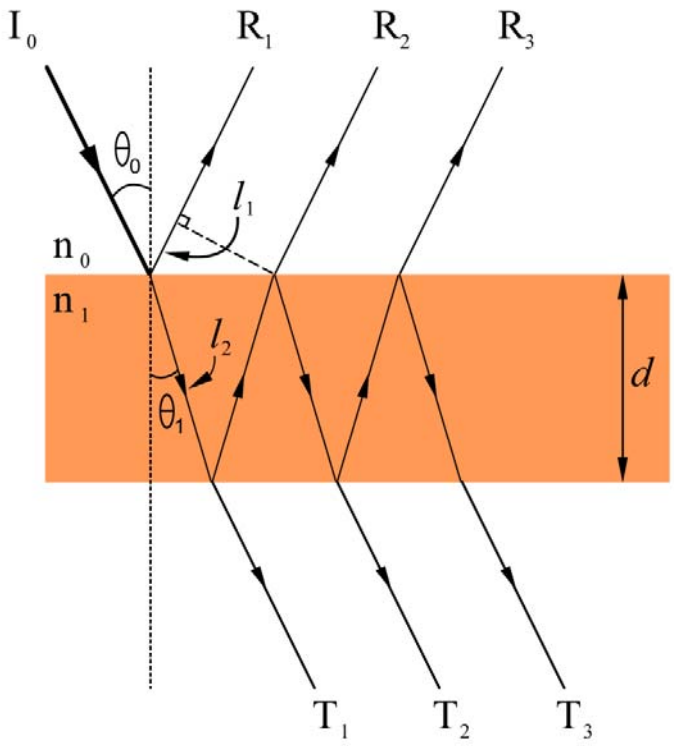

Figure 1.1 Scheme showing the combination of refraction and reflection in order to produce interference.

The phase difference (γ) between the two rays for constructive interference is

$$\gamma - \frac{2\pi}{\lambda} L \qquad \text{(Eq. 1.5)}$$

Since the condition for constructive interference is $\gamma = 2m\pi$, then $m\lambda = L$, where m is the order of reflection and λ is the wavelength of the incident light,

$$m\lambda - 2d\sqrt{n^2 - n_0{}^2 \sin^2 0} \qquad \text{(Eq. 1.6)}$$

This relation is analogous to Bragg's law because the optical reflection surface is considered as atomic emitters in the lattice.

Considering a Bragg reflector with alternating layers of high and low refractive index materials, the relation for diffraction in the condition of normal incidence and non-absorbing materials can be simplified and described by the Bragg-Snell law:[36, 37]

$$m\lambda = 2(n_l d_l + n_h d_h) \qquad \text{(Eq. 1.7)}$$

where n_l and n_h are the refractive indices of the low and high refractive index materials respectively, and d_l and d_h are corresponding thicknesses. If the central wavelength of the photonic band is defined as λ_0, the bandwidth of the photonic stop band $\Delta\lambda_0$ can be calculated: [6]

$$\Delta\lambda_0 = \frac{4\lambda_0}{\pi} \arcsin\left(\frac{n_h - n_l}{n_h + n_l}\right) \qquad \text{(Eq. 1.8)}$$

The reflectivity depends on the number of bilayers (N) in the Bragg stack and the contrast of refractive index:

$$R = \left[\frac{n_0 - n_s(n_l/n_h)^{2N}}{n_0 + n_s(n_l/n_h)^{2N}}\right]^2 \qquad \text{(Eq. 1.9)}$$

where n_0 is the refractive index of the surrounding and n_s that of the substrate.[36]

A similar method can be applied to more complex systems such as 3D colloidal photonic crystals.[38] In practical conditions, the colloidal spheres are usually embedded in a matrix material such as solvents or polymers, and then the refractive index n can be taken as an average of the refractive indices of the colloids and the interstitial space for 3D photonic crystals like opals.

$$n_{avg} = \varphi\, n_{spheres} + (1 - \varphi) n_{background} \quad \text{(Eq. 1.10)}$$

where φ is the solid fraction in the material.[39, 40] By approximation, the average index for 3D opals can be calculated:

$$n_{avg} = (\sum_i n_i^2 V_i)^{\frac{1}{2}} \quad \text{(Eq. 1.11)}$$

Where n_i and V_i are the refractive index and volume fraction of each component respectively. The spacing between close-packed planes, d_{hkl} can be expressed:

$$d_{hkl} = \frac{D\sqrt{2}}{\sqrt{h^2+k^2+l^2}} \quad \text{(Eq. 1.12)}$$

Here D is the interparticle spacing, and h, k, and l are the indices of the Miller planes. For (111) planes, $d_{hkl} = D\sqrt{\frac{2}{3}}$. If $n_0 \approx 1$, then for the first order (m = 1):[41]

$$\lambda = 1.633 (\sum_i n_i^2 V_i - sin^2\alpha)^{\frac{1}{2}} \quad \text{(Eq. 1.13)}$$

Although this expression does not take all conditions into account, such as the coupling of incident light and diffracted light due to strong scattering,[42] it predicts the reflection peak maxima in relatively good agreement with experimental observations.

1.1.2 General Strategies for Photonic Crystals Fabrication

Ever since the concept of photonic crystals was developed when two milestone papers were published by John[4] and Yablonovitch[5] in 1987, there has been a considerable effort to develop novel methods to fabricate artificial photonic crystals. Generally, the fabrication methods can be classified into two categories: the top-down and bottom-up approaches. Typical top-down approaches mainly rely on producing microstructures with desired morphology and order from bulk materials by lithography-based microfabrication techniques.[35, 43-45] The advantage of this type of technique is that long-range ordering of photonic crystal structure with arbitrary complexity can be achieved.[46] Two-dimensional semiconducting photonic crystals are successful examples fabricated by this type of method. However, for 3D photonic crystals, lithography techniques turn out to be not as efficient as for 2D crystals because of their complicated and laborious fabrication procedures.[19, 22] Although new progress of top-down approaches made so far shows promise for the rapid production of defect free photonic structures with relatively large area, using methods such as multi-beam interference lithography,[47] phase mask interference lithography,[48] and two-photon lithography,[49] these unconventional microfabrication approaches involve high cost and complicated procedures. Thus bottom-up approaches that are based on self-assembly processes have become more attractive.

Compared with the expensive lithography-based top-down strategies, bottom-up approaches are low cost and low-energy consumption methods that can assemble pre-prepared building blocks into ordered structures.[39, 50] Building blocks with different properties can be applied to fabricate photonic crystals with assorted functions and morphologies.[51, 52] Importantly, uniformity of the building blocks is a prerequisite to

achieve high-quality photonic crystals with the self-assembly process. Colloidal particles or block copolymers are therefore typical building blocks as they are easy to prepare into monodisperse units. The approach by self-assembly of block copolymers is simple and efficient for preparing relatively large area photonic structures comparable to wafer size.[28, 53] By utilizing various structures that block copolymers can form in their equilibrium states from microphase separation, different photonic structures assembled by the building blocks can be achieved in different dimensions.[54-56] However, a major drawback in a block copolymer photonic crystal system is that it is hard to achieve desired photonic structures with long-range ordering and large PBG due to the traps from existing nonequilibrium states and the small dielectric contrast between copolymer microdomains.[57] Various ways have been developed to improve the ordering and orientation of the block copolymer nanostructures and enhance the dielectric contrast between the microdomains. For instance, for directed assembly on templated substrates,[58, 59] application of an external field[60-62] or annealing[63] can be used to improve the long range order while preferentially doping high dielectric nanocrystals with optical transparency into the block copolymer microdomains can enlarge the photonic band gap,[28] although the improvement has been limited.

Self-assembly of monodisperse colloidal spheres on the submicron scale is one of the most powerful approaches for fabricating photonic crystals, because desired photonic crystals can be easily assembled using designed building blocks with special structure, size, composition and properties.[25, 64, 65] Thanks to well-developed colloidal synthesis method, various colloids are available to be incorporated into photonic crystals. Typical

materials include SiO_2 and PS colloids, as well as other uniform oxides (such as ZnO and TiO_2) and polymers (such as poly(methyl methacrylate), PMMA).[66-68] Further modifications of the colloids provide an alternative way to prepare multi-functional photonic crystals.[69-71] By controlling the physical conditions and taking advantage of different forces in the assembly process, assorted photonic crystals with different dimensional periodic structures can be formed, like 2D non-close-packed arrays by spin coating[72-74] or 3D opals by capillary force.[75] During the past two decades, a number of self-assembly methods have been successful in the fabrication of photonic crystals with different purposes, such as sedimentation and electrophoretic deposition.[3, 76-78] Among these methods, one utilizing repulsive electrostatic interactions demonstrates greater potential over others in successful assembly of photonic crystals with a higher degree of order and larger domain size.[79-83] High charge density on the colloidal surface and high particle volume fraction with low ionic strength in solution guarantee strong repulsions between colloids, which results in ordered structures with non-close-packed features.[40, 84] Structures with long-range order can be achieved when spatial physical confinement is provided.[85, 86] As demonstrated by Xia et al., continuous sonication helps colloidal systems reach the thermodynamic equilibrium state, in which colloids are set in the colloidal crystalline lattice sites.[87, 88] The surface morphology and the layer number of the resulting structure can be precisely controlled and large area crystals can be obtained.[89] Pioneered by Asher and Ozin groups, functional colloidal crystals have been prepared by similar approaches such as chemical or biological sensors.[90-93] However, all

these methods suffer from long preparation time from days to weeks and the polycrystalline nature of the crystal hampers the practical applications.

1.2 Responsive Photonic Crystals

In the past two decades, there has been increasing interest in exploring novel photonic structures with new properties, among which photonic crystals with a tunable stop band that can be conveniently controlled by external stimuli are highly desirable for their potential applications. Responsive photonic crystals (RPCs) are widely applicable in areas such as biological and chemical sensing, tunable color displays, and many optically active components.[1, 33, 94]

1.2.1 Strategies to Create Responsive Photonic Crystals

Considerable effort has been devoted to achieving responsive photonic crystals with fast response to external stimuli and well controlled tunability of the optical properties. To reach this goal, it is necessary to return to the mechanism, based on which the photonic crystal band gap is tuned upon the application of external stimulus. The tunable optical properties of the photonic structure are related to the changeable PBG characteristics through the application of chemical stimuli, mechanical forces, electrical/magnetic fields, or light. As discussed in section 1.1.1, based on the deduced equations, the bandgap characteristics of the photonic crystals largely depend on the contrast of refractive indices between the ordered dielectric materials, the lattice constants or spatial symmetry of the crystals and the filling factor/volume fraction. In other words, any one of these parameters in the photonic structures that is stimulus-responsive can be used for the creation of the responsive photonic crystals.[1, 33]

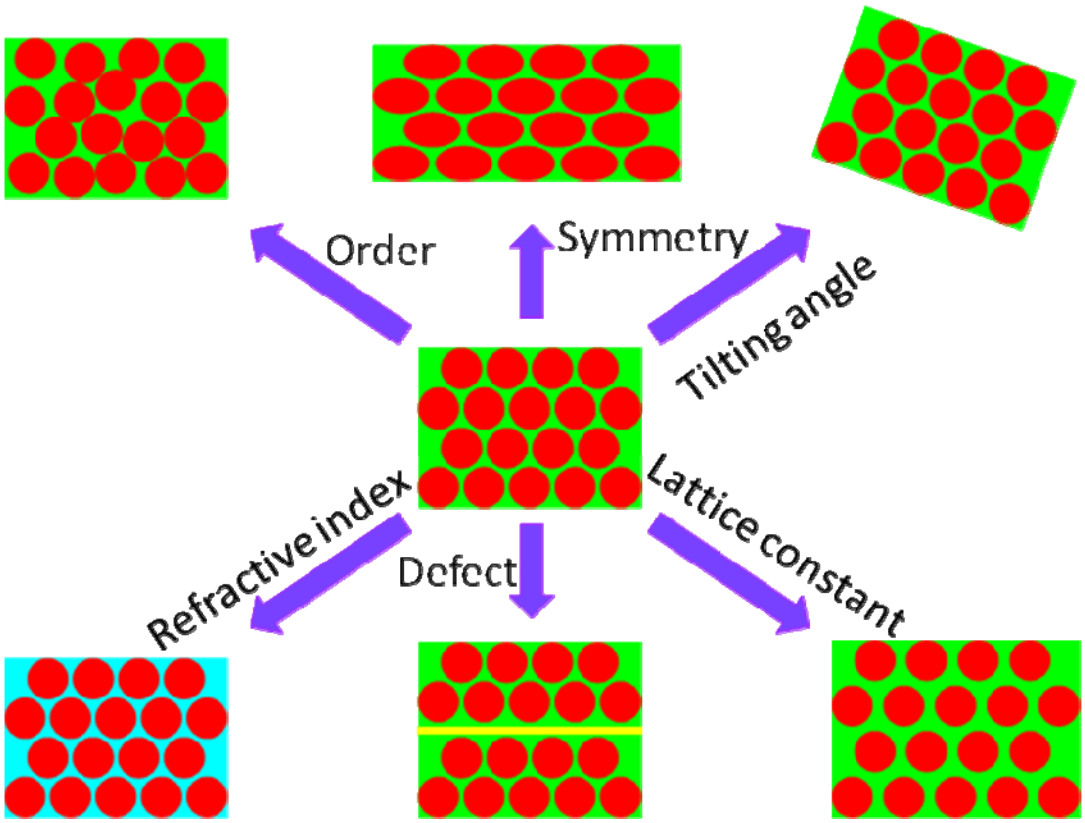

Figure 1.2 Schematic illustration of the parameters that can be tuned in a responsive photonic crystal structure

Figure 1.2 summarizes the factors that can be employed to change the photonic properties of the ordered structures. First, the effective refractive index is one of the most extensively studied parameters to tune the optical properties. Methods that can reversibly and efficiently change the refractive index can be utilized. Currently, the tuning of the refractive index can be achieved either by addition of new solvents, molecules, or liquid crystal into the structure or utilizing the phase transition of the building blocks according to their own physical properties.[95-97]

Second, adjusting the lattice parameter or crystal structure such as symmetry is another typical strategy to achieve the responsive property. Building blocks that undergo expansion or contraction upon external stimuli including mechanical stress, charge induced deformation or polymer phase transition are chosen to build responsive photonic crystals.[98, 99] Another way is based on utilization of a responsive matrix surrounding the building blocks, which exhibits structural deformation by solvent swelling/deswelling, and phase transition.[40, 100] Recently, hydrogel assisted responsive photonic crystals have been intensively studied, because functional photonic crystals with different purposes can be easily prepared by embedding photonic units into different responsive hydrogels. The smart responsive photonic crystals can be applied as sensors in chemistry or biology.

Third, the orientation of the photonic crystal can also be controlled to effectively change the optical properties when illuminated by fixed incident light. Anisotropic structures or properties from the structures are critical to induce the stimulus-responsive rotation.[101, 102] In addition, the introduction of defects into ordered photonic structures can enable the tuning of optical properties as long as these defects are responsive to a

certain stimulus reversibly. Many materials such as liquid crystals or responsive polymer can be used as defects, making it an effective way to manipulate the photonic properties.[103-105] Based on these tunable parameters, diverse responsive photonic crystals that fulfill specific needs can be achieved and will be discussed in the following section.

1.2.2 Various Responsive Photonic Crystals

To achieve responsive photonic crystal with controllable optical properties, stimulus-responsive material should be incorporated into either the building blocks or the surrounding matrix. There are a large number of candidate materials that can be employed to construct RPCs, allowing the fabricated photonic crystals feature different functions. Classified by external stimuli, photonic crystals can be categorized in to following types.

Mechanically Responsive Photonic Crystals. As the most straightforward way to design RPCs, mechanically induced shape changes such as contraction or expansion can act as an effective strategy to tune the photonic properties.[106] Generally, photonic crystals are embedded inside a stretchable polymer matrix, which is elastic by application of external stress.[107] The tuning range is related to the elastic properties of the polymer matrix when responding to stretching or to the original interparticle spacing when pressing can initiate the diffraction change. The reversibility can be achieved once the mechanical stress is released. In 1994, Asher et al. developed a mechanical RPC based on polystyrene photonic crystals embedded in a film from copolymerization of N-vinylpyrrolidone and acrylamide.[39] The diffraction of the film is sensitive to stretching with a 35 nm shift, as shown in Figure 1.3. The relatively small tuning range due to the

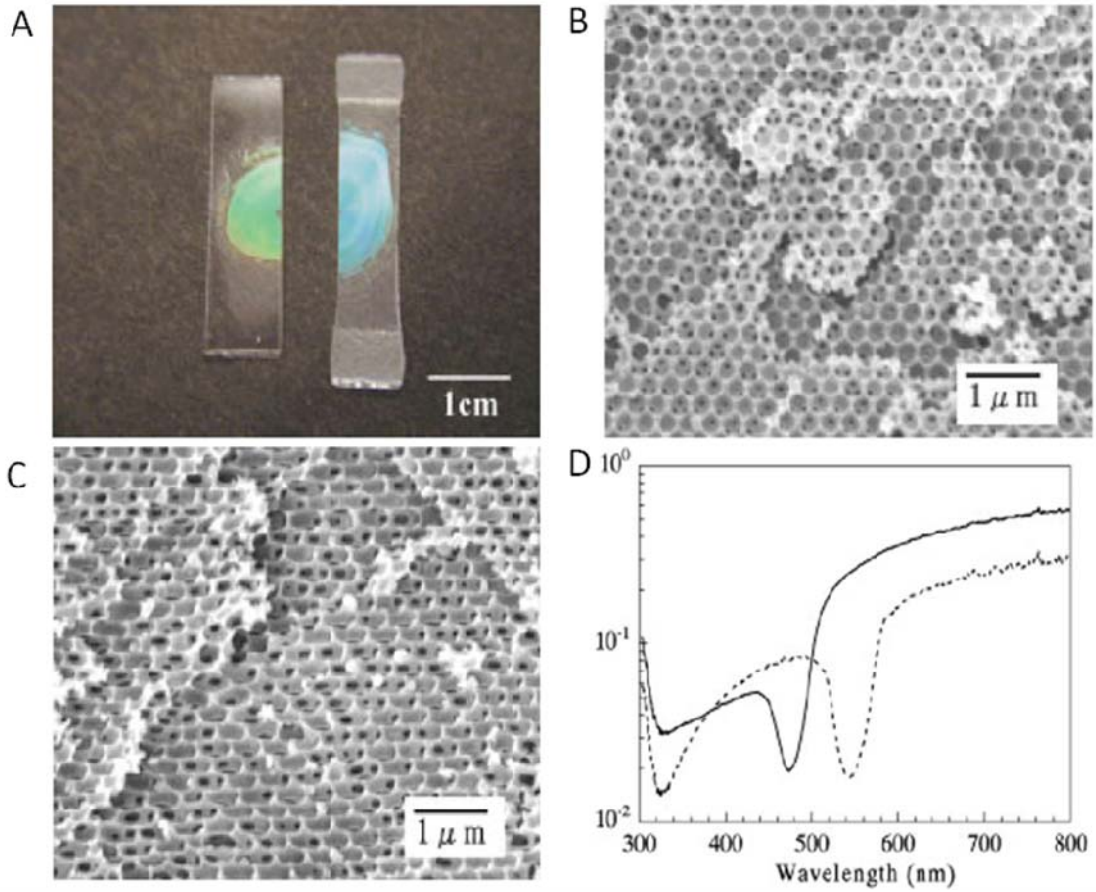

Figure 1.3 (A) Photograph of PMMA inverse opal film (left) and the film after stretching (right). (B, C) Cross-sectional SEM images of PMMA inverse opal film before and after horizontal stretching. (D) Transmission spectra of PMMA film before (dotted line) and after (sollid line) stretching. (Copyright © 2011 Wiley Periodicals, Inc., A Wiley Company)

poor mechanical strength can be further improved by using more elastic polymer matrix. However, the recovery time is not satisfactory when hydrogels are employed as the responsive matrix, resulting from their elastic properties with low polymer content. Later, a water-free, highly mechanically responsive photonic crystal was fabricated by Foulger et al.,[108] which was synthesized through a second polymerization when another polymer, 2-methoxyethyl acrylate (MOEA) was swelled into the primary hydrogel. This new mechanical RPC exhibited a larger tuning range and a much higher response rate within 100ms. Further modification with functional composite such as electroactive materials can render the system responsive to other stimulus like electrical field.

Thermo-responsive photonic crystals. Generally, thermo-responsive photonic crystals can be classified into two categories: one is based on polymer swelling and the other utilizes phase change of inorganic materials. A large portion of the research has been focused on the polymer based thermo RPCs since the original development by Asher et al. of the first successful responsive photonic crystals using responsive polymer matrix.[40, 109] Any thermosensitive polymer, which undergoes a volume phase transition around its lower critical solution temperature, could be used as the responsive matrix material to a temperature stimulus. One of the most widely studied thermosensitive polymers is poly(N-isopropylacrylamide) (NIPAM), whose hydrophilicity can change around its lower critical solution temperature (LCST) 32 ^{o}C. In the case when temperature is higher than its LCST, the formed polymer matrix can expel water and shrink, resulting in the gradual decrease of interparticle spacing and corresponding blue-shift of the diffraction peak. When the temperature is lower than its LCST, the polymer

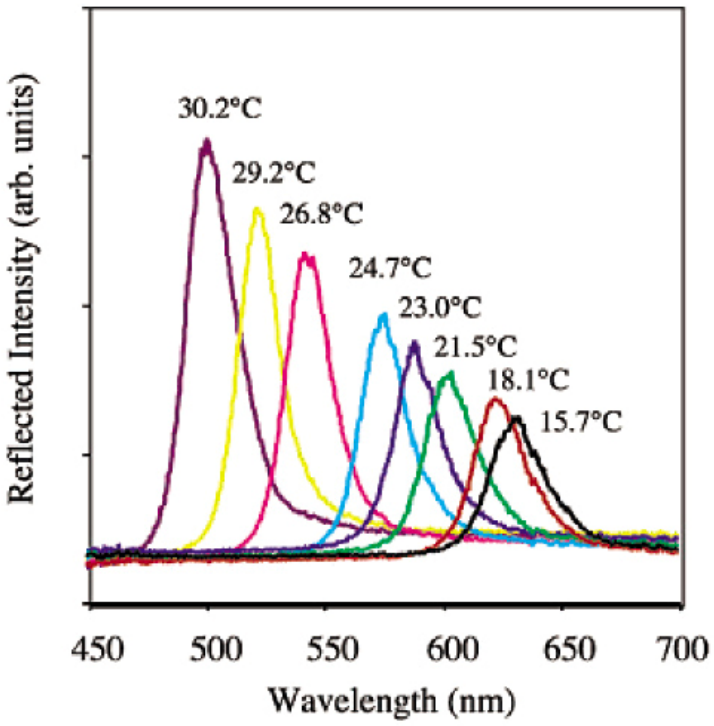

Figure 1.4 Temperature dependence of the reflection spectra of porous NIPAM gel built with a colloidal crystal template composed of 210-nm silica particles. (Copyright © 2011 American Chemical Society)

matrix can absorb water molecules and swell. The optical properties can be switched reversibly as the temperature changes and the tuning range of the diffraction is very broad to cover the whole visible range.[110]

Later, Takeoka and Watanabe discovered that the responsive photonic properties can still be retained after removing the originally incorporated colloidal crystals, with only the thermosensitive matrix left.[111] As shown in Figure 1.4, they used silica colloidal crystals as an example, and the reversible photonic response to temperature change was maintained because the voids left over were still periodic. The tunability can be controlled by the degree of cross-linking of the polymer matrix.

Multi-stimuli RPCs can be developed by modifying the thermo-responsive polymer molecules with other functional groups. Copolymerization is one of the typical approaches to synthesize the bi-stimuli responsive photonic crystals. For example, methacrylic acid (MAAc) can be copolymerized with NIPAM, which allows the resulting photonic gel not only respond to the change in temperature but also to the pH value of the exposed environment.[112] This kind of responsive gel was found to be able to switch its colors induced by electrochemical reaction around the electrode, because the pH value around the anode electrode was shifted with the electrolysis of water. By incorporating different functional prepolymers into the structures, different bistimuli responsive photonic crystals can be fabricated with response to stimulus other than temperature such as light or mechanical stress at the same time.[98, 113] The tuning range of the photonic signals of the bistimuli responsive photonic crystals can be extended with the help of lithographic techniques.

However, the low response rate and limited operation temperature range are difficulties that challenge the use of responsive polymeric photonic crystals in practical applications. To solve these problems, inorganic materials whose refractive index can be controlled by temperature serve as alternative candidates for thermo-responsive photonic crystals. The change in refractive index with temperature is based on the corresponding phase transition, by which higher response rate can be achieved. For instance, Se/Ag_2Se core/shell particles were used as building blocks to fabricate thermally switchable photonic crystals by the Xia group.[30] The reversible diffraction wavelength change can be related to the temperature variation around the phase transition temperature of Ag_2Se. Other inorganic materials like Si, $BaTiO_3$ or VO_2 have also been incorporated into responsive photonic crystals.[114-116] However, the changes in refractive index are small so that the tuning range of the diffraction peak is not broad enough.

Chemically Responsive Photonic Crystals. Similar strategies can also be applied to fabricate photonic crystals that are responsive to chemical stimuli. One is based on the polymer swelling and shrinkage when the components of RPCs are exposed to specific chemical species, resulting in the change of photonic properties. The other can be categorized as porous chemical PRCs in which by tuning the average refractive index is tuned. Chemical species such as biomolecules, solvent, vapor and various ions can be employed as stimuli as long as they can change the corresponding optical properties of the RPCs.

Among the polymer based chemical RPCs, responsive hydrogels are the most popular type. Hydrogel polymers are usually modified with functional groups that can

recognize a specific stimulus, which can induce a volume change once the stimulus in the surrounding chemical environment changes. Asher *et al.* lead a pioneering study in the field of chemical responsive hydrogel based photonic crystals, and various ion-responsive PCs have been developed in their group.[100, 117, 118] Ion recognition groups were first functionalized on the polymer chains, including crown ether, 4-vinylbenzo-[18]crown-6 and 8-hydroxyquinoline. Based on the specific selection of metal ions by the polymer matrix, Donnan osmotic pressure that is related to the amount of target ions in the environment can induce an expansion/contraction of the gel. Thus, the diffraction will shift when the polymer swells/deswells. According to the different number of bonded charges, the volume change of the RPCs as well as the shift in diffraction wavelength can be different, allowing the detection of the target concentration. Similarly, the pH RPCs can be fabricated with hydrogel that is responsive to H^+ ions.[41] Complex optical response can be achieved in some special chemical environments, such as the recently developed porous poly(NIPAM-[Ru complex]) photonic gel with optical response and a self-sustaining peristaltic motion.[119]

Others based on refractive index tuning are capable of detecting many different molecules as solvents and vapors. Porous structure is crucial to achieve a large tuning range of the optical response.[95] The surface properties of the structure and the properties of target molecules can greatly affect the response of RPCs to the stimuli. In addition, the composition and pore size are also related to the sensitivity. By either infiltration or physical adsorption of the target species, effective refractive indexes of RPCs change together with their optical diffraction. Mesoporous Bragg stacks, one of the most popular

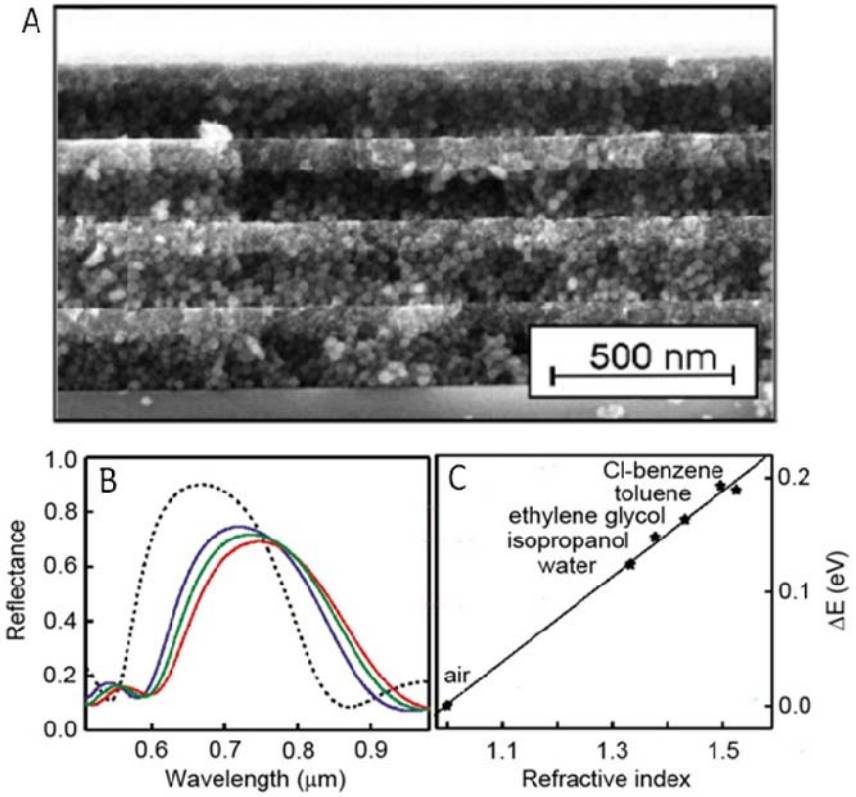

Figure 1.5 (A) SEM image of the cross section of an eight-layer Bragg reflector made of silica and titania nanoparticles deposited alternately on the substrate. (B) Reflection of the Bragg reflector infiltrated with water (blue line), ethylene glycol (green line) and Cl-benzene (red line). (C) Relationship between the Bragg peak position shift and the refractive index. (Copyright © 2011 American Chemical Society)

system for RPCs, show high sensitivity and good selectivity when proper materials are chosen with advanced microstructures. The mesoporous TiO_2/SiO_2 Bragg stacks fabricated by Ozin and Miguez and porous silicon Bragg stacks have been demonstrated as promising candidates for chemical sensors (Figure 1.5).[120, 121] More complicated structures with larger surface areas and modified surface properties show the possibility to enhance the selectivity and sensitivity of the RPCs.

Electrically Responsive Photonic Crystals. RPCs whose optical properties can be controlled by external electrical field have been intensively studied because of their great potential in advanced physics and optics. Generally, assembled photonic crystals or inverse ones are infiltrated with electrically responsive hydrogel polymers or liquid crystals that are very sensitive to electric fields. The resulting structures show electrical field controllable optical properties by either changing the polymer matrix volume or adjusting the effective refractive index of the system.

Recently, a unique electrical RPC based on a metallopolymer matrix with opal structure embedded inside has been developed by the Ozin group, as shown in Figure 1.6.[91, 122] The metallopolymer network has a characteristic property that its volume can change through swelling induced by redox reaction. Polyferrocenylsilane derivative molecules comprise the functional part that can contract or expel according to the applied potential. As electrons can be extracted or injected from the polymer networks, anions can diffuse in or out to neutralize the system, causing the volume of the polymeric matrix to change as well as the diffraction from the opal inside. Bistable states can be achieved in this composite film but the response time is relatively long, the tuning range is narrow

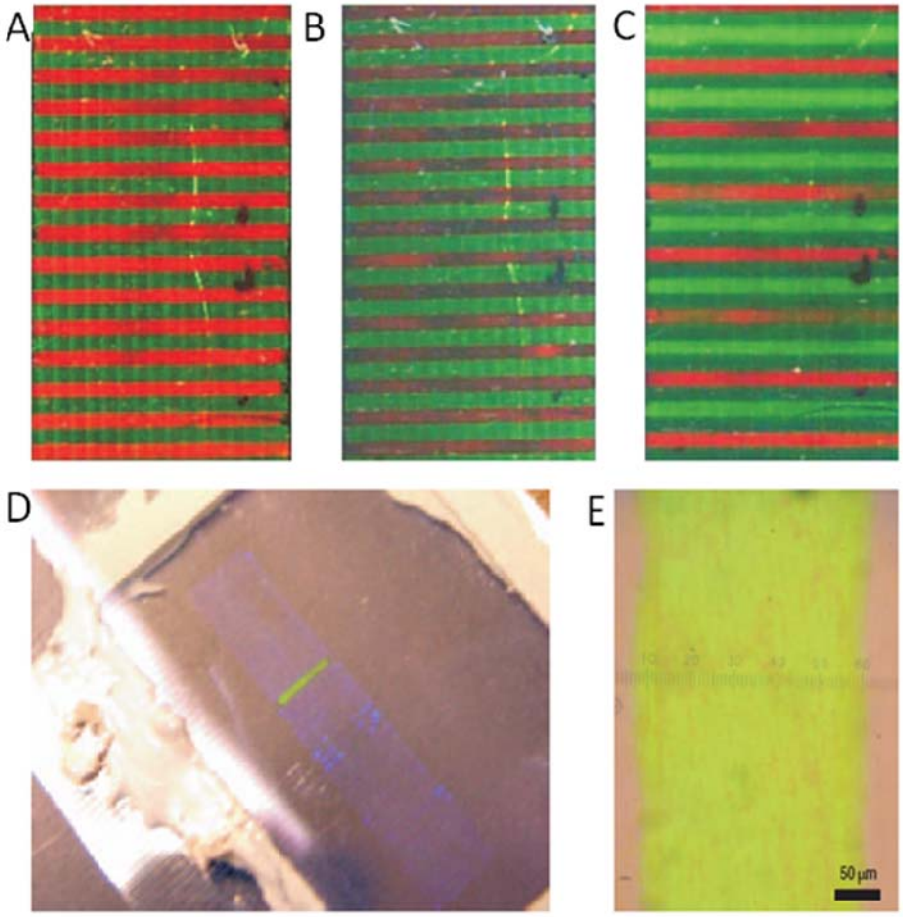

Figure 1.6 Images of P-Ink pixel arrays. (A–C), Pictures of a P-Ink film coated onto an array of 0.3-mm ITO lines. Every other line was oxidized to various degrees to generate coloured patterns. (A), Alternating dark green and red stripes made by applying a voltage to every other line in the array. (B), The lines have been shifted into the near infrared by applying a higher voltage and are thus transparent, allowing the black background behind the sample to be visualized. (C), By applying different voltages to individual lines, multicolour lines are also possible. (D), Image of an oxidized single line, showing a vivid green on pale violet. (E), The line shown in (D), visualized in an optical microscope, demonstrating a 25-mm edge resolution adequate for display application. (Copyright © 2011 Nature Publish Group)

and the required voltage is high, owing to the limited diffusion of the electrolyte. However, an inverse opal can be applied to solve this problem effectively because of its large porosity. In another version, polyelectrolyte hydrogel can be used as a responsive matrix to external electrical fields.[123] By combined local pH change and Donnan osmotic pressure, the hydrogel also undergoes a volume change due to the potential variation, but the durability and the response are unsatisfactory. In addition, electrophoresis can be employed as the electrophoretic force on the charged polymer matrix leading to shrinking or swelling, as well as an optical diffraction shift.[124] But the retarded response rate and the high required voltage limit the practical use.

Compared with other approaches, liquid crystal based electrical RPCs have attracted more attention since the orientation of the anisotropic liquid crystal molecules shows effective influence on the average refractive index.[125] Enhanced response time that is comparable to or faster than the conventional twisted nematic cell can be achieved. However, the reorientation is limited because the motion of liquid crystal molecules near the solid substrate surface is blocked, thus only a small tuning range can be achieved. By selecting different liquid crystals such as 5CB or PCH5 or using other photonic crystals, electrical RPCs with improved sensitivity, tuning range and response rate can be fabricated.[126, 127]

Optically Responsive Photonic Crystals. In the past two decades, optical RPCs have been studied extensively as the diffraction properties can be effectively controlled with high precision. The basic strategy is similar to the above-mentioned RPCs, and is based on the tuning of average refractive index or lattice constant induced by optical

stimulus. Led by the Asher and Sato groups, many interesting optical RPCs have been developed. Irradiation sensitive polymers or photochromic dye aggregates, whose photoisomerization can change upon the variation of the optical stimulus, were infiltrated into the assembled photonic crystals.[52, 128] Thus the matrix volume may alter as the charge distribution in the polymer network changes. However, the RPC based on Spirobenzopyran chromophore has limited wavelength shift and a relatively long response time.[129] Photochromic dye aggregate functionalized RPCs can achieve relatively larger tuning ranges as long as the change of their refractive index is large enough at their electronic oscillation frequency.[130] Liquid crystals that are responsive to optical variations can also be employed to fabricate a switchable optical RPC because the phase transition between nematic and isotropic states is induced by irradiation. The reflection can be controlled on or off upon the light irradiation due to the changed refractive index after the photoisomerization.[131] By infiltrating an anisotropic inverse opal with liquid crystals, a birefrigent photonic crystal can be fabricated. Gu et al. have discovered that when two pieces of the birefrigent photonic crystal with different PBG were stacked together with perpendicular elongation directions, polarization of incident light together with the relative intensity of the two diffractions can be identified.[132]

Magnetically responsive photonic crystals. When magnetic responsive materials have been incorporated into the photonic system, the resulting magnetically RPCs can exhibit controllable diffraction by external magnetic field manipulation. In this special class of RPCs, a magnetic component is directly incorporated in to the building blocks in most cases. Since a magnetic field can induce magnetic attraction to the nearby

building blocks and a magnetic packing force to change the concentration gradient of the building blocks, the corresponding optical performance can be tuned.[133, 134] Superparamagnetism is required to achieve good reversibility. Previously, Asher et al. have fabricated a colloidal magnetically RPC based on superparamagnetic non-close-packed 3D PS photonic crystals.[135] The prepared RPC exhibited a magnetic field controlled response when the field strength was changed. Then, hydrogel polymers such as PAAm or PHEMA were employed to infiltrate the assembled crystals and form a solid sensitive film.[101] However, an enlarged tuning range is desirable since interparticle separation in the magnetically RPCs is limited when the structure is created by a conventional colloidal self-assembly process. A chainlike magnetically RPCs have been fabricated by Bibette et al, which took advantage of the periodic assembly of magnetic emulsion droplets in a magnetic field.[136] The emulsion droplet was not thermodynamically stable, which affected its long term durablity.[137] However, interest in the study of this kind of magnetically RPCs has kept increasing because the system displays attractive advantages such as fast response time, contactless control from the stimuli and easy integration into advanced devices

1.2.3 Challenges in Constructing Responsive Photonic Crystals

Responsive photonic crystals with high potential for practical applications generally require a large tuning range of the diffraction properties in either wavelength or intensity, a quick response rate, good reversibility, easy and precise control by external stimuli, and the potential for integration into advanced devices.[33] After years of study, the creation of responsive photonic crystals with all the features mentioned above

remains difficult due to limited tunability of the band gap, a slow response to external stimuli, incomplete reversibility, and difficulty of integration into existing photonic devices. The narrow tuning range originates from the limited stimuli induced variations in the crystal structure or effective refractive index, while the slow response results from retarded physical or chemical changes caused by the external stimuli. Stability is another big issue because the photonic performance can change after repeated cycles of tuning. Additionally, stimuli that are easy to control, safe to use and available in general labs is preferred in the design of RPCs. Furthermore, conventional methods for the fabrication of RPCs usually require tedious steps and long periods to complete, especially for the colloidal crystals with a relatively large area. Thus, fabrication approach with high efficiency and low cost is highly desired. Intrigued by these challenges, researches have worked intensively to develop novel responsive materials or new responsive mechanisms that can fulfill the desired properties.

1.3 Focus of This Work

The objective of this work is to develop a new type of magnetic responsive photonic crystal structure featuring fast response, excellent reversibility, large tuning range and high stability, which can be further applied in practical applications such as color displays. The reason for choosing magnetic field as the stimulus will be discussed in the following section, together with the obstacles now faced in this area. Finally, a brief description of my work will be provided.

1.3.1 Advantages of Magnetically Responsive Photonic Crystals

Although in principle the stimulus can be any chemical/physical means that can effectively cause changes in the average refractive indices of the structures, the lattice constants and symmetry of the colloidal arrays, the magnetic based stimulus exhibits several advantages over the others.[138-140] First, contactless control can be achieved using a magnetic field, which endows the magnetic RPCs with the potential to be integrated into advanced devices. Second, the magnetic field strength can be easily and precisely controlled by a simple magnet, which assures good control over responsive photonic properties. Third, since the magnetic interactions can be quickly built up within microseconds, a fast response of the magnetic RPC can be achieved. In addition, the magnetic interactions can help in the assembly of photonic structures with a much higher efficiency compared to conventional methods. Thus, adding magnetic components to colloidal building blocks provides an opportunity for efficient assembly of photonic structures, together with a convenient and precise control of the properties of the photonic crystals through an external magnetic field.

1.3.2 The Present Obstacles for Magnetic RPCs

Previously, Bibette et al. reported that γ-Fe_2O_3 nanoparticles could be introduced into emulsion droplets, which were able to form one dimensional chain structures and diffract visible light in the presence of an external magnetic field. Because emulsions are not thermodynamically stable, the unachieved long-term stability of oil droplets may limit their practical applications.[136] Besides, Asher et al. have developed a much more stable magnetic RPC by embedding superparamagnetic iron oxide nanoparticles into monodisperse polymer colloids through an emulsion polymerization process.[135, 141] By

introducing a high density of charges to the colloid surface, they were able to create 3D photonic crystals by taking advantage of the strong repulsive electrostatic interactions. Field-responsive diffraction in the visible spectrum was thus realized with a considerably larger tuning range. However, the percentage of magnetic components that can be incorporated into the building block is limited to about 17 wt% by the emulsion polymerization process. If the loading of magnetic materials in the building blocks can be significantly increased, in principle, it is possible to greatly improve the performance of system including the response speed and the diffraction tuning range.

In fact, an ideal magnetic RPC can be fabricated by using colloids made of pure magnetic materials, which can possess a faster response to the external field.[33, 139, 142] Such colloidal building blocks are preferred to have a uniform shape with a narrow size distribution and a tunable size, in order to enable precise control of the lattice constant and eliminate crystal defects as much as possible. The particle size is expected to be in the range of 100–200 nm so that the assembled structures will have periodicities comparable to wavelengths in the visible or near infrared range. In addition, superparamagnetism is required for the building blocks in the aim of creating a reversible optical response because significant magnetic interactions need to be initiated only through the application of external magnetic fields. The magnetic moment of each colloid has to be high enough so that strong interactions can be induced in a moderate magnetic field, improving the photonic response and lowering the responsive field strength threshold. More importantly, these magnetic particles are expected to have high surface charges and good solubility in the dispersion, thus producing sufficient repulsions

to balance the magnetically induced attractive force during assembly. The presence of both attractive and repulsive interactions with comparable strengths is believed to be the key to a successful self-assembled magnetically RPC. The main challenge along this path lies in the production of magnetic colloidal building blocks with controllable size, morphology, stability, surface structure, and magnetic properties.

1.3.3 Achievement of this work

To address the above-mentioned issues, I have focused on the development of a highly magnetically responsive photonic structure with rapid and full reversibility, which shows great potential in applications such as responsive color displays. In chapter 2, the colloidal photonic crystals with magnetically tunable stop bands covering the entire visible spectrum will be discussed, including the fabrication of superparamagnetic building blocks-- magnetite colloidal nanocrystal clusters (CNCs) and the resulting responsive photonic properties. The optical response of these photonic crystals to external magnetic stimuli is rapid and fully reversible.

To better understand the dynamic assembly process in the magnetic responsive system, a method of combining magnetic assembly with sol–gel processes has been developed to study the assembled structures by physically fixing them. In chapter 3, the convenient and flexible approach for the fabrication of individually fixed nanochains with a magnetically responsive photonic property will be demonstrated. The chain length and diffraction property can be well controlled. The fixed photonic nanochains exhibit long-term structural/optical stability and can be conveniently incorporated into many liquid or solid matrices.

For practical uses, long-term stability of such field-responsive photonic materials is required. However, in previous systems, the diffraction properties may change during storage because the electrostatic attractions between particles can vary once the surfactants gradually detach from the particle surface. In chapter 4, a novel water based etching method will be firstly introduced. Then in chapter 5, greatly improved magnetically responsive photonic structures with widely tunable optical properties and long-term stability can be achieved on the basis of this method.

In certain applications, long period application of a magnetic field with a high gradient is needed, but the gradient induced magnetic packing force can destroy the ordered photonic structure and thus diminish the diffraction. A new mechanism of stabilizing the magnetic photonic crystals against packing force while keeping the tunability will be shown in Chapter 6. By taking advantage of agarose gel as a matrix to prevent the photonic structures inside from aggregating, the system shows remarkable stability against an external magnetic field. Other features such as fast, reversible, and tunable optical response to external magnetic fields are maintained in this system.

The ability to stabilize the assemblies of the magnetic particles by a hydrogel matrix for a long period allows the fabrication of field-responsive polymer composite films for potential applications as color displays or sensors. In chapter 7, a simple demonstration of a magnetic responsive color display will be provided, in which a bistable color-reflective magnetic tunable photonic film with thermally erasable property can be fabricated by a magnetic field induced phase separation process and further stabilized by agarose gel. This bistable photonic film exhibits excellent cycling stability

and durability over a long period. The simple fabrication process, easy control over the color change, the superior stability over cycling and prolonged field exposure, and the low cost and energy saving properties allow broad potential applications including outdoor displays.

1.4 References

(1) C. I. Aguirre, E. Reguera, A. Stein, *Adv. Funct. Mater.*, 2010, **21**,2565.
(2) Y. Fukata, *Basic Concepts and Applications of Colored Materials*, Kodansha Springer, Tokyo, **2007**.
(3) J. V. Sanders, *Nature*, 1964, **204**,1151.
(4) S. John, *Phys. Rev. Lett.*, 1987, **58**,2486.
(5) E. Yablonovitch, *Phys. Rev. Lett.*, 1987, **58**,2059.
(6) J. D. Joannopoulos, S. G. Johnson, J. N. Winn, R. D. Meade, *Photonic Crystals: Molding the Flow of Light*, 2nd ed., Princeton University Press, Princeton, NJ, **2008**.
(7) E. Yablonovitch, *Sci. Am.*, 2001, **285**,47.
(8) C. López, *J. Opt. A: Pure Appl. Opt.*, 2006 **8**,R1.
(9) J. Hung, M. H. Kok, W. Y. Tam, *Appl. Phys. Lett.*, 2009, **94**,014102.
(10) V. N. Bogomolov, S. V. Gaponenko, I. N. Germanenko, A. M. Kapitonov, E. P. Petrov, N. V. Gaponenko, A. V. Prokofiev, A. N. Ponyavina, N. I. Silvanovich, S. M. Samoilovich, *Phys. Rev. E*, 1997, **55**,7619.
(11) T. F. Krauss, *Nat. Mater.*, 2003, **2**,777.
(12) M. Srinivasarao, *Chem. Rev.*, 1999, **99**,1935.
(13) A. R. Parker, V. L. Welch, D. Driver, N. Martini, *Nature*, 2003, **426**,786.
(14) A. R. Parker, R. C. McPhedran, D. R. McKenzie, L. C. Botten, N. A. P. Nicorovici, *Nature*, 2001, **409**,36.
(15) P. Vukusic, J. R. Sambles, *Nature*, 2003, **424**,852.
(16) Y. Akahane, T. Asano, B.-S. Song, S. Noda, *Nature*, 2003, **425**,944.
(17) D. J. Norris, *Nat. Mater.*, 2007, **6**,177.
(18) Y. Chen, J. Au, P. Kazlas, A. Ritenour, H. Gates, M. McCreary, *Nature*, 2003, **423**,136.
(19) S. Ogawa, M. Imada, S. Yoshimoto, M. Okano, S. Noda, *Science*, 2004, **305**,227.
(20) A. Birner, R. B. Wehrspohn, U. M. Gösele, K. Busch, *Adv. Mater.*, 2001, **13**,377.
(21) H. Masuda, M. Ohya, H. Asoh, M. Nakao, M. Nohtomi, T. Tamamura, *Jpn. J. Appl. Phys.*, 1999, **38**,L1403.
(22) S. Y. Lin, J. G. Fleming, D. L. Hetherington, B. K. Smith, R. Biswas, K. M. Ho, M. M. Sigalas, W. Zubrzycki, S. R. Kurtz, J. Bur, *Nature*, 1998, **394**,251.
(23) S. Noda, K. Tomoda, N. Yamamoto, A. Chutinan, *Science*, 2000, **289**,604.

(24) M. Campbell, D. N. Sharp, M. T. Harrison, R. G. Denning, A. J. Turberfield, *Nature*, 2000, **404**,53.
(25) Y. Xia, B. Gates, Y. Yin, Y. Lu, *Adv. Mater.*, 2000, **12**,693.
(26) R. C. Schroden, M. Al-Daous, C. F. Blanford, A. Stein, *Chem. Mater.*, 2002, **14**,3305.
(27) A. Urbas, Y. Fink, E. L. Thomas, *Macromolecules*, 1999, **32**,4748.
(28) Y. Fink, A. M. Urbas, M. G. Bawendi, J. D. Joannopoulos, E. L. Thomas, *J. Lightwave Technol.*, 1999, **17**,1963.
(29) A. K. Arora, B. V. R. Tata, *Ordering and Phase Transitions in Colloidal Systems*, VCH, Weinheim, **1996**.
(30) U. Jeong, Y. Xia, *Angew. Chem. Int. Ed.*, 2005, **44**,3099.
(31) K. Lee, S. A. Asher, *J. Am. Chem. Soc.*, 2000, **122**,9534.
(32) M. Born, E. Wolf, *Interferece and Diffraction of Light*, 7th ed., Cambridge University Press, New York, **2001**.
(33) J. Ge, Y. Yin, *Angew. Chem. Int. Ed.*, 2011, **50**,1492.
(34) G. R. Fowles, *Introduction to Modem Optics*, 2nd ed., Dover Pub. Inc., New York, USA, **1989**.
(35) H. Benisty, C. Weisbuch, D. Labilloy, M. Rattier, C. J. M. Smith, T. F. Krauss, R. M. de la Rue, R. Houdre, U. Oesterle, C. Jouanin, D. Cassagne, *J. Lightwave Technol.*, 1999, **17**,2063.
(36) L. D. Bonifacio, B. V. Lotsch, D. P. Puzzo, F. Scotognella, G. A. Ozin, *Adv. Mater.*, 2009, **21**,1641.
(37) Y. Lu, H. Xia, G. Zhang, C. Wu, *J. Mater. Chem.*, 2009, **19**,5952.
(38) P. A. Rundquist, P. Photinos, S. Jagannathan, S. A. Asher, *J.Chem.Phys.*, 1989, **91**,4932.
(39) S. A. Asher, J. Holtz, L. Liu, Z. Wu, *J. Am. Chem. Soc.*, 1994, **116**,4997.
(40) J. M. Weissman, H. B. Sunkara, A. S. Tse, S. A. Asher, *Science*, 1996, **274**,959.
(41) Y. J. Lee, P. V. Braun, *Adv. Mater.*, 2003, **15**,563.
(42) W.L. Vos, R. Sprik, A. van Blaaderen, A. Imhof, A. Lagendijk, G. H. Wegdam, *Phys. Rev. B*, 1996, **53**,16231.
(43) T. F. Krauss, R. M. De La Rue, S. Brand, *Nature* 1996, **383**,699
(44) O. Painter, R. K. Lee, A. Scherer, A. Yariv, J. D. O'Brien, P. D. Dapkus, I. Kim, *Science*, 1999, **284**,1819.
(45) S. Noda, A. Chutinan, M. Imada, *Nature*, 2000, **407**,608.
(46) O. Toader, S. John, *Science*, 2001, **292**,1133.
(47) M. Miyake, Y.-C. Chen, P. V. Braun, P. Wiltzius, *Adv. Mater.*, 2009, **21**,3012.
(48) T. Y. M. Chan, O. Toader, S. John, *Phys. Rev. E*, 2006, **73**.
(49) S. Jeon, V. Malyarchuk, J. A. Rogers, *Opt. Express*, 2006, **14**,2300.
(50) H. Fudouzi, Y. N. Xia, *Langmuir*, 2003, **19**,9653.
(51) B. Gates, Y. Xia, *Adv. Mater.*, 2001, **13**,1605.
(52) Z. Z. Gu, A. Fujishima, O. Sato, *J. Am. Chem. Soc.*, 2000, **122**,12387.
(53) A. Urbas, R. Sharp, Y. Fink, E. L. Thomas, M. Xenidou, L. J. Fetters, *Adv. Mater.*, 2000, **12**,812.
(54) F. S. Bates, *Science*, 1991, **251**,898.

(55) M. F. Schulz, A. K. Khandpur, F. S. Bates, K. Almdal, K. Mortensen, D. A. Hajduk, S. M. Gruner, *Macromolecules*, 1996, **29**,2857.
(56) J. G. McGrath, R. D. Bock, J. M. Cathcart, L. A. Lyon, *Chem. Mater.*, 2007, **19**,1584.
(57) J. H. Moon, S. Yang, *Chem. Rev.*, 2010, **110**,547.
(58) S. O. Kim, H. H. Solak, m. P. Stoykovich, N. J. Ferrier, J. J. d. Pablo, P. F. Nealey, *Nature*, 2003, **424**,411.
(59) M. P. Stoykovich, M. Müller, S. O. Kim, H. H. Solak, E. W. Edwards, J. J. de Pablo, P. F. Nealey, *Science*, 2005, **308**,1442.
(60) C. Park, C. De Rosa, L. J. Fetters, B. Lotz, E. L. Thomas, *Adv. Mater.*, 2001, **13**,724.
(61) D. E. Angelescu, J. H. Waller, D. H. Adamson, P. Deshpande, S. Y. Chou, R. A. Register, P. M. Chaikin, *Adv. Mater.*, 2004, **16**,1736.
(62) N. E. Voicu, S. Ludwigs, U. Steiner, *Adv. Mater.*, 2008, **20**,3022.
(63) C. Harrison, Z. Cheng, S. Sethuraman, D. Huse, P. M. Chaikin, D. A.. Vega, J. M. Sebastian, R. A. Register, D. H. Adamson, *Phys. Rev. E*, 2002, **66**,011706.
(64) F. Marlow, M. P. Sharifi, R. Brinkmann, C. Mendive, *Angew. Chem. Int. Ed.*, 2009, **121**,6328.
(65) F. Marlow, M. P. Sharifi, R. Brinkmann, C. Mendive, *Angew. Chem. Int. Ed.*, 2009, **48**,6212.
(66) R. K. Iler, *The Chemistry of Silica*, Wiley, New York, **1979**.
(67) W. Stöber, A. Fink, E. Bohn, *J. Colloid Interface Sci.*, 1968, **26**,62.
(68) E. Matijevic, *Langmuir*, 2002, **10**,8.
(69) M. Ohmori, E. Matijevic, *J. Colloid Interface Sci.*, 1992, **150**,594.
(70) W. P. Hsu, R. Yu, E. Matijevic, *J. Colloid Interface Sci.*, 1993, **156**,56.
(71) A. P. Philipse, M. P. B. van Bruggen, C. Pathmamanoharan, *Langmuir*, 2002, **10**,92.
(72) H. W. Deckman, J. H. Dunsmuir, S. Garoff, J. A. McHenry, D. G. Peiffer, *J. Vac. Sci. Technol., B*, 1988, **6**,333.
(73) P. Jiang, T. Prasad, M. J. McFarland, V. L. Colvin, *Appl. Phys. Lett.*, 2006, **89**,011908.
(74) S. Venkatesh, P. Jiang, B. Jiang, *Langmuir*, 2007, **23**,8231.
(75) P. Jiang, J. F. Bertone, K. S. Hwang, V. L. Colvin, *Chem. Mater.*, 1999, **11**,2132.
(76) K. E. Davis, W. B. Russel, W. J. Glantschnig, *Science*, 1989, **245**,507.
(77) P. N. Pusey, W. van Megen, *Nature*, 1986, **320**,340.
(78) L. V. Woodcock, *Nature*, 1997, **388**,236.
(79) P. Pieranski, *Contemp. Phys.*, 1983, **24**,25.
(80) W. Van Negen, I. Shook, *Adv. Colloid Interface Sci.*, 1984, **21**,119.
(81) S. A. Asher, P. L. Flaugh, G. Washinger, *Spcetroscopy*, 1986, **1**,26.
(82) T. Okubo, *Langmuir*, 2002, **10**,3529.
(83) E. A. Kamenetzky, L. G. Magliocco, H. P. Panzer, *Science*, 1994, **263**,207.
(84) D. H. Van Winkle, C. A. Murray, *Phys. Rev. A*, 1986, **34**,562.
(85) P. Pieranski, L. Strzelecki, B. Pansu, *Phys. Rev. Lett.*, 1983, **50**,900.
(86) S. Neser, C. Bechinger, P. Leiderer, T. Palberg, *Phys. Rev. Lett.*, 1997, **79**,2348.

(87) S. H. Park, Y. Xia, *Langmuir*, 1998, **15**,266.
(88) S. H. Park, D. Qin, Y. Xia, *Adv. Mater.*, 1998, **10**,1028.
(89) B. Gates, D. Qin, Y. Xia, *Adv. Mater.*, 1999, **11**,466.
(90) G. A. Ozin, L. Cademartiri, *Small*, 2009, **5**,1240.
(91) A. C. Arsenault, H. Miguez, V. Kitaev, G. A. Ozin, I. Manners, *Adv. Mater.*, 2003, **15**,503.
(92) X. Xu, A. V. Goponenko, S. A. Asher, *J. Am. Chem. Soc.*, 2008, **130**,3113.
(93) M. Ben-Moshe, V. L. Alexeev, S. A. Asher, *Anal. Chem.*, 2006, **78**,5149.
(94) D. P. Puzzo, A. C. Arsenault, I. Manners, G. A. Ozin, *Angew. Chem. Int. Ed.*, 2009, **48**,943.
(95) C. F. Blanford, R. C. Schroden, M. Al-Daous, A. Stein, *Adv. Mater.*, 2001, **13**,26.
(96) P. A. Snow, E. K. Squire, P. S. J. Russell, L. T. Canham, *J. Appl. Phys.*, 1999, **86**,1781.
(97) S. Chan, S. R. Horner, P. M. Fauchet, B. L. Miller, *J. Am. Chem. Soc.*, 2001, **123**,11797.
(98) J. H. Kang, J. H. Moon, S. K. Lee, S. G. Park, S. G. Jang, S. Yang, S. M. Yang, *Adv. Mater.*, 2008, **20**,3061.
(99) J. D. Debord, S. Eustis, S. B. Debord, M. T. Lofye, L. A. Lyon, *Adv. Mater.*, 2002, **14**,658.
(100) J. H. Holtz, S. A. Asher, *Nature*, 1997, **389**,829.
(101) X. L. Xu, S. A. Majetich, S. A. Asher, *J. Am. Chem. Soc.*, 2002, **124**,13864.
(102) J. Arriaga, L. Dobrzynski, B. Djafari-Rouhani, *J. Appl. Phys.*, 2008, **104**,063108/1.
(103) F. Fleischhaker, A. C. Arsenault, Z. Wang, V. Kitaev, F. C. Peiris, G. von Freymann, I. Manners, R. Zentel, G. A. Ozin, *Adv. Mater.*, 2005, **17**,2455.
(104) F. Fleischhaker, A. C. Arsenault, V. Kitaev, F. C. Peiris, G. von Freymann, I. Manners, R. Zentel, G. A. Ozin, *J. Am. Chem. Soc.*, 2005, **127**,9318.
(105) M. Qi, E. Lidorikis, P. T. Rakich, S. G. Johnson, J. D. Joannopoulos, E. P. Ippen, H. I. Smith, *Nature*, 2004, **429**,538.
(106) K. Sumioka, H. Kayashima, T. Tsutsui, *Adv. Mater.*, 2002, **14**,1284.
(107) S. H. Foulger, P. Jiang, A. C. Lattam, D. W. Smith, J. Ballato, *Langmuir*, 2001, **17**,6023.
(108) S. H. Foulger, P. Jiang, A. Lattam, D. W. Smith, J. Ballato, D. E. Dausch, S. Grego, B. R. Stoner, *Adv. Mater.*, 2003, **15**,685.
(109) J. D. Debord, L. A. Lyon, *J. Phys. Chem. B*, 2000, **104**,6327.
(110) Z. B. Hu, X. H. Lu, J. Gao, *Adv. Mater.*, 2001, **13**,1708.
(111) Y. Takeoka, M. Watanabe, *Langmuir*, 2003, **19**,9104.
(112) M. Honda, T. Seki, Y. Takeoka, *Adv. Mater.*, 2009, **21**,1801.
(113) K. Matsubara, M. Watanabe, Y. Takeoka, *Angew. Chem. Int. Ed.*, 2007, **46**,1688.
(114) N. Tetreault, H. Miguez, S. M. Yang, V. Kitaev, G. A. Ozin, *Adv. Mater.*, 2003, **15**,1167.
(115) A. B. Pevtsov, D. A. Kurdyukov, V. G. Golubev, A. V. Akimov, A. A. Meluchev, A. V. Sel'kin, A. A. Kaplyanskii, D. R. Yakovlev, M. Bayer, *Phys. Rev. B*, 2007, **75**,153101/1.

(116) J. Zhou, C. Q. Sun, K. Pita, Y. L. Lam, Y. Zhou, S. L. Ng, C. H. Kam, L. T. Li, Z. L. Gui, *Appl. Phys. Lett.*, 2001, **78**,661.
(117) C. E. Reese, S. A. Asher, *Anal. Chem.*, 2003, **75**,3915.
(118) S. A. Asher, V. L. Alexeev, A. V. Goponenko, A. C. Sharma, I. K. Lednev, C. S. Wilcox, D. N. Finegold, *J. Am. Chem. Soc.*, 2003, **125**,3322.
(119) S. Shinohara, T. Seki, T. Sakai, R. Yoshida, Y. Takeoka, *Angew. Chem. Int. Ed.*, 2008, **47**,9039.
(120) S. Y. Choi, M. Mamak, G. von Freymann, N. Chopra, G. A. Ozin, *Nano Lett.*, 2006, **6**,2456.
(121) M. C. Fuertes, F. J. Lopez-Alcaraz, M. C. Marchi, H. E. Troiani, V. Luca, H. Miguez, G. Juan de Avila Arturo Soler-Illia, *Adv. Funct. Mater.*, 2007, **17**,1247.
(122) A. C. Arsenault, D. P. Puzzo, I. Manners, G. A. Ozin, *Nat. Photonics*, 2007, **1**,468.
(123) K. Ueno, K. Matsubara, M. Watanabe, Y. Takeoka, *Adv. Mater.*, 2007, **19**,2807.
(124) K. Ueno, J. Sakamoto, Y. Takeoka, M. Watanabe, *J. Mater. Chem.*, 2009, **19**,4778.
(125) R. Wilk, N. Vieweg, O. Kopschinski, M. Koch, *Opt. Express*, 2009, **17**,7377.
(126) M. H. Song, B. Park, S. Nishimura, T. Toyooka, I. J. Chung, Y. Takanishi, K. Ishikawa, H. Takezoe, *Adv. Funct. Mater.*, 2006, **16**,1793.
(127) D. Kang, J. E. Maclennan, N. A. Clark, A. A. Zakhidov, R. H. Baughman, *Phys. Rev. Lett.*, 2001, **86**,4052.
(128) M. Kamenjicki Maurer, I. K. Lednev, A. Mikhonin, R. Kesavamoorthy, S. A. Asher, *Adv. Funct. Mater.*, 2003, **13**,774.
(129) M. Kamenjicki Maurer, I. K. Lednev, S. A. Asher, *Adv. Funct. Mater.*, 2005, **15**,1401.
(130) Z. Z. Gu, T. Iyoda, A. Fujishima, O. Sato, *Adv. Mater.*, 2001, **13**,1295.
(131) S. Kubo, Z. Z. Gu, K. Takahashi, Y. Ohko, O. Sato, A. Fujishima, *J. Am. Chem. Soc.*, 2002, **124**,10950.
(132) Z.-Y. Xie, L.-G. Sun, G.-Z. Han, Z.-Z. Gu, *Adv. Mater.*, 2008, **20**,3601.
(133) Y. Saado, M. Golosovsky, D. Davidov, A. Frenkel, *Phys. Rev. B*, 2002, **66**,195108/1.
(134) Z. Cun, C. Liangshui, X. Hua, G. Zhongze, *Macromol. Rapid Commun.*, 2009, **30**,1945.
(135) X. L. Xu, G. Friedman, K. D. Humfeld, S. A. Majetich, S. A. Asher, *Adv. Mater.*, 2001, **13**,1681.
(136) F. Leal Calderon, T. Stora, O. Mondain Monval, P. Poulin, J. Bibette, *Phys. Rev. Lett.*, 1994, **72**,2959.
(137) J. Bibette, *J. Magn. Magn. Mater.*, 1993, **122**,37.
(138) G. M. Whitesides, M. Boncheva, *Proc. Natl. Acad. Sci. USA*, 2002, **99**,4769.
(139) J. Ge, Y. Yin, *J. Mater. Chem.*, 2008, **18**,5041.
(140) J. Ge, J. Goebl, L. He, Z. Lu, Y. Yin, *Adv. Mater.*, 2009, **21**,4259.
(141) X. L. Xu, G. Friedman, K. D. Humfeld, S. A. Majetich, S. A. Asher, *Chem. Mater.*, 2002, **14**,1249.
(142) J. Ge, L. He, Y. Hu, Y. Yin, *Nanoscale*, 2011, **3**,177.

Chapter 2

Magnetically Responsive Photonic Crystals

2.1 Introduction

Colloidal crystals, typically self-assembled from monodisperse colloidal building blocks into periodic structures, are one class of photonic band gap materials that can be fabricated at low cost and on a large scale.[1-5] They have attracted much attention because of their promise in optoelectronic applications that require the manipulation of photons, for example, as photonic components in telecommunication devices, lasers, and sensors.[6-14] It is highly desirable for the envisioned applications that a photonic crystal possesses a tunable stop band that can be conveniently controlled by external stimuli. Considerable effort has been devoted to achieving this goal by changing the refractive indices of the materials and the lattice constants or spatial symmetry of the crystals through the application of chemical stimuli, mechanical forces, electrical fields, or light.[13, 15-20] However, the wide use of these systems as optoelectronic devices is hampered by the limited tunability of the stop band (changes in peak position are typically in the range of tens of nanometers), the slow response to the external stimuli, and the difficulty of integration into existing photonic systems.[20-25]

Adding magnetic components to the colloidal building blocks provides an effective means for convenient and precise control over the properties of photonic crystals through an external magnetic field.[26-31] In fact, an ideal magnetic responsive photonic crystal can be fabricated by using colloids made of pure magnetic materials,

thus favoring a faster response to the external field. Such colloids are better to have a controllable size, a uniform shape, and a narrow size distribution, so that the periodicity can be precisely tuned. The particle size is preferred to be in the range of 100–200 nm so that the assembled structures will have periodicities comparable to the wavelength of the visible or near infrared light. Again, the superparamagnetic-to ferromagnetic transition must be avoided, which usually occurs when crystal size is larger than 30 nm.[29, 32] Superparamagnetism is a prerequisite in order to achieve a reproducible and reversible photonic response because no significant magnetic interactions will remain after removing the external magnetic field.[33] High magnetic moment of each colloid is desired so that strong magnetic interactions can be induced by a moderate magnetic field, ensuring a rapid photonic response. More importantly, these magnetic particles are expected to possess a high charge density, thus producing sufficient repulsive force to balance the magnetically induced attractive force during assembly. The presence of both attractive and repulsive interactions with comparable strengths is believed to be the key of a successful self-assembly process.

The pioneer work by Asher and coworkers focused on similar approach by fabricating colloidal photonic crystals using highly charged polystyrene microspheres containing superparamagnetic nanoparticles.[26, 27, 34] In this case, the magnetic forces exerted on the colloids are weak relative to interparticle electrostatic forces because of the low loading of the magnetic materials, leading to a limited tuning range, a long response time, and consequently limited practical applications. Preparation of polymer microspheres with increased loading of magnetic materials is practically difficult within

the typically used emulsion polymerization schemes. In addition, Bibette et al. discovered that emulsion droplets containing γ-Fe_2O_3 nanoparticles can form one dimensional chain structures and diffract visible light upon the application of an external magnetic field.[35] However, emulsion droplets are not thermodynamically stable, which may limit their practical applications.[36] In principle, colloidal particles of pure magnetic materials such as iron oxide can be directly used as the building blocks for constructing colloidal photonic crystals. Such effort, however, is limited by the superparamagnetic-to-ferromagnetic transition that occurs as particles are grown into larger domains.[36]

Here, we developed a high-temperature hydrolysis method for the preparation of polyacrylate-capped superparamagnetic magnetite (Fe_3O_4) colloidal nanocrystal clusters (CNCs) with tunable sizes from 30 to 180 nm.[37] Each cluster is composed of many magnetite crystallites of approximately 10 nm, thus retaining the superparamagnetic properties at room temperature. Such superparamagnetic clusters can be directly employed for constructing colloidal photonic crystals with highly tunable stop bands that can be moved across the entire visible spectral region owing to the highly charged polyacrylate-capped surfaces and the strong interaction of the magnetite CNCs with a magnetic field.[38] Our approach employs simple and inexpensive synthetic methods and yields photonic crystals with wide and reversible tunability, and an instant response to external magnetic fields; as such, it could lead to many critical applications that would not otherwise be accessible.

2.2 Experimental Section

2.2.1 Materials.

Diethylene glycol (DEG, reagent grade), ethanol (denatured), and sodium hydroxide (NaOH, 98.8%) were purchased from Fisher Scientific. Anhydrous iron(III) chloride (FeCl3, 98%) was purchased from Riedel-deHaën. Poly(acrylic acid) (PAA,MW) 1800) was obtained from Sigma-Aldrich. All chemicals were directly used as received without further treatment.

2.2.2 Synthesis of Superparamagnetic Fe_3O_4 CNCs.

Magnetite colloidal nanocrystal clusters (CNCs) with a tunable average size in the range from ~30 to ~180 nm were synthesized in solution at high temperature. A NaOH/DEG stock solution was prepared by dissolving 50 mmol of NaOH in 20 mL of DEG and then heating it at 120 °C for 1 h under nitrogen. In a typical synthesis, a mixture of 4 mmol of PAA, 0.4 mmol of $FeCl_3$, and 17 mL of DEG was heated to 220 °C in a nitrogen atmosphere for 30-60 min with vigorous stirring to form a transparent, light yellow solution. A total of 1.75 mL of NaOH/DEG stock solution was then injected into the above solution which slowly turned black after about 2 min. The resulting mixture was further heated for 1 h. These colloids were first washed with a mixture of deionized (DI) water and ethanol and then with pure water several times. Finally the cleaned colloids were dispersed in 3 mL of DI water.

2.2.3 Characterization of Fe_3O_4 CNCs.

TEM Characterization. A Tecnai T12 transmission electron microscope (TEM) was used to characterize the morphology and size distribution of the Fe_3O_4 CNCs. Colloids dispersed in water at an appropriate concentration were cast onto a carbon-coated copper grid, followed by evaporation under vacuum at room temperature. A Zeiss

AXIO Imager optical microscope was used to observe the visible-range diffraction by CNC solutions enclosed in glass capillaries and the assembly of Fe_3O_4 CNCs under a magnetic field.

Diffraction Measurements. The diffraction spectra of the photonic crystals were measured by using an Ocean Optics HR2000CG-UV-NIR spectrometer coupled to a six-around-one reflection/backscattering probe. Incident light emerges from six fibers, and the light back-diffracted by the colloidal crystals is collected by a central fiber. In a typical measurement, a thin glass vessel containing the solution of F_3O_4 CNCs was placed between the NdFeB magnet and reflection probe. The probe was perpendicular to the glass vessel and parallel to the direction of the magnetic field. Reflection peaks were measured with the magnet fixed at a certain distance from the samples. For measuring the diffraction of photonic crystals in modulated magnetic fields, a tubular electromagnet (Magnetic Sensor Systems, E-20-100-27) controlled by a function generator was used to produce periodical magnetic fields. The spectra integration time of collecting the signals was set to be 500 ms for constant magnetic fields and 200 or 100 ms for modulated magnetic fields.

In Situ Observation of the Assembly of Fe_3O_4 CNCs. A 5 μL Fe_3O_4 CNC solution was sandwiched between two thin ¾'' X ¾'' cover glass slides to form a thin liquid film and then transferred onto the stage of an optical microscope for in situ observation. A NdFeB magnet was placed on another stage beneath the sample stage and could be manually moved vertically to change the magnet-sample distance.

2.3 Results and Discussion

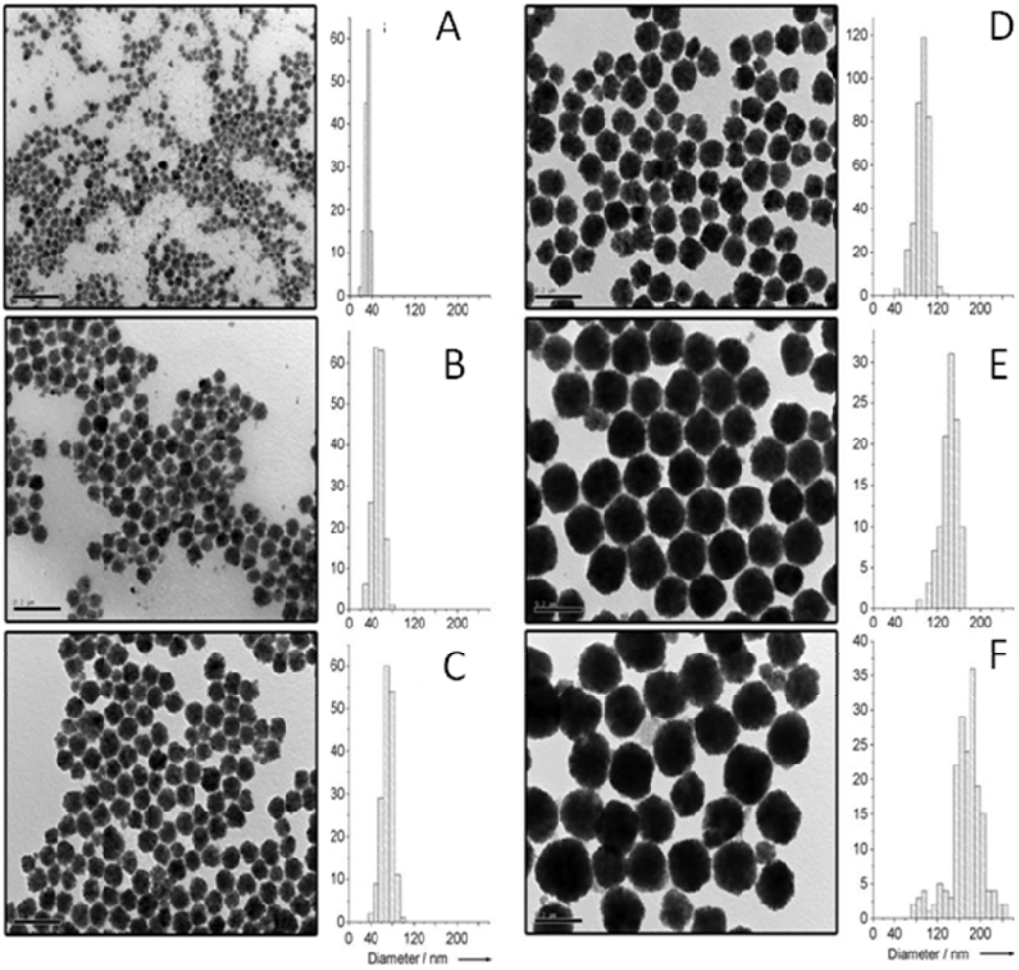

Figure 2.1 Representative TEM images of magnetite CNCs at the same magnification. The average diameters of the CNCs, obtained by measuring about 150 clusters for each sample, are 31 (A), 53 (B), 71 (C), 93 (D), 141 (E), and 174 nm (F). All scale bars are 200 nm.

2.3.1 Synthesis Strategy for Fe_3O_4 CNCs

Water soluble magnetite CNCs were produced through a high temperature hydrolysis reaction of $FeCl_3$ with NaOH in the presence of PAA.[37] The solvent, DEG, partially reduces trivalent iron at the reaction temperature (220 °C) and finally produces Fe_3O_4 particles through dehydration.[39, 40] Depending on the relative ratios of reagents, this system allows the production of single crystalline nanodots and polycrystalline flowerlike three dimensional clusters.[41] Under optimized conditions, uniform CNCs with average diameters tunable from ~30 to ~180 nm can be produced by adjusting the amount of NaOH (Figure 2.1). As shown in Figure 2.2, each CNC is composed of small primary nanocrystals of ~10 nm, thus retaining superparamagnetism at room temperature while showing much higher saturation magnetization than individual nanodots. Polyacrylate binds to the particle surface through the strong coordination of carboxylate groups with iron cations. The uncoordinated carboxylate groups on the polymer chains extend into the aqueous solution, rendering the particle surfaces highly charged. After removing excess surfactant through repeated cleaning by centrifugation, the CNCs form a stable aqueous dispersion. The PAA coating confers excellent stability against aggregation upon the particles. For example, the particles can be separated from the solution and dried at 60 °C overnight. After storing in powder form for several months, they can still be dispersed instantly in water without detectable aggregation.

Solutions of the Fe_3O_4 CNCs show brilliant colors when an external magnetic field is applied, indicating the formation of ordered structures.[38] This effect, observable in the direction parallel to the external field, results from Bragg diffraction of ambient

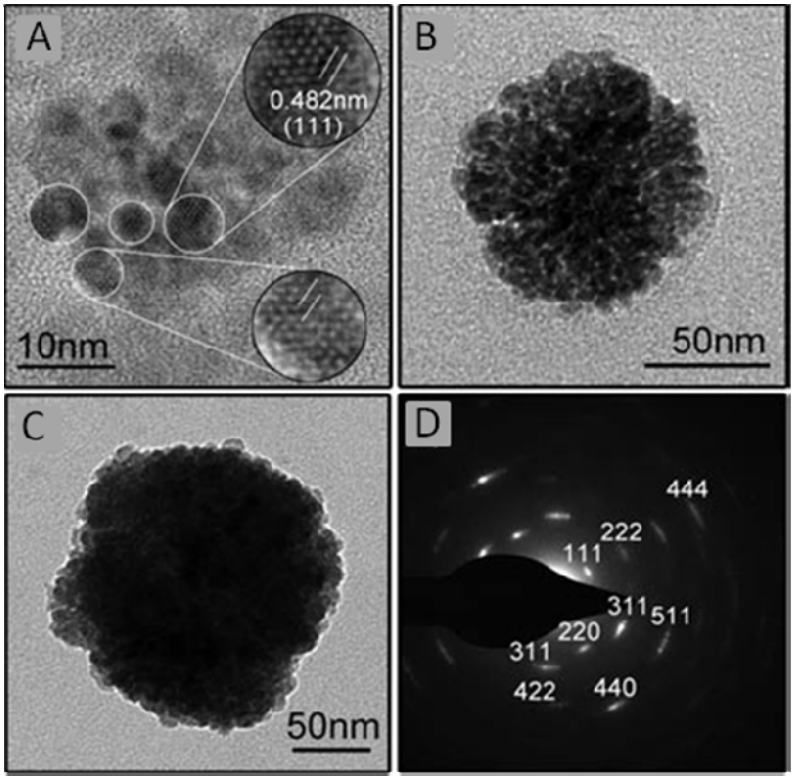

Figure 2.2 (A) Typical HRTEM image of a 31-nm cluster. (B, C) High magnification TEM images of 93- and 174-nm CNCs. (D) SAED pattern of the cluster in (C).

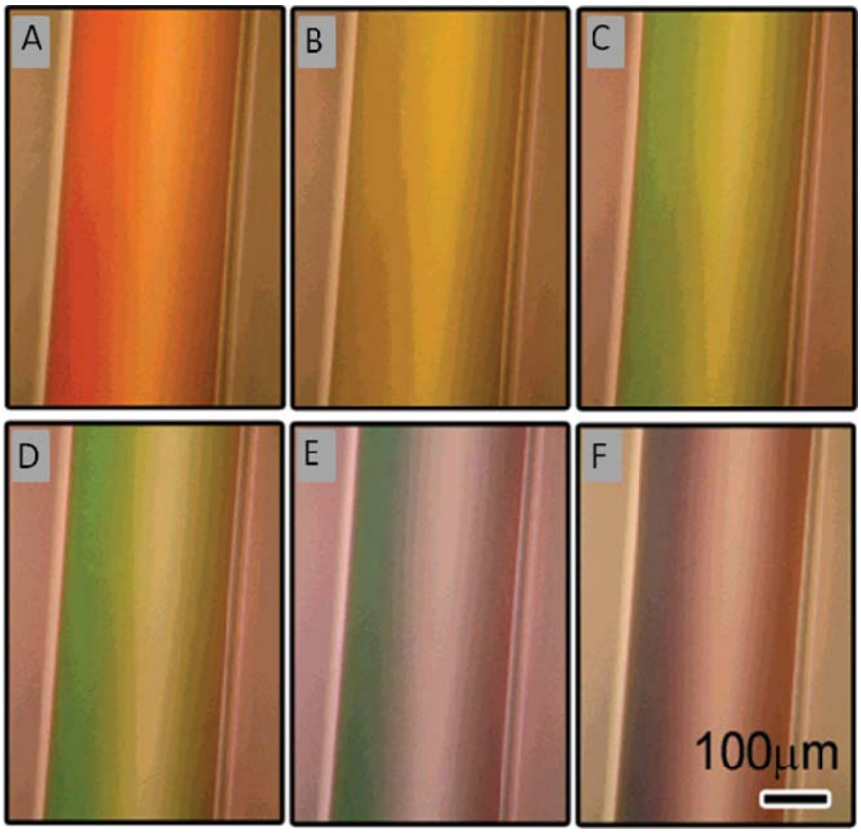

Figure 2.3 Optical microscope images of a 120 nm Fe_3O_4 CNC solution enclosed in a glass capillary under an increasing (from A to F) magnetic field.

light by the periodically ordered structures self-assembled from CNCs under the magnetic field.[35, 42] The diffraction wavelength can be tuned from longer to shorter values by simply increasing the magnetic field strength. A magnetic field with strength above 100 G is sufficient to induce the ordering of CNCs and the color change in a bulk solution enclosed in a glass vial. This system also allows for convenient miniaturization while maintaining an optical response to the external field. We have demonstrated this advantage by simply placing a 120 nm Fe_3O_4 CNC solution into a glass capillary with an inner diameter of ~ 265 μm. As shown in the optical microscopy images in Figure 2.3, a magnet placed beneath the capillary drives the color change progressing from red to yellow, green, and blue by simply changing the magnet-capillary distance. The optical response of the small volume sample to the external field is rapid and reversible, demonstrating the feasibility of miniaturization of the system for integration into optoelectronic devices.

2.3.2 Self-Assembly of CNCs in External Magnetic Fields.

The self-assembly behavior of the CNCs in response to external magnetic fields has been studied in situ through optical microscopy. A thin film of CNC solution is formed by sandwiching a CNC droplet between two cover glasses, and then mounted on the sample stage of the microscope. A magnet is placed on another stage underneath the sample so that the magnet can be moved vertically for convenient control of the sample magnet distance. Without an external magnetic field, the superparamagnetic colloids are well dispersed in water and their Brownian motion makes it difficult to capture a clear image of the particles. When a magnetic field is vertically applied and gradually

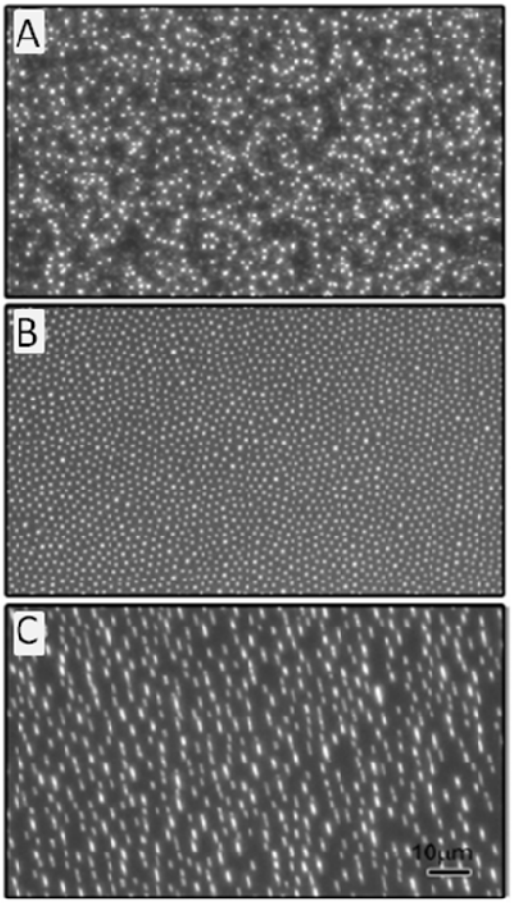

Figure 2.4 (A and B) Optical microscope images showing the assembly of Fe_3O_4 CNCs dispersed in a liquid film encapsulated between two glass slides in a magnetic field parallel to the viewing angle. The field strength increases from (A) to (B). (C) Optical microscope image illustrating the assembly of CNCs into chainlike structures by slight tilting of the magnetic field (~15° from the view angle).

strengthened, the movement of particles slows down. At first sight, the increased magnetic field appears to induce a decrease of the particle number density, as can be seen by comparing the dark-field optical microscopy images in Figure 2.4 A and B. A careful inspection also indicates short-range hexagonal order of the particle assembly (Figure 2.4 B). A slight tilt (~15°) of the magnet reveals that each bright spot is, in fact, a chain of particles lined up along the magnetic field (Figure 2.4 C). The chains appear longer when the magnetic field is tilted further away from vertical orientation. The formation of chains along the magnetic field explains why the particle number density seemingly decreases upon application of the field. We also observed that the separation between the chains (~2 μm) does not change significantly upon further increase of the magnetic field beyond the value necessary for hexagonal ordering to emerge.

The strong optical diffraction is believed to result from periodicity formed along the magnetic field. In the plane perpendicular to the magnetic field, the short-range order and the large interparticle distance of the assembled structure make it unlikely to diffract visible light. Only in the direction of the external field, chainlike structures form with an interparticle distance (periodicity) comparable to the wavelength of visible light. As schematically shown in Figure 2.5A, the Fe_3O_4 colloidal crystal is highly anisotropic in structure so that it appears more like arrays of parallel CNC chains. The structural anisotropy also leads to the anisotropic optical responses. Figure 2.5B and C shows the optical response of a sample confined in a rectangular cuvette when observed parallel and perpendicular to the magnetic field, respectively. A strong visible Bragg diffraction can be noticed when observed in the direction parallel to the magnetic field, while only a

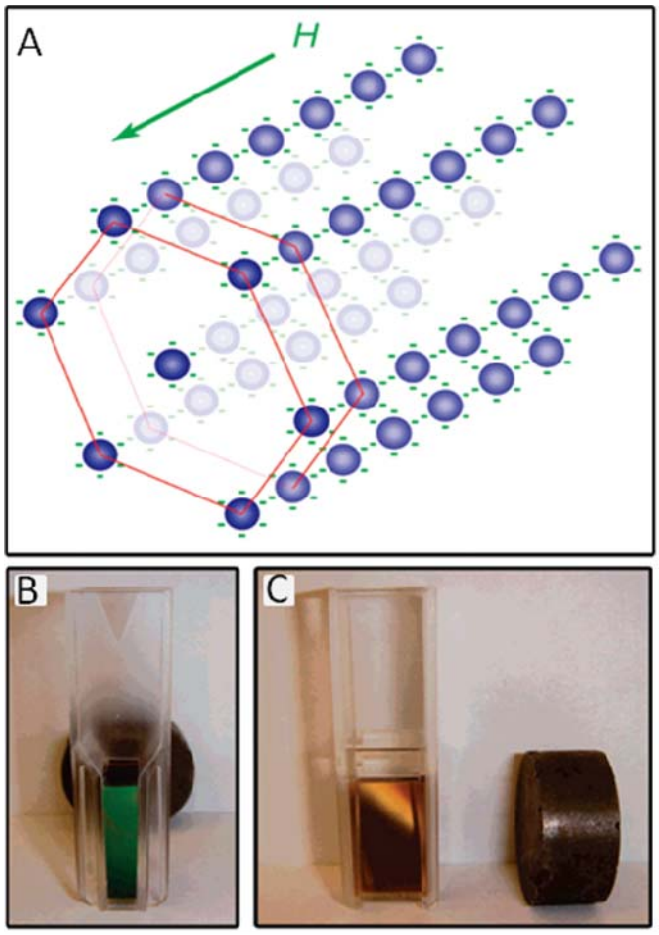

Figure 2.5 (A) Schematic illustration of the structure of Fe_3O_4 colloids self-assembled in the presence of an external magnetic field. (B and C) Digital photos of a CNC solution captured from the direction (B) parallel and (C) perpendicular to the magnetic field.

golden luster can be captured in the perpendicular direction. When highly charged superparamagnetic colloids are assembled in an external magnetic field, the final ordered structure is the balanced result of both electrostatic interactions and induced magnetic forces.[27] In the absence of a magnetic field, the Fe_3O_4 CNCs disperse well in water at a typical concentration of 8.4 mg/mL. At this concentration, the average interparticle distance is apparently large so that no strong electrostatic repulsive interaction is present to drive the self-assembly of CNCs into ordered arrays. This is different from the previously reported case of magnetically tunable colloidal crystals where charged superparamagnetic polystyrene spheres are highly concentrated so that the strong electrostatic repulsive forces drive the self assembly of the particles into ordered structures even without an external magnetic field. In the current work, the electrostatic interactions do not contribute to the ordering of the CNCs until the magnetic field is applied. The application of a magnetic field to superparamagnetic colloids in solution results in additional magnetic packing forces and magnetic dipole-dipole interactions.[43, 44] The magnetic packing force $F_m = \nabla(\mu B)$, with μ being the induced magnetic moment and B being the strength of the external field, is exerted on every particle and attracts them toward the maximum of local magnetic gradient.[27] The magnetic dipolar interactions can be either attractive or repulsive, strongly depending on the relative orientation of the two magnetic moments. Considering in the current case where the induced magnetic dipoles are parallel to the magnetic field, a magnetic attractive force $F_m = 6(\mu^2/d^4)$ exists when two identical interacting dipoles are aligned with their connecting line parallel to the direction of the magnetic field, while a repulsive force $F_m = 3(\mu^2/d^4)$ presents when the

two dipoles are positioned with their connecting line perpendicular to the field (d is the spacing between the two magnetic dipoles). Our estimation shows that the magnetic packing force is relatively small in comparison to the magnetic attractive force. For example, a 120 nm cluster shows a magnetic moment μ of ~ 6.3 X 10^{-14} emu in a 235G magnetic field and experiences a magnetic packing force of 1.3 X 10^{-11} dyn in a gradient of 200 G/cm. With a 197.4 nm nearest-neighbor spacing d derived from the diffraction peak position, the interparticle attractive force $F_m = 6(\mu^2/d^4)$ is estimated to be 1.6 X 10^{-7} dyn. Therefore, the magnetic attractive force is believed to play a dominant role in bringing CNCs together. The electrostatic repulsive force (F_{er}) for the same sample in a 235 G field with a 197.4 nm interparticle spacing is also calculated and compared to the induced magnetic forces. The unbounded carboxylate groups on the particle surface were first converted to the acid form using slightly excessive diluted HCl. The amount of free carboxylate groups was estimated by matching the pH of a pure PAA solution to that of the sample. The ionic strength (I) of the solution is thus estimated to be 3.4 X 10^{-4} mol/L. The Debye-Hückel length κ^{-1} was calculated to be 16.56 nm according to its definition $\kappa^{-1} = \varepsilon kT/2000N_A e^2 I)^{1/2}$, where ε is the dielectric constant, k is Boltzmann's constant, T is the absolute temperature in kelvins, N_A is Avogadro's number, and e is the elementary charge.[45] The zeta potential (ζ) was measured to be -51 mV. Since the 120 nm cluster shows a magnetic moment μ of 6.3 X 10^{-14} emu in a 235 G magnetic field and a 197.4 nm spacing d can be derived from the diffraction peak, the particle diameter (r) and interparticle surface-to-surface distance (h) are 60 and 77.4 nm, respectively. Using the formula $F_{er} = \pi\varepsilon\zeta^2 r e^{-\kappa h}$, the electrostatic repulsive force is calculated to be 2.4 X 10^{-7} dyn,

which is comparable to the estimated magnetic attractive force. When the electrostatic repulsive force and magnetic attractive force reach a balance, the CNCs form chainlike structures along the external magnetic field with regular interparticle spacing of a few hundred nanometers. The repulsive forces, both electrostatic and magnetic, keep the CNC chains away from each other so that they may self-organize into short-range ordered structures.

2.3.3 Tuning the Diffraction Wavelength by Varying the External Magnetic Field Strength.

The spacing between neighboring CNCs within each chain can be changed by varying the strength of external magnetic fields. By moving a magnet closer to the sample, one can conveniently increase the strength of the field and therefore the induced magnetic attractive force, in turn bringing CNC particles closer together until the magnetic attractive force is balanced by the increased interparticle electrostatic repulsion. Figure 2.6A shows the photos of an aqueous solution of 120-nm CNCs in response to a varying magnetic field achieved by controlling the distance between the magnet and the sample. Figure 2.6B shows the reflection spectra of an aqueous solution of CNCs in response to a varying magnetic field. By moving the magnet closer to the sample, the local magnetic field increases gradually and the diffraction peak blue shifts. The spatial dependence of the magnetic field strength of the NdFeB magnet used in this work is displayed in Figure 2.6C. By using Bragg's law $\lambda=2nd\sin\theta$, where λ is the diffraction wavelength, n is the refractive index of water, d is the lattice plane spacing, and $\theta = 90°$ is

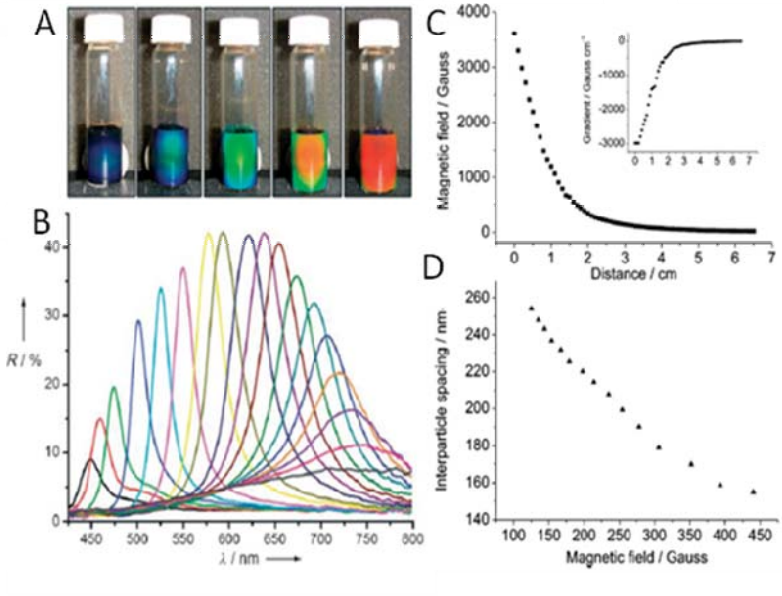

Figure 2.6 (A) Photographs of colloidal crystals formed in response to an external magnetic field; the magnet–sample distance decreases gradually from right to left. (B) Dependence of the reflection spectra at normal incidence of the colloidal crystals on the distance of the sample from the magnet. Diffraction peaks blue-shift (from right to left) as the distance decreases from 3.7 to 2.0 cm with step size of 0.1 cm. The average diameter of the CNCs in this sample is 120 nm. (C) Spatial distribution of the magnetic field strength and gradient (inset) measured using a Hall probe. (D) Relation between the estimated interparticle spacing along the magnetic field and the strength of the magnetic field.

the Bragg angle, we are able to estimate the interparticle spacing within a single chain. As a result, the reflection spectra in Figure 2.6C can be re-plotted in Figure 2.6D, showing a very clear trend for the dependence of the interparticle spacing on the strength of the magnetic field. Changes in the reflection spectra due to repositioning of the magnet are reversible, with the diffraction peak intensity and position being well reproduced at a fixed sample-magnet distance.

2.3.4 Tuning the Diffraction Wavelength by Electrostatic Interactions.

Electrostatic interactions also contribute significantly to the assembly of CNC particles. In principle, in a magnetic field with fixed strength, any changes leading to stronger electrostatic repulsion between CNCs will increase the interparticle distance, therefore red-shifting the diffraction peak. When a stronger magnetic field is applied to balance the increased electrostatic repulsion, the CNCs are organized with improved long-range order so that the diffraction intensity increases. These intuitive considerations have been observed experimentally. Immediately following synthesis, the system contains a large amount of free sodium polyacrylate and other ions, which effectively screen the electrostatic repulsive interactions. Only after prewashing with mixtures of ethanol and DI water does the colloidal aqueous solution display diffraction under a magnetic field. Furthermore, the overall diffraction intensities increase significantly after additional cycles of cleaning. Figure 2.7 shows the variation of magnetically induced reflection spectra of a 130nm CNC solution with the number of additional washing cycles (1-5 for a-e, respectively). The diffraction spectra obtained at a certain magnet-sample distance in different washing cycles are plotted in the same color. At a fixed magnetic

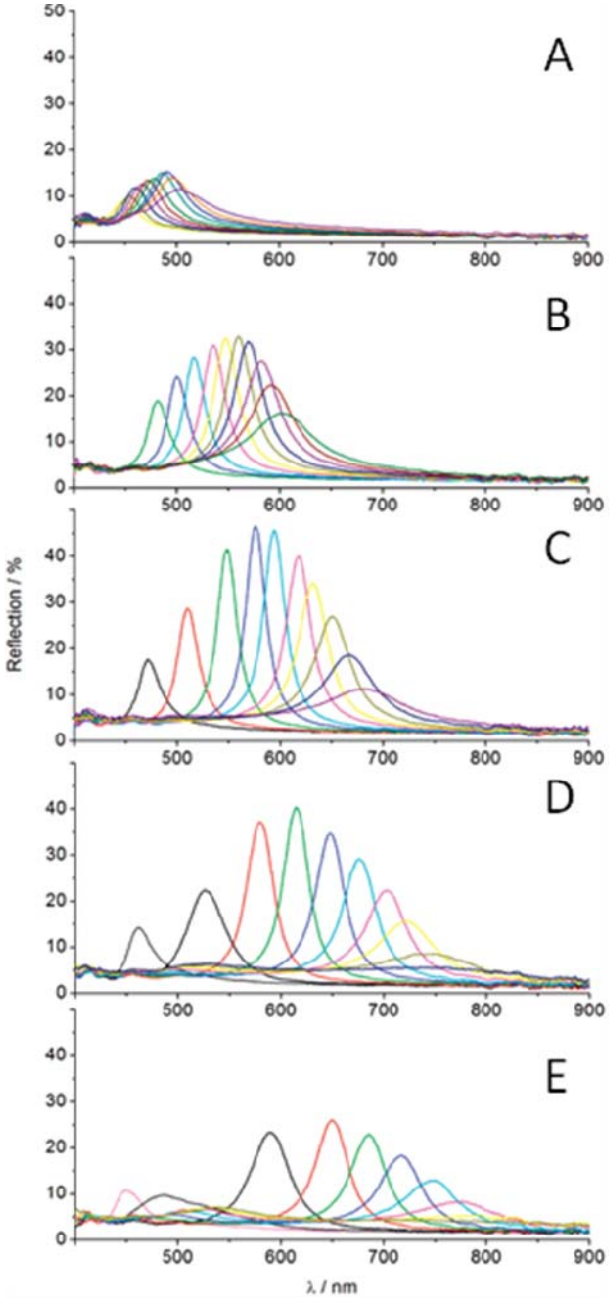

Figure 2.7 Reflection spectra of a 130 nm CNC solution after additional washing cycles (1-5 for a-e, respectively) with pure DI water. The starting sample was precleaned with a mixture of ethanol and water to remove most of the solvent and extra surfactants. Diffraction peaks blue-shift as the magnet-sample distance decreases from (A) 3.5 to 2.6 cm, (B) 3.1 to 2.2 cm, (C) 2.9 to 2.0 cm, (D) 2.8 to 1.9 cm, and (E) 2.7 to 1.8 cm. Peaks obtained at a specific distance were plotted in the same color.

strength, the diffraction peaks consistently red-shift with an increased number of washing cycles, indicating the increase of repulsive electrostatic interactions as more stray electrolytes are removed from the solution.[46, 47] With increasing numbers of washing cycles, stronger magnetic fields (or shorter sample-magnet distances) are required to keep the CNC solution diffractive at a given wavelength. Since the magnetic attractive force, scales with the square of induced magnetic moment, a higher magnetic strength is required to induce a strong enough attractive force to balance the electrostatic separation so that CNCs can be assembled into ordered arrays. On the other hand, the additional cleaning cycles significantly expand the range of wavelengths that the diffraction peak can be magnetically tuned over. For example, the diffraction maximum can be effectively tuned between 450 and 500 nm after a single water cleaning cycle with the sample-magnet distance in the range 2.6-3.5 cm, while the same sample after the fifth round of cleaning shows diffraction peaks tunable from 450 to 780 nm for the sample-magnet distance changing from 1.8 to 2.7 cm. The diffracted intensity increases monotonically in the first three cleaning cycles, and then it fades slightly in further washing processes. The optimal assembly condition after three times of water cleaning favors the long-range order of the CNC arrays and therefore the strong diffractions. When the electrostatic repulsion is further enhanced by additional cleaning, more intense magnetic fields are required to induce a strong enough magnetic attractive force to balance the electrostatic force. This can be experimentally achieved by moving the magnet closer to the sample. However, when the magnet-sample distance is smaller than 2.3 cm, the magnetic packing force starts to affect the assembly behavior of the CNCs as

the gradient of the magnetic field increases dramatically. The packing force applies to every particle and attracts them toward the maximum of local magnetic gradient, thus disturbing the long-range order inside the CNC chains and diminishing the diffracted intensity. Moving the magnet even closer further increases the magnetic packing force, eventually destabilizing the dispersion and precipitating CNCs on the glass vial wall.

We have also systematically studied the influence of the electrolyte concentration on the optical response of the samples. Figure 2.8 summarizes the change in position and intensity of the diffraction peak for a cleaned CNC solution with varying NaCl concentrations (0-1 mM) for nine sample-magnet distances. Due to screening by the counter ions present in a double layer around each particle, the magnitude of the electrostatic repulsive force decreases strongly with increasing concentration of electrolytes.[47, 48] As a result, the diffraction peak blue-shifts. From Figure 2.8A, it is obvious that the peak shift is more significant at lower ionic strength for the same amount of variation in the magnetic field. Data on the diffracted intensity as a function of electrolyte concentration and magnet-sample distance are displayed in Figure 2.8B, illustrating that maximum diffraction intensity is achieved at an optimal balance between magnetic and electrostatic interactions. For a strong magnetic field (magnet-sample distance 2.3-2.7 cm), bright diffractions are achievable at a low electrolyte concentration (C_{NaCl} = 0), where the induced magnetic attraction is strong enough to counter electrostatic repulsion. Increasing the electrolyte concentration reduces interparticle electrostatic repulsion. Apparently, as the repulsive forces weaken, positional order

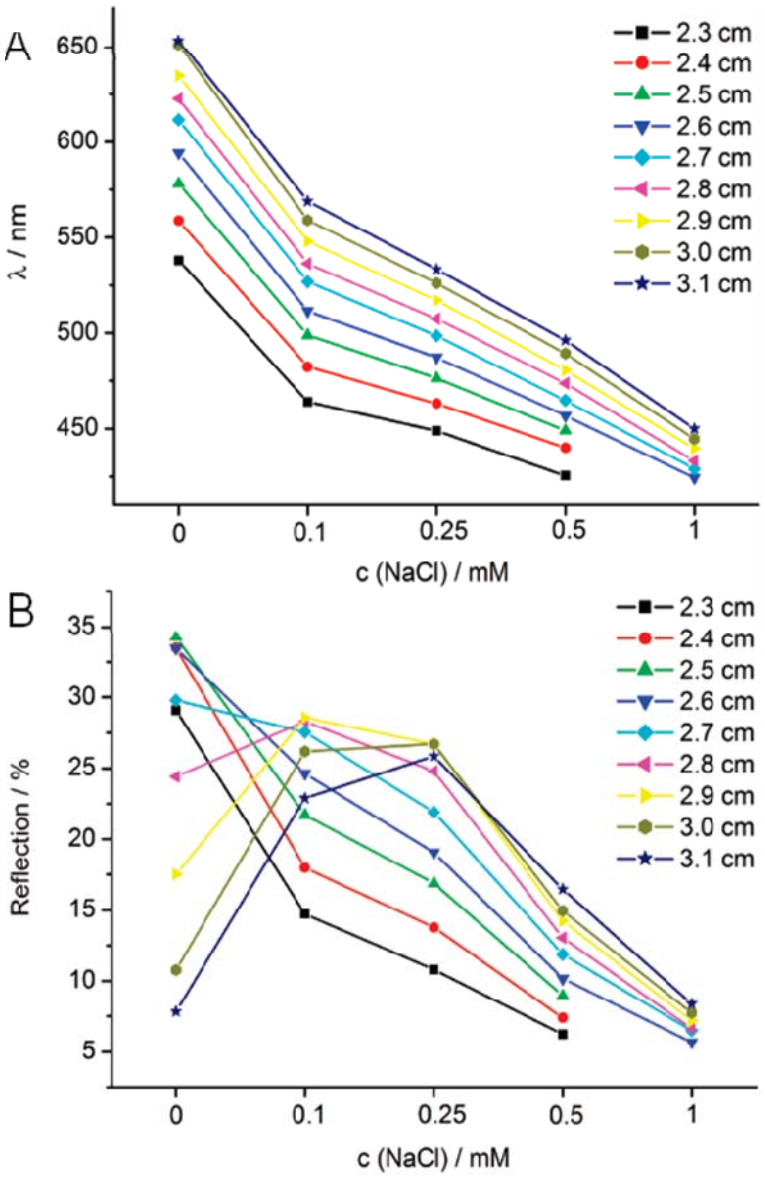

Figure 2.8 Influence of additional electrolyte NaCl on the (A) wavelength and (B) intensity of the diffraction peaks.

weakens monotonically, leading to the steady decrease in the diffraction intensity with increased electrolyte concentration. For samples in a weaker magnetic field (magnet-sample distance 2.8 to 3.1 cm), the induced magnetic attractive force has the appropriate magnitude to counter the reduced electrostatic force achieved at a certain, nonzero electrolyte concentration. As a result, the diffraction intensity in this case first increases with the addition of NaCl, reaches a maximum at C_{NaCl} = 0.1-0.25 mM, and eventually decreases at even higher NaCl concentrations where the electrostatic force becomes too weak to produce optimal ordering within chains of particles.

2.3.5 Size Dependence of the Tuning Range of Diffractions.

The range of the diffraction wavelengths that can be tuned by the external magnetic field has been found to relate to the mean size of the Fe_3O_4 CNCs. Figure 2.9 shows the TEM images and reflection spectra of four representative samples with sizes of ≈91±11, 108±23, 130±20, and 180±26 nm as determined by measuring the size of ~200 clusters in TEM images for each sample. There is a consistent correlation between average particle size and the wavelength of the diffraction peaks. Comparatively speaking, smaller CNCs form ordered structures only under stronger magnetic fields with the formed structures preferably diffracting blue light (Figure 2.9A). Larger clusters diffract red light in a relatively weak magnetic field, and the ordered structures become unstable when the magnetic field strength is increased (Figure 2.9D). Medium-size clusters (~100-150 nm) self-assemble into stable ordered structures in both weak and strong magnetic fields, making their diffractions tunable from blue to green, yellow, and red (Figure 2.9B and C). The size-dependent optical property can be attributed to the

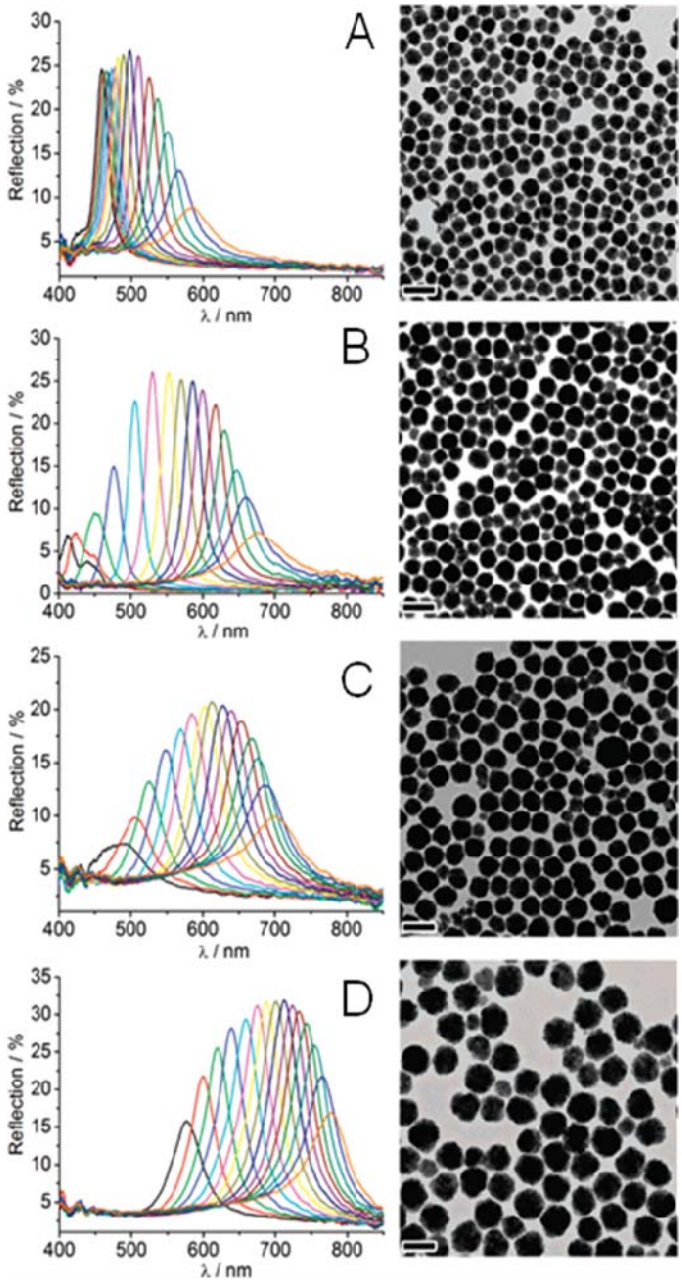

Figure 2.9 Dependence of the tuning range for diffraction on particle size. The average diameter of Fe3O4 CNCs in (a-d) is estimated to be 91, 108, 130, 180 nm, respectively, from TEM images. All scale bars correspond to 200 nm. For each sample, the diffraction peak blue-shifts as the magnet-sample distance decreases from (A) 2.6 to 1.2 cm, (B) 3.2 to 1.8 cm, (C) 3.5 to 2.1 cm, and (D) 3.7 to 2.3 cm.

strong size-dependent magnetic moments of the CNC particles. As reported previously, the saturated magnetic moments of individual particles increases dramatically when the particle size changes from a few nanometers to ~180 nm. When CNCs are small, they need a strong external field and short interparticle distances to induce enough magnetic attractive force for assembly into ordered structures. When CNCs are large, strong attraction can be induced even under relatively weak external fields so that the particles can be easily assembled at relatively large interparticle separations. The high value of magnetic moment of large CNCs also significantly increases the magnetic packing force, which makes the ordered structure unstable in strong external magnetic fields.

Interestingly, the tuning range of the diffraction wavelength can be broadened by mixing CNCs with two different sizes. Although a broad particle size distribution severely deteriorates the optical response of the CNCs, a mixture of two monodisperse colloids with different average particle sizes still displays reasonably strong diffraction. Figure 2.10 shows the reflections of two samples with sizes of~75 and 116 nm and their 1:1 (in mass ratio) mixture in response to external magnetic fields, with the spectra recorded at the same magnet-sample distance coded in the same color. The corresponding TEM images are also included as insets. Since the average sizes of the original samples are close to each other, their mixture displays single diffraction peaks in a magnetic field with fixed strength. The tuning range has been slightly broadened in comparison to those of the original samples. Apparently, ordered structures still form in a solution of CNCs with mixed sizes under external fields. Careful comparison of the spectra for the samples before and after mixing reveals two interesting features that can

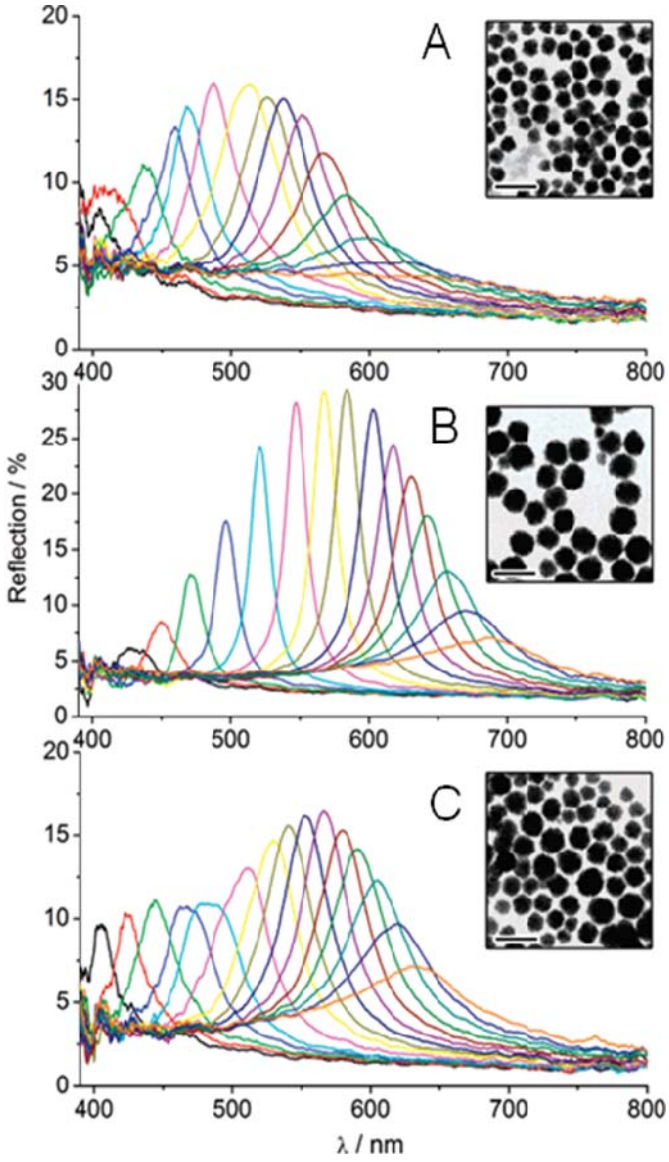

Figure 2.10 Reflection spectra of (A)~75 nm and (B)~116 nm Fe_3O_4 CNCs and (C) their 1:1 (in mass ratio) mixture in response to external magnetic fields. Since (A) and (B) are similar in size, the mixture shows slight broadening of the diffraction tuning range. In all cases, diffraction peaks blue-shift as the magnet-sample distance decreases from 3.3 to 1.9 cm. The scale bars correspond to 200 nm.

help to elucidate the assembled structures in the mixed solutions. First, each diffraction peak of the mixture at a specific field strength is positioned between the peaks of the two original samples. However, the former is not the result of a simple overlay of the latter two, suggesting that the average interparticle distance of the CNCs in the mixture has a value between those in the original samples. Second, the overall diffracted intensity is lower than those of the original samples, especially in the longer wavelength, indicating considerable disruption to long-range order resulting from the mixing of particle populations of two different sizes.

By mixing two samples with a large size difference, we have been able to further increase the tuning range of the diffractions. Different from the previous case, the reflection spectra of the mixture seem to be the simple overlay of those of the two original samples. In a weak magnetic field, the optical response appears to result from the ordering of large particles and the solution displays red diffractions, while in a strong field the diffraction is mainly due to the ordering of small particles and the solution shows blue color. In a magnetic field of intermediate strength, the large and small particles appear to assemble independently so that the reflection spectra are split into two peaks.

2.3.6 The Concentration Effect.

Unlike traditional three-dimensional photonic crystals which are assembled from highly concentrated colloids, the system described in this work displays stronger diffraction at optimally diluted conditions. Figure 2.11 shows the reflection spectra of a sample in five different concentrations by dilution from 33.6 to 2.1 mg/mL. For each

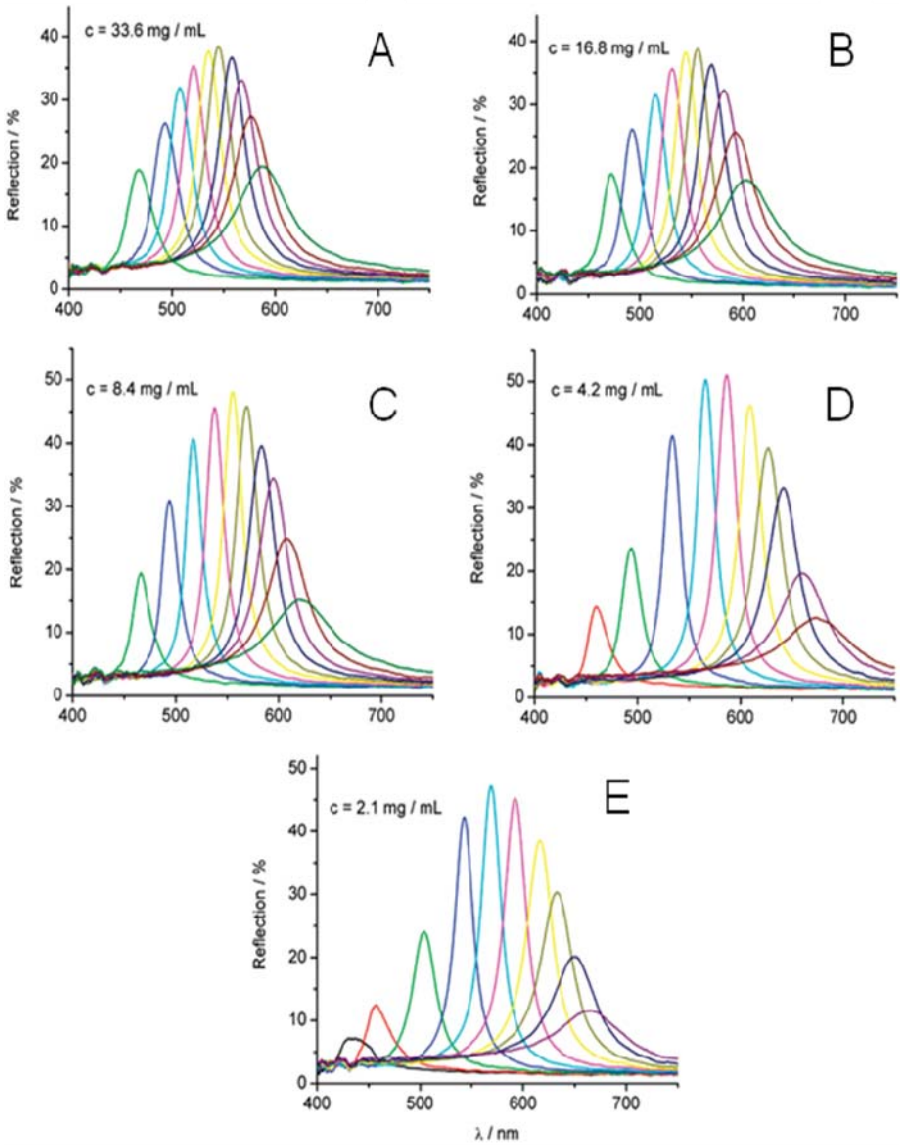

Figure 2.11 Influence of CNC concentration on the diffraction tuning range. Diffraction peaks blue-shift as the magnet-sample distance decreases from (A-C) 3.0 to 2.1 cm, (D) 2.9 to 2.0 cm, and (E) 2.8 to 1.9 cm. Peaks obtained at a specific magnet-sample distance were assigned the same color.

concentration, reflection spectra obtained at the same sample magnet distance were plotted in the same color. Overall, the system shows a trend of red-shifting of the diffraction peaks upon dilution. There are very small changes in the peak positions and widths when the system is diluted from high concentrations (33.6 mg/mL) to the medium value (8.4 mg/mL), suggesting that a high particle concentration does not significantly change the assembly behavior of the CNCs (Figure 2.11A-C). The magnetic fields that are required to initiate the ordering of the CNC particles are also similar in strength for these three concentrations. The intensity of the diffractions, on the other hand, is lower at higher concentrations, probably due to the increased absorption at a higher loading of Fe_3O_4 materials. Further dilution of the system from 8.4 to 4.2 and eventually to 2.1 mg/mL greatly red-shifts the diffraction peaks, while the peak intensities remain almost unchanged. Interestingly, the strengths of the magnetic fields have to be increased to organize the particles in diluted solutions to display strong diffractions. It is therefore believed that the electrostatic repulsive interactions are enhanced upon dilution, probably because such dilution also decreases the concentration of electrolytes. We found that a concentration in the range 4.2-8.4 mg/mL was optimal in terms of diffraction intensity and tuning range. If the solution is diluted to a concentration below 1.0 mg/mL, almost no visible diffraction can be observed.

2.3.7 Fast Response to Modulated Magnetic Fields.

The Fe_3O_4 colloidal solutions possess a fast optical response to the external magnetic field, a feature critical for applications. To characterize the response time, we recorded the change of reflections in the presence of a periodically on-off magnetic field

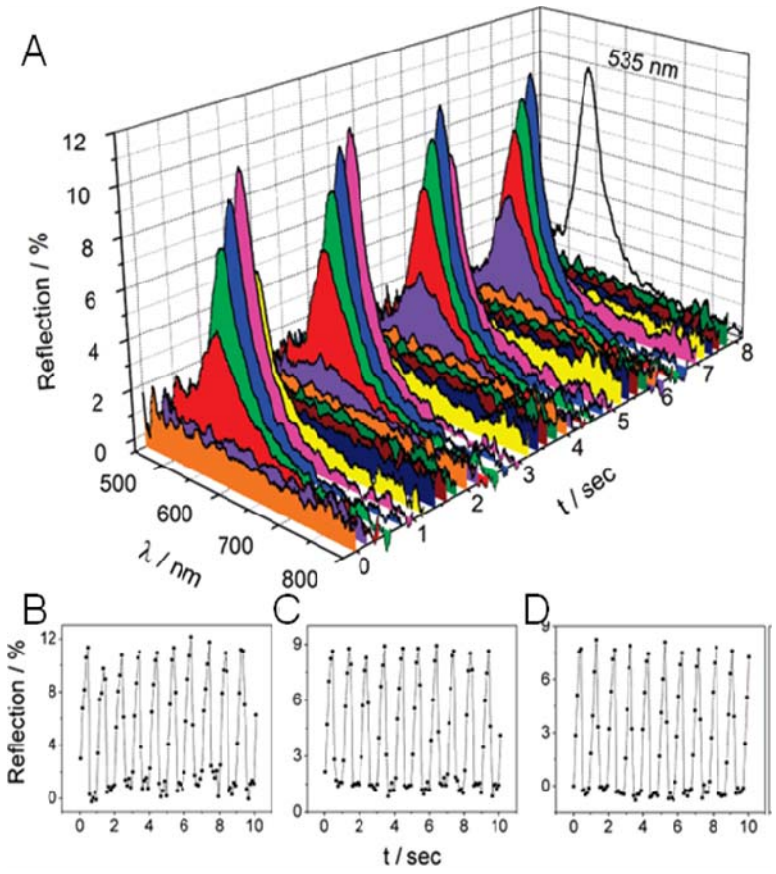

Figure 2.12 (A) Modulated diffractions of a 130 nm CNC solution in a 0.5 Hz periodic magnetic field, with a spectra integration time of 200 ms. (B-D) Variation of the diffraction peak intensity at (B) 470 nm, (C) 535 nm, and (D) 654 nm for 70, 130, and 180 nm colloidal photonic crystals in a 1 Hz periodic magnetic field, with a spectra integration time of 100 ms.

with a controllable switching frequency. Figure 2.12A shows successive reflection spectra recorded for a solution containing 130 nm Fe_3O_4 CNCs in response to a 0.5 Hz periodic magnetic field. The green diffraction at ~535 nm clearly switches on and off with the same frequency as the external field. The reflected intensity continues to increase (albeit at a sharply decreasing rate) through the "on" phase of the cycle; however, no significant sharpening or shift of the diffraction peak is visible during that phase. A reasonable interpretation is that smaller structures with a distribution of interparticle spacings mimicking the equilibrium distribution form quite fast (in a period shorter than the integration time of our spectrometer, 200 ms). On the other hand, the growth, alignment, and merging of these ordered chains into longer ones appears to proceed over a longer time (on the scale of seconds).

Similar modulation can be obtained for 70 and 180 nm Fe_3O_4 CNCs, which periodically diffract blue and red light at~470 and ~654 nm, respectively. Figure 2.12B-D shows the intensity change of the peaks at 470, 535, and 654 nm for the three samples in a faster, 1Hz alternating magnetic field. One can clearly see that the peak intensity increases gradually during the "on" stage of the magnetic field, indicating continuous improvement of the long-range order of the CNCs. The diffraction peak disappears completely within 100-200 ms after the magnetic field is off, which is much faster than the development of perfect translational order under a magnetic field. Carefully comparing the intensity profile of the diffraction peaks of three samples with the same frequency, one can find that the "blue" sample of smaller CNCs with a diffraction peak at

470 nm takes less time than the "red" sample of larger CNCs to reach maximum intensity, probably due to the smaller size and higher mobility.

On the basis of visual observations, we believe the colloidal solution confined in a glass capillary may respond to the external magnetic field at even higher frequencies. However, no such measurements have been attempted at higher switching speed due to the limitation of the integration time of our charge-coupled device (CCD) detectors. The nucleation of an initial region with regular interparticle and interchain distances might be facilitated by the boundary conditions in a confined volume, suggesting the study of ordering kinetics in a range of confined volumes as an interesting area of research. On the other hand, the rapid switching rate of the described systems in response to external magnetic signals implies wide potential use in telecommunication and optoelectronic devices.

2.4 Conclusions

Colloidal photonic crystals with magnetically tunable stop bands covering the entire visible spectrum have been fabricated from superparamagnetic magnetite CNCs. Superparamagnetic colloidal nanocrystal clusters of magnetite with highly charged surfaces have been assembled into ordered structures in solution under external magnetic fields. The ordering of the particles was achieved as the balanced interactions including the electrostatic forces and externally induced magnetic forces. Although the assembled structures are three-dimensional, long range order is only achieved along the direction of the magnetic field with interparticle spacing comparable to the wavelength of visible light. As a result, the colloidal solutions show strongly diffraction in the visible spectrum in the

direction of external magnetic fields. Since the interparticle spacing is determined by the relative strengths of electrostatic repulsions and magnetic attractions, the diffraction peaks can be tuned across the entire visible spectrum by simply changing the strength of the magnetic field. The concentration of stray electrolytes also has a strong effect on the optical response of the solution, as it changes the strength of the interparticle electrostatic repulsion. Other factors including the size, size distribution, and concentration of the colloids have also been examined to optimize the diffraction intensity and tuning range. With further demonstrations of their rapid, reversible, and fully tunable field-responsive photonic properties, it is believed that such field-responsive photonic materials will provide a new platform for the fabrication of novel optical microelectromechanical systems, sensors, and color display units.

2.5 Reference

(1) A. Blanco, E. Chomski, S. Grabtchak, M. Ibisate, S. John, S. W. Leonard, C. Lopez, F. Meseguer, H. Miguez, J. P. Mondia, G. A. Ozin, O. Toader, H. M. van Driel, *Nature*, 2000, **405**,437.
(2) O. D. Velev, A. M. Lenhoff, E. W. Kaler, *Science*, 2000, **287**,2240.
(3) P. Jiang, G. N. Ostojic, R. Narat, D. M. Mittleman, V. L. Colvin, *Adv. Mater.*, 2001, **13**,389.
(4) J. H. Holtz, S. A. Asher, *Nature*, 1997, **389**,829.
(5) Y. Xia, B. Gates, Y. Yin, Y. Lu, *Adv. Mater.*, 2000, **12**,693.
(6) J. R. Lawrence, Y. Ying, P. Jiang, S. H. Foulger, *Adv. Mater.*, 2006, **18**,300.
(7) E. A. Kamenetzky, L. G. Magliocco, H. P. Panzer, *Science*, 1994, **263**,207.
(8) C. Lopez, *Adv. Mater.*, 2003, **15**,1679.
(9) M. Ben-Moshe, V. L. Alexeev, S. A. Asher, *Anal. Chem.*, 2006, **78**,5149.
(10) K. Lee, S. A. Asher, *J. Am. Chem. Soc.*, 2000, **122**,9534.
(11) S. A. Asher, V. L. Alexeev, A. V. Goponenko, A. C. Sharma, I. K. Lednev, C. S. Wilcox, D. N. Finegold, *J. Am. Chem. Soc.*, 2003, **125**,3322.
(12) Y. J. Lee, P. V. Braun, *Adv. Mater.*, 2003, **15**,563.
(13) S. Y. Choi, M. Mamak, G. von Freymann, N. Chopra, G. A. Ozin, *Nano Lett.*, 2006, **6**,2456.
(14) A. C. Sharma, T. Jana, R. Kesavamoorthy, L. J. Shi, M. A. Virji, D. N. Finegold, S. A. Asher, *J. Am. Chem. Soc.*, 2004, **126**,2971.

(15) S.-L. Kuai, G. Bader, P. V. Ashrit, *Appl. Phys. Lett.*, 2005, **86**,221110.
(16) F. Fleischhaker, A. C. Arsenault, V. Kitaev, F. C. Peiris, G. von Freymann, I. Manners, R. Zentel, G. A. Ozin, *J. Am. Chem. Soc.*, 2005, **127**,9318.
(17) Z. Z. Gu, A. Fujishima, O. Sato, *J. Am. Chem. Soc.*, 2000, **122**,12387.
(18) S. Kubo, Z. Z. Gu, K. Takahashi, A. Fujishima, H. Segawa, O. Sato, *J. Am. Chem. Soc.*, 2004, **126**,8314.
(19) H. Fudouzi, Y. Xia, *Langmuir*, 2003, **19**,9653.
(20) C. I. Aguirre, E. Reguera, A. Stein, *Adv. Funct. Mater.*, 2010, **20**,2565.
(21) T. S. Shim, S. H. Kim, J. Y. Sim, J. M. Lim, S. M. Yang, *Adv. Mater.*, 2010, **22**,4494.
(22) E. Yablonovitch, *Nat. Mater.*, 2003, **2**,648.
(23) J. Xia, Y. Ying, S. H. Foulger, *Adv. Mater.*, 2005, **17**,2463.
(24) E. T. Tian, J. X. Wang, Y. M. Zheng, Y. L. Song, L. Jiang, D. B. Zhu, *Journal of Materials Chemistry*, 2008, **18**,1116.
(25) Y. Xia, B. Gates, Z.-Y. Li, *Adv. Mater.*, 2001, **13**,409.
(26) X. Xu, G. Friedman, K. D. Humfeld, S. A. Majetich, S. A. Asher, *Adv. Mater.*, 2001, **13**,1681.
(27) X. Xu, G. Friedman, K. D. Humfeld, S. A. Majetich, S. A. Asher, *Chem. Mater.*, 2002, **14**,1249.
(28) H. Gu, K. Xu, C. Xu, B. Xu, *Chem. Comm.*, 2006,941.
(29) U. Jeong, X. Teng, Y. Wang, H. Yang, Y. Xia, *Adv. Mater.*, 2007, **19**,33.
(30) Y. Saado, M. Golosovsky, D. Davidov, A. Frenkel, *Phys. Rev. B*, 2002, **66**,195108.
(31) I. L. Lyubchanskii, N. N. Dadoenkova, M. I. Lyubchanskii, E. A. Shapovalov, T. Rasing, *J. Phys. D: Appl. Phys.*, 2003, **36**,R277.
(32) B. Gates, Y. Xia, *Adv. Mater.*, 2001, **13**,1605.
(33) A. Petri-Fink, M. Chastellain, L. Juillerat-Jeanneret, A. Ferrari, H. Hofmann, *Biomaterials*, 2005, **26**,2685.
(34) S. Sacanna, A. P. Philipse, *Langmuir*, 2006, **22**,10209.
(35) J. Bibette, *J. Magn. Magn. Mater.*, 1993, **122**,37.
(36) F. Bai, D. Wang, Z. Huo, W. Chen, L. Liu, X. Liang, C. Chen, X. Wang, Q. Peng, Y. Li, *Angewandte Chemie International Edition*, 2007, **46**,6650.
(37) J. Ge, Y. Hu, M. Biasini, W. P. Beyermann, Y. Yin, *Angew. Chem. Int. Ed.*, 2007, **46**,4342.
(38) J. Ge, Y. Hu, Y. Yin, *Angew. Chem. Int. Ed.*, 2007, **46**,7428.
(39) H. Deng, X. L. Li, Q. Peng, X. Wang, J. P. Chen, Y. D. Li, *Angew. Chem. Int. Ed.*, 2005, **44**,2782.
(40) Y. G. Sun, B. Mayers, T. Herricks, Y. N. Xia, *Nano Lett.*, 2003, **3**,955.
(41) J. Ge, Y. Hu, M. Biasini, C. Dong, J. Guo, W. P. Beyermann, Y. Yin, *Chem. Eur. J.*, 2007, **13**,7153.
(42) F. L. Calderon, T. Stora, O. Mondain Monval, P. Poulin, J. Bibette, *Phys. Rev. Lett.*, 1994, **72**,2959.
(43) R. W. Chabay, B. A. Sherwood, *Electric and Magnetic Interactions*, Wiley, New York, **1995**.

(44) Y. Kraftmakher, *Eur.J. Phys.*, 2007, **28**,409.
(45) D. Myers, *Surfaces, Interfaces, and Colloids: Principles and Applications*, 2nd ed., Wiley VCH, New York, **1999**.
(46) B. V. Derjaguin, L. Landau, *Acta Physicochim URSS*, 1941, **14**,633.
(47) E. J. W. Verwey, J. T. G. Overbeek, *Theory of Stability of Lyophobic Colloids*, Elsevier, Amsterdam, **1948**.
(48) J. C. Crocker, D. G. Grier, *Phys. Rev. Lett.*, 1994, **73**,352.

Chapter 3

Magnetically Responsive Photonic Nanochains

3.1 Introduction

Responsive photonic materials are of great interest due to their broad applications relevant to controlling of colors.[1, 2] With the advantages of high efficiency and low production cost, self-assembly of colloidal building blocks into photonic crystal structures has been widely studied especially for those applications that can tolerate defects.[3-5] While many studies have focused on the tuning the refractive index of the components or the periodicity of the ordered structures by incorporating active materials that can respond to the changes in the environment,[6-8] we have recently developed a magnetically tunable photonic crystal structure by assembling uniform superparamagnetic colloidal particles into one-dimensional (1D) chain-like arrays in various liquid media.[9-14] The dynamic ordering of the magnetic colloids with controllable periodicity along the direction of external field renders the system a fast, fully reversible photonic response across the visible-near-infrared spectrum. However, the structure of the dynamic chain remains unclear as only hypothesis has been proposed to explain the corresponding photonic properties. In order to further confirm the proposed structure and obtain more profound understanding on the assembled process, a fixed structure which preserves the original assembled characteristics is preferred.

By taking advantage of the magnetic property of the materials, we have been able to develop an alternative method for fixing the assembled chain by a polymer matrix and

produce tunable photonic materials by magnetically manipulating the orientation of photonic crystal structures.[15] This was achieved by embedding aligned chains of periodically arranged SPM particles in polymer microspheres so that their relative orientation and correspondingly the diffraction property can be tuned by rotating the external magnetic fields. Although this method acts as an indirect method to help proving the chainlike structures from the insect image of smashed microspheres, a more visualizing method is desired to directly show the assembled structure. Optimally, single magnetic chains with fixed ordered structure are the best demonstration and good examples for fundamental study in the assemble process.

In addition, the division of bulk photonic crystals into many small units of tens of micrometers brings the benefits of easy fabrication, actuation and broader applications, as the color of these units can be controlled individually or collectively as needed by using external magnetic fields. Thus, it has been our great interest to extend this principle to the fabrication of magnetically responsive photonic structures with significantly reduced dimensions so that color manipulation with significantly higher resolution can be realized. The ideal case is to fix individual magnetic particle chains whose optical diffraction can be fully controlled through magnetic alignment. In additional to color displays, these optically active magnetic nanochains may find great use in fields such as bio- and chemical sensors and biomedical labeling and imaging.[16-19] Such structure however has been very difficult to achieve by using the emulsion method that was employed for making the magnetochromatic microspheres.

Herein, we present a convenient and flexible approach for the fabrication of individually fixed chains with magnetically responsive photonic property by combining magnetic assembly with sol-gel processes. The process involves initial coating the superparamagnetic Fe_3O_4 colloidal nanocrystal clusters (CNCs) with a thin layer of silica, assembling them into chains by applying magnetic field, and further overcoating the chains with an additional layer of silica to stabilize the chain structure. The key is to induce chaining of magnetic particles by brief exposure to external fields during their silica coating process so that the particles temporary stay connected, allowing additional silica deposition to fix chains into mechanically robust rods or wires. The process is highly controllable: the periodicity can be varied by using Fe_3O_4 CNCs of different sizes; the interparticle spacing can be fine tuned by adjusting the timing of magnetic field exposure; the length of the chains can be controlled by changing the duration of the magnetic field exposure. The resulting photonic chains disperse randomly in solution in the absence of magnetic field, but align themselves and show diffraction color instantly when an external field is applied. As the periodic structure has already been created, only a weak external field (ca. 50 Gauss (G)) is sufficient to fully align the photonic chains. Compared with the magnetically tunable photonic crystals that we developed previously, the fixed photonic nanochains have long-term optical stability, improved tolerance to environmental variances such as ionic strength, and greater convenience for incorporation into many liquid or solid matrices without the need of complicated surface modification procedures.

3.2 Experimental section

3.2.1 Chemicals.

Iron(III) chloride anhydrous ($FeCl_3$, 98%) was purchased from Riedel-de Haën, German. Diethylene glycol (DEG, reagent grade), ethyl alcohol (denatured), hexane (99.9%), and sodium hydroxide (NaOH, 98.8%) were purchased from Fisher Scientific. Ammonium hydroxide solution (28%) was obtained from Fluka. Poly(acrylic acid) (PAA, *M*w = 1800), tetraethylorthosilicate (TEOS, 98%) were purchased from Sigma-Aldrich.

3.2.2 Synthesis of Fe_3O_4@SiO_2 photonic chains.

Superparamagnetic Fe_3O_4 CNCs were synthesized using a high-temperature hydrolysis reaction that we reported previously.[11] In a typical synthesis of photonic chains, 3 mL of aqueous solution of CNCs (ca. 8.6 mg Fe_3O_4/1 mL H_2O) was dispersed in a mixture of ammonium hydroxide (1 mL) and ethanol (20 mL) under sonication. TEOS (170 μL) was quickly injected after the mixture was transferred into a three-neck flask under mechanical stirring at 600 rpm. After 12 min, 2 mL of the mixture was transferred to a glass vial (23 X 85 mm) and placed above a 3" X 1/4" Neodymium disc magnet at a distance of 4 cm for 1 second. After removed from the magnetic field and kept still for another 15 min, the sample was washed with ethanol 3 times and redispersed in ethanol (4 mL).

3.2.3 Characterization.

A Tecnai T12 transmission electron microscope and a Philips FEI XL 30 scanning electron microscope were used to characterize the morphology of the photonic chains. A Zeiss AXIO Imager optical microscope was used to investigate the chain lengths and

observe the "on"/ "off" switch of diffraction from the photonic chains in response to the change in the external magnetic field. The diffraction spectra were measured by an Ocean Optics HR 2000CG-UV-NIR spectrometer coupled with a six-around-one reflection/backscattering probe. The probe was perpendicular to the glass cell. The spectra integration time of collecting the signals was set to be 300 ms.

3.3 Results and Discussion

3.3.1 Synthesis Strategy

Figure 3.1A illustrates the fabrication process for Fe_3O_4@SiO_2 photonic chains. Superparamagnetic Fe_3O_4 CNCs are synthesized using a high-temperature hydrolysis reaction that we reported previously.[11] After cleaning, the aqueous dispersion of Fe_3O_4 particles is mixed sequentially with ammonium hydroxide (NH_4OH) and ethanol. Since the Fe_3O_4 CNCs are covered with a layer of polyacrylate (PAA), they tend to aggregate in ethanol. The aggregates can be temporarily broken up under sonication. Tetraethoxysilane (TEOS) is injected after the dispersion is quickly transferred into a flask under mechanical stirring. Upon hydrolyzation and condensation, a thin layer of silica starts to deposit on the surface of Fe_3O_4 particles, gradually improving their dispersity in ethanol.[20] If the silica layer is allowed to continuously grow beyond 20 nm in thickness, the resulting Fe_3O_4@SiO_2 core-shell particles become highly dispersible in ethanol solutions. However, if a magnetic field is applied during the early stage of silica coating, the magnetic dipole-dipole interaction brings the particles together to form 1D chains. Due to their low dispersibility, the particles tend to remain in the linear chain

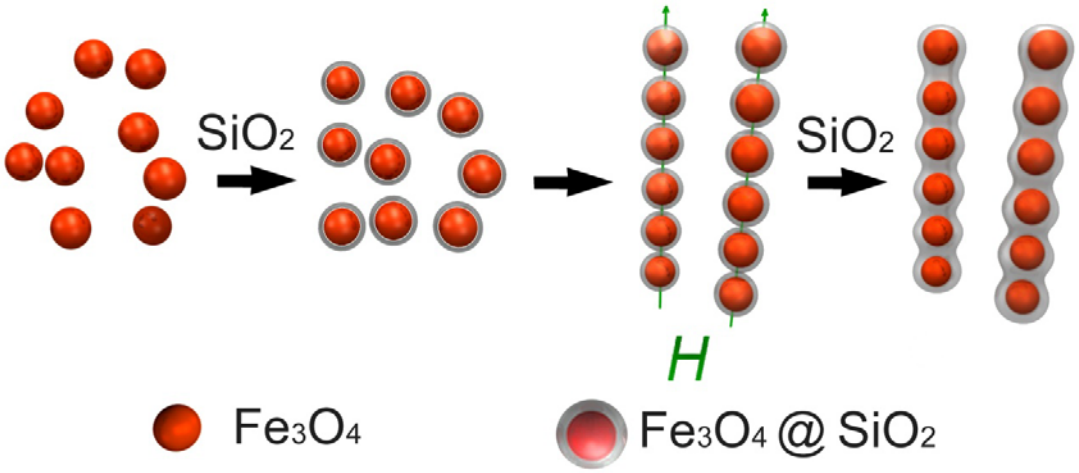

Figure 3.1 Schematic illustration of the fabrication process of the fixed 1D nanochains containing periodically arranged Fe_3O_4 particles. The key is to induce chaining of the uniform magnetic particles by a brief magnetic exposure during their silica coating process and then allow additional silica deposition to further stabilize the chain structures.

structure even after the external field is removed. We believe the growing silica surface may also benefit the connection between neighboring particles through the condensation reaction of surface silanol groups.[21] Continued deposition of silica covers the entire surface of each chain, producing peapod-like structures with further increased mechanical stability. The final products are 1D chains containing periodically arranged uniform Fe_3O_4 CNCs which can effectively diffract visible light.

3.3.2 Effect of External Magnetic Field Strength

The strength of magnetic field is an important parameter for the successful fabrication of photonic nanochains. The magnetic field should be strong enough to induce chaining of magnetic particles and overcome the electrostatic force to ensure close contact of neighboring particles before additional silica coating. As reported previously, the required field strength decreases with the increase in the size of magnetic CNCs.[10] For medium size (~160 nm) particles, field strength of 570 G is used. If the external magnetic field strength is too strong (> 800 G), the magnetic particles will aggregate immediately into large objects without a chance of retaining the chain structure. In addition, a uniform magnetic field is required for producing photonic chains with uniform lengths. This has been achieved by simply using the central portion of a large diameter disk magnet, although further improved field uniformity might be possible with specially designed electromagnets.

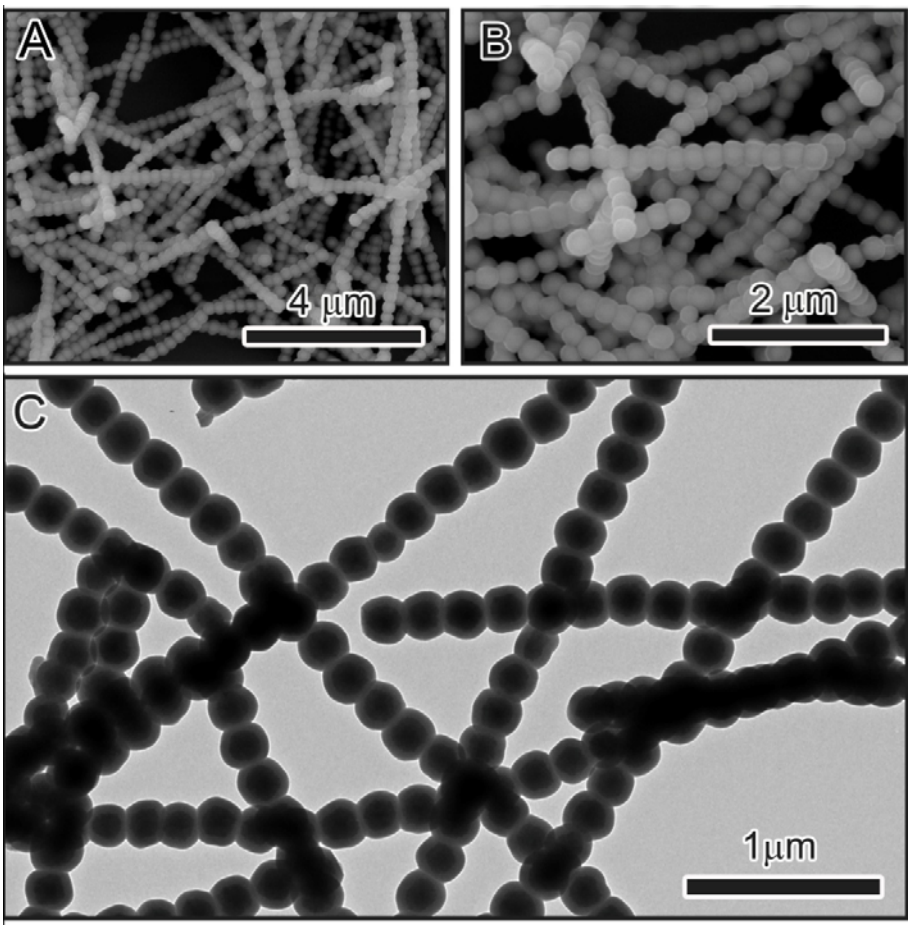

Figure 3.2 (A, B) SEM and (C) TEM images of typical photonic nanochains. The particles in chains are permanently fixed by silica coating so that they remain stable when dispersed in solution or dried on solid substrates.

The chain structure has been characterized by using both scanning and transmission electron microscopy. As shown in Figure 3.2A and B, the product deposited on a silicon substrate clearly shows 1D chain structures, which appear in the form of many linearly connected spheres. The core-shell structure can be better appreciated in the TEM image in Figure 3.2C. The periodically arranged Fe_3O_4 cores and the smooth silica coating can be identified by the contrast between the core and the shell. Note that the magnetic cores are not in direct contact with each other, confirming the initial silica deposition before the chain formation.

The photonic chains can diffract visible light and display brilliant colors owing to the periodic arrangement of the Fe_3O_4 particles. In the absence of external magnetic fields, the chains are randomly oriented so that their bulk solution only shows the native brown color of iron oxide. When an external field is applied, all the chains are aligned along the field direction so that the dispersion shows distinctive colors. We used optical microscope operated in the dark-field to clearly observe the magnetic alignment of the chains and the corresponding photonic response. As shown in Figure 3.3, without magnetic field the chains are randomly dispersed in solution so that no uniform colors can be observed. The slightly colored background is due to the automatic color adjustment of the digital camera when a few vertically oriented chains diffract light. When a vertical magnetic field is applied, all the chains align themselves along the field direction and appear as brightly colored dots to the viewers. All the photonic chains within one sample show a single color because the particles arrange in the same periodicity.

Similar to the magnetic particle arrays that we reported previously, the diffraction wavelength of the photonic chains can be controlled through the periodicity of particle arrays. A convenient way to change the periodicity is to use Fe_3O_4 CNCs of different sizes. As shown in Figure 3.3, photonic chains assembled from large CNCs (~ 182 nm in diameter) diffract red light, while those from medium-size particles (~ 160 nm) diffract green light and those from small CNCs (~ 113 nm) preferably diffract blue light. As we reported previously, uniform CNCs can be produced with average diameters ranging from ~30 to 200 nm,[11] so it should be possible to produce photonic chains with diffraction wavelength across a wide range of spectrum from near UV to near IR.

3.3.3 Effect of Magnetic Field Exposure Timing

The timing of magnetic field exposure is critically important to the success of the chain fixing. It has to be performed when the surface of F_3O_4 has been covered with a thin silica layer, which is typically ~ 5 min after the addition of TEOS. Exposing the dispersion to magnetic field too early will result in large irregular aggregates because of the low dispersity of the particles in solution. On the other hand, exposure to magnetic field has to be done before the particles gain high dispersity in solution, which typically occurs when the thickness of silica layer is above 20 nm. Otherwise, the temporarily formed particle chains by brief magnetic exposure cannot be maintained during the subsequent additional silica coating. Interestingly, controlling the timing of magnetic exposure also allows fine tuning the interparticle spacing within photonic chains. Because silica deposition is a slow and continuous process, the thickness of initial silica

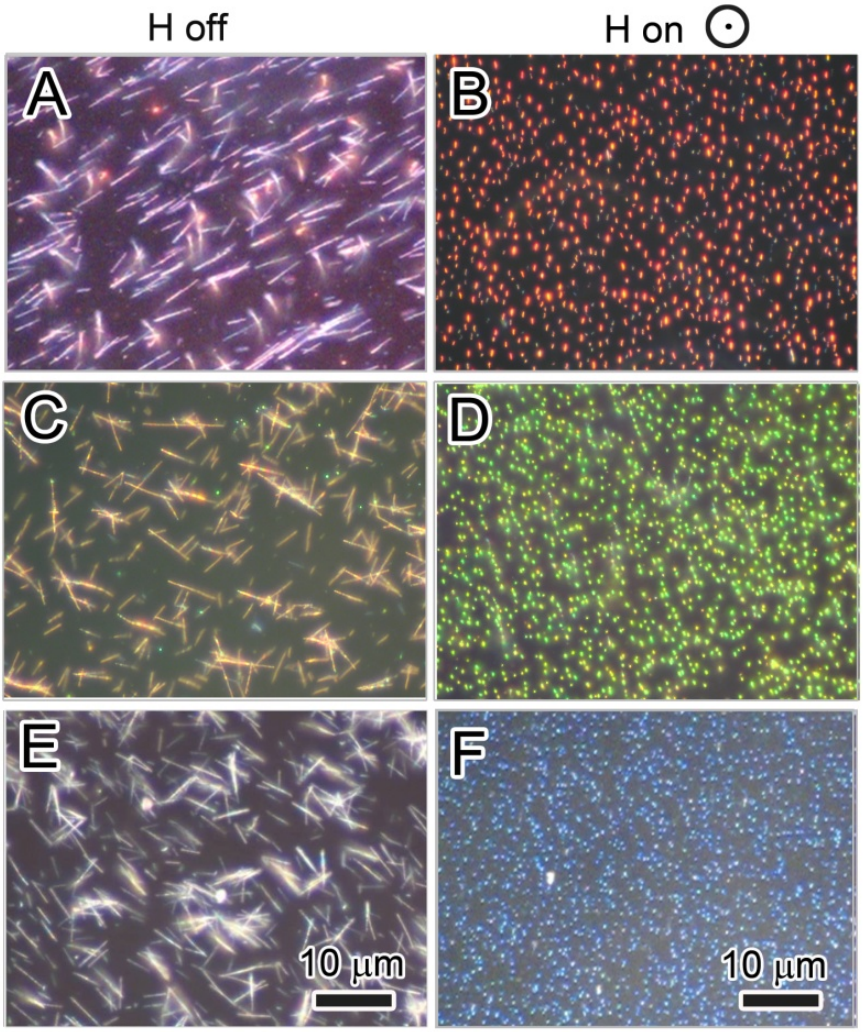

Figure 3.3 Dark-field optical microscopy images of magnetic photonic chains with different diffraction colors switched between "off" (A, C, E, without magnetic field) and "on" (B, D, F, with vertical magnetic field) states. These photonic chains diffract at different wavelengths because they were prepared using Fe_3O_4 CNCs of different average sizes: (A, B) 182 nm; (C, D) 160 nm; (E, F) 113 nm. All images are at the same scale.

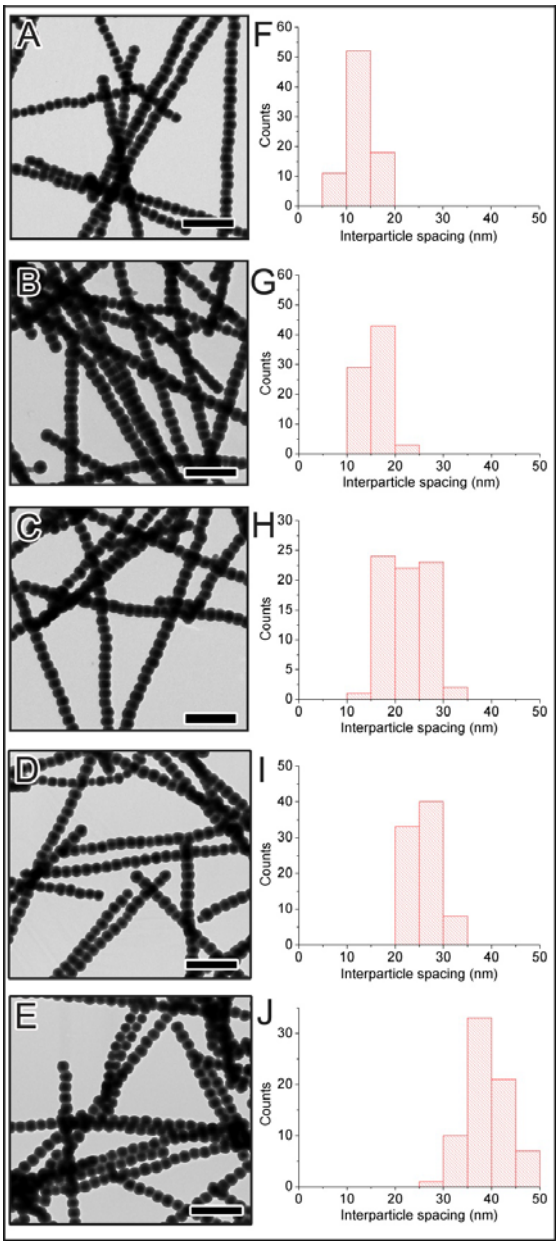

Figure 3.4 Representative TEM images and corresponding interparticle spacing distributions of photonic chains prepared by changing the timing of magnetic exposure during silica coating. The duration of magnetic exposure is 1 s. All scale bars are 1 μm.

layer varies when the magnetic field is applied at different times (Figure 3.4). If the magnetic field is applied at a later stage, a relatively thicker silica layer will be deposited, resulting in a larger interparticle spacing and subsequently diffraction at longer wavelength. Figure 3.5A shows TEM images of photonic chains produced from CNCs with a diameter of ~160 nm by applying external magnetic fields at different times. The interparticle separation gradually increases when the timing of magnetic exposure changes from 6 to 8, 10, 11 and 16 min after injecting TEOS. Figure 3.5B and C summarize the interparticle spacing and correspondingly the diffraction wavelength of these five samples. The application of a magnetic field at an early stage (6 min) results in a thin layer of silica between neighboring particles (~15 nm) and thereby a diffraction with relative short wavelength (~517 nm). When the magnetic field is applied at a later stage (16 min), the interparticle spacing increases to ~39 nm and the diffraction red-shifts to ~593 nm. According to Bragg's equation, the change in diffraction wavelength ($\Delta\lambda$) should be proportional to the interparticle spacing variation (ΔD): $\Delta\lambda=2n_{SiO2}\Delta D$. This is verified by plotting $\Delta\lambda$ against ΔD using the experimental data (Figure 3.5D inset). The refractive index of the silica calculated from the slope of the linear fit of the plot is 1.43, which is in good accordance with the literature reported value.[22] Because the chain structure cannot be retained when the initial silica coating is beyond 20 nm in thickness, the silica layer between neighboring CNCs can only be tuned within the limit of ~10-40 nm with the corresponding diffraction peak shift of ~80 nm.

3.3.4 Nanochains' Length Control

The length of the chains can be controlled by the duration of applied magnetic field.

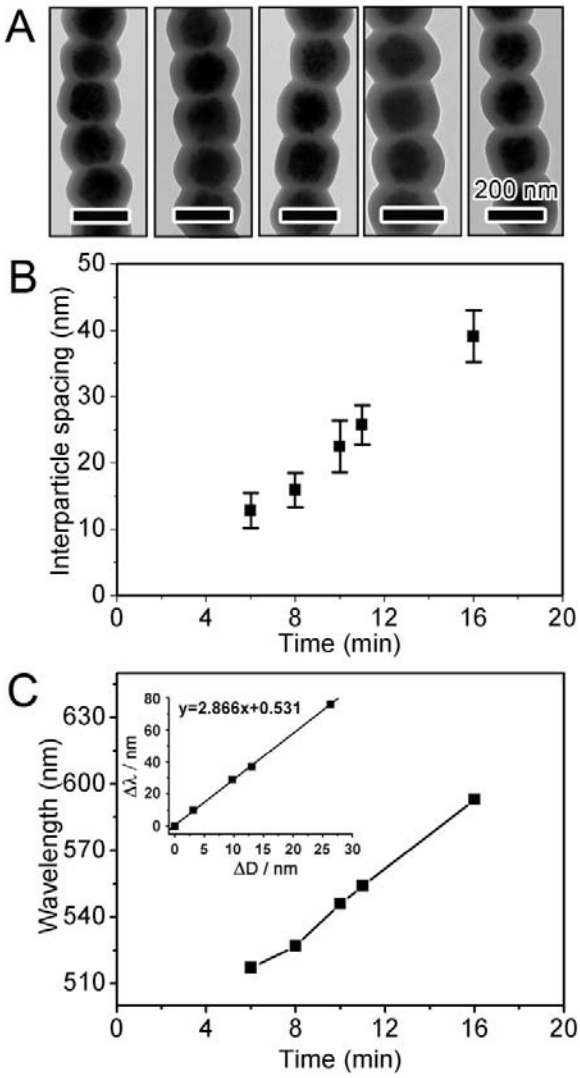

Figure3.5 A) Representative TEM images of photonic chains with different interparticle spacing controlled by applying magnetic fields at different times after injecting TEOS (left to right): 6 min; 8 min; 10 min; 11 min; 16 min. All scale bars correspond to 200 nm. B) The dependence of interparticle spacing on the timing of magnetic exposure. C) The dependence of diffraction wavelength of the photonic chains on the timing of magnetic exposure. The inset plots the shift in diffraction wavelength against the change in interparticle spacing.

As shown in Figure 3.6, the chain length can be controlled over a range of two to tens of micrometers by adjusting the magnetic field duration from ~ 0.5 second to ~ 4 seconds. Upon a very brief exposure (0.5 s) to external field, the Fe_3O_4 CNCs only assemble locally to form short chains of two micrometers (Figure 3.6A). Increasing the field duration allows more extensive particle assembly and chain recombination, producing longer chains with lengths of several tens of micrometers (Figure 3.6B-D). Retaining the dispersion in the magnetic field for even longer time leads to random aggregation of chains. In addition, the thickness of outer silica coating can be controlled by using different amount of TEOS precursor, as demonstrated in Figure 3.7. The thickness control provides opportunity to tune the mechanic strength of the generated magnetic chains.

3.3.5 Magnetic Response of Photonic Nanochains

Since photonic chains contain many magnetic particles, their response to external magnetic field is very sensitive. We have observed a measurable reflection with intensity of 4.5% due to partial chain alignment upon the application of a low magnetic field of only ~ 4 G, while in our previously reported unfixed system a minimum of 50 G is typically required for observable diffraction because magnetic particles need to be assembled from dispersed form into periodic arrays first. In the current system, a magnetic field of 50 G is sufficient to align all the photonic chains along the field direction, producing diffraction with a maximum intensity. As shown in figure 3.8A, the diffraction peak position will keep the same (ca. 526 nm) as the periodicity in the nano flashlights is fixed. The intensity of the diffraction peak will first increase steadily with

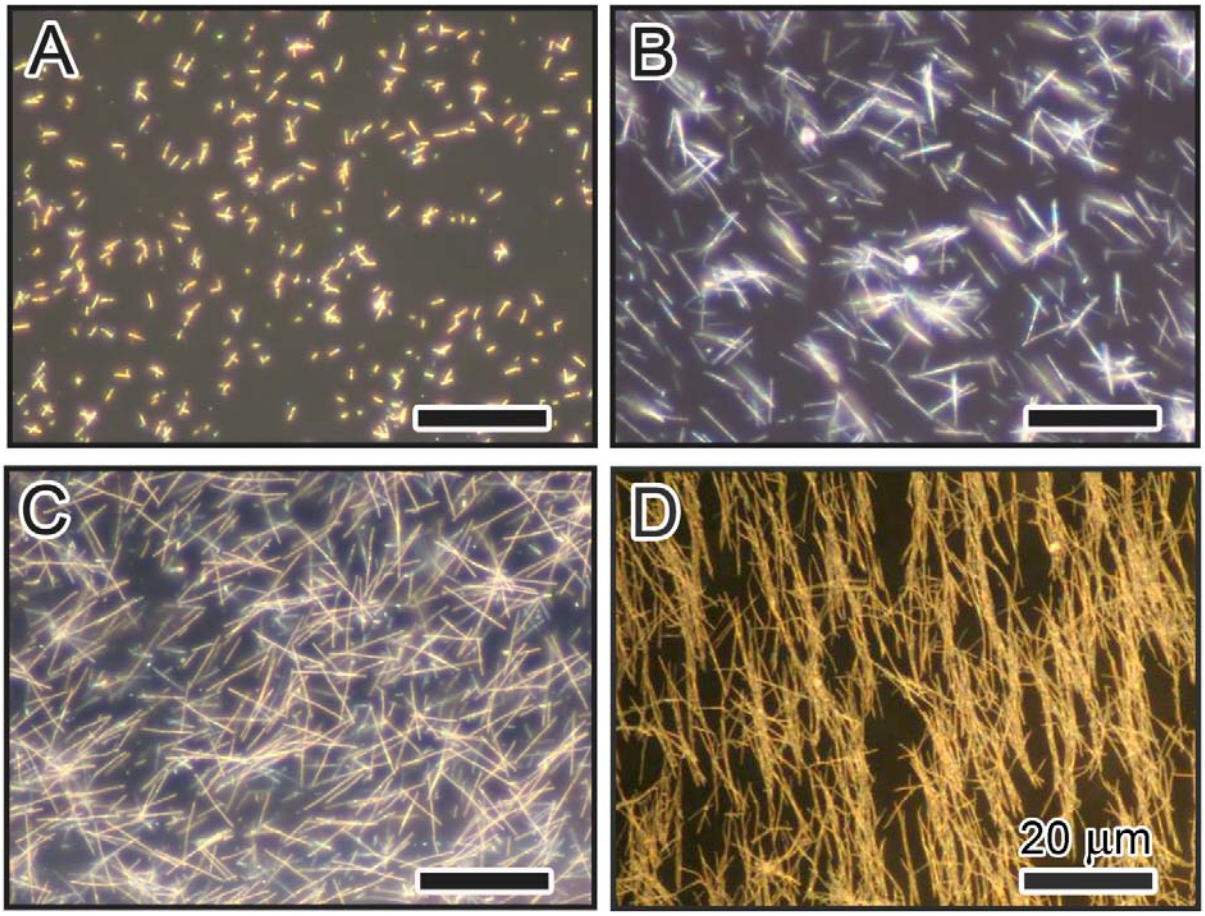

Figure 3.6 Dark-field optical microscopy images of photonic chains with different lengths obtained by applying magnetic field for different duration: A) 0.5 s; B) 1 s; C) 2 s; D) 4s. The field strength of magnetic exposure is estimated at ~ 570 G and field gradient ~ 197 G/cm. All images are at the same scale.

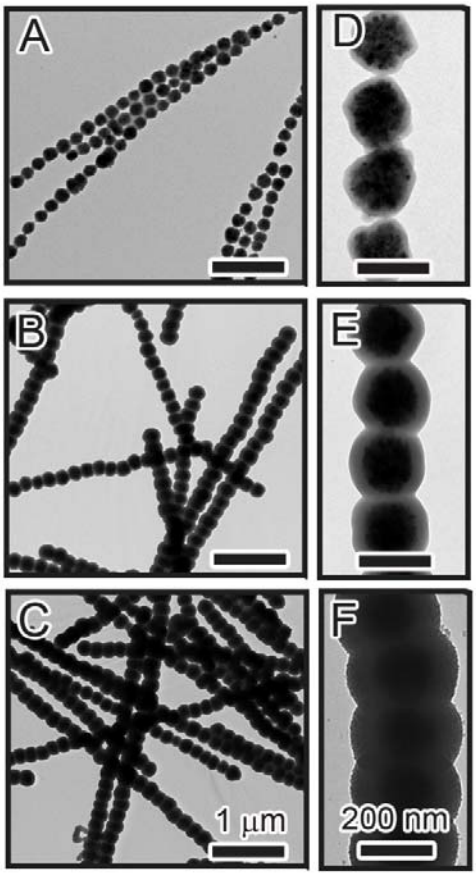

Figure 3.7 TEM images of photonic chains with silica coating of different thicknesses controlled by using different amounts of TEOS precursor: A) 100 μL; B) 140 μL; C) 180 μL; D-F) Corresponding TEM images at a higher magnification.

the enhancement of the magnetic field when the magnet moves toward the sample from 170 mm to 70 mm and then decrease with further increased magnetic field from 70 mm to 0 mm. A lower intensity in a relatively weak magnetic field results from the lack of energy to overcome the thermo energy for Brownian movement. As the switching of the diffraction only involves chain rotation, it could be accomplished rapidly and reversibly in a sufficiently strong magnetic field (> 50 G), as can be appreciated in the video shown in the Supporting Information. We have been able to observe switching of the photonic chain between diffraction "on" and "off" stages at a frequency of 2 Hz. Another good feature of the current system is the optical stability. In the previous reported case where the magnetic particle arrays are not fixed, they can gradually aggregate and reassemble into large objects when exposed to a magnetic field for long time (> 10 min), leading to a decrease in diffraction intensity. In this system, the photonic chains act as rigid magnetic rods which remain separated from each other in magnetic fields due to the magnetically induced repulsive force in the perpendicular direction of the field. We have observed a stable diffraction (in both intensity and wavelength) over a period over 4 hours for photonic chains aligned in a magnetic field of 50 G (Figure 3.8B).

3.4 Conclusion

In summary, we have developed a simple but effective process for the fabrication of magnetically responsive photonic nanochains, each of which is composed of an array of magnetic Fe_3O_4 particles fixed within a silica shell. The fixed structure further confirms the proposed consumption of the single particle chain. These photonic chains can be aligned in magnetic fields and diffract visible light. The key of the fabrication process is

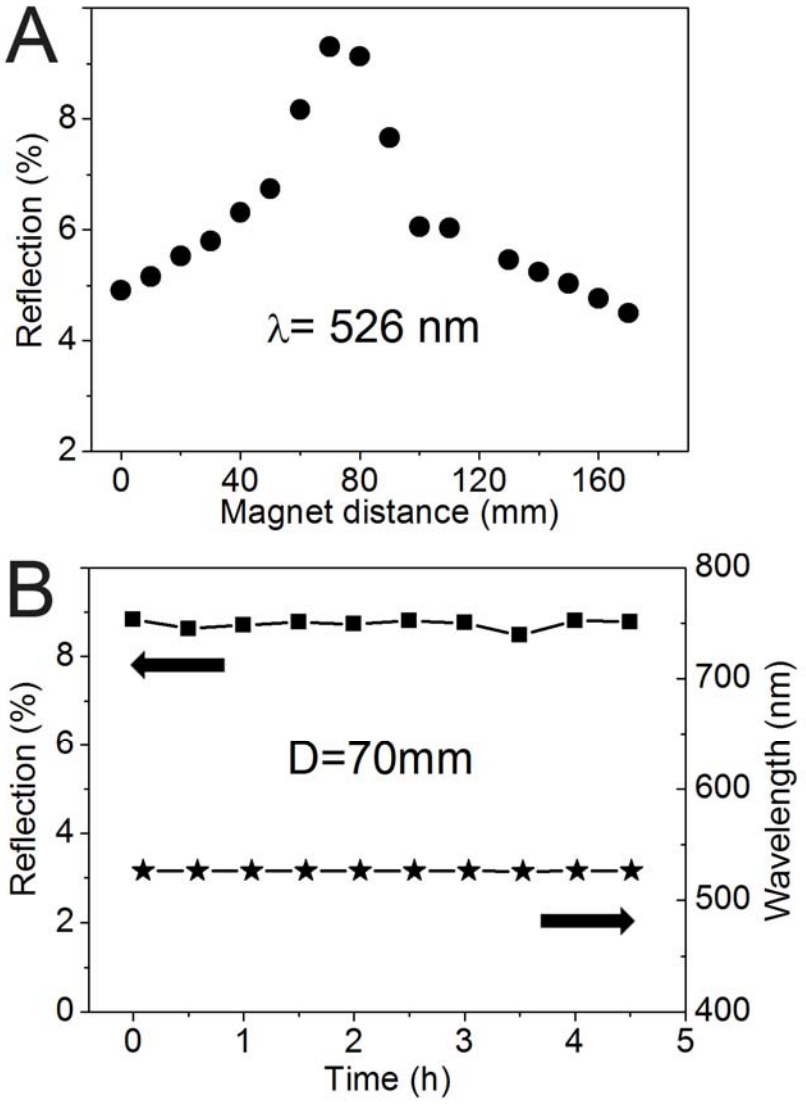

Figure 3.8 A) Plot of the diffraction peak intensities in response to external magnetic fields: the magnet-sample distance decreases from 170 to 0 mm with 10 mm in each step. Corresponding nano flashlights are prepared with 150 nm Fe_3O_4 CNCs. B) Plots of reflection intensities by the nano flashlights in a magnetic field with the magnet-sample distance of 70mm over time (Top plot); corresponding diffraction wavelength over time (Bottom plot).

to induce chaining of the uniform magnetic particles during their silica coating process and then allow additional silica deposition to wrap entire chains into mechanically robust rods/wires. The diffraction wavelength of these photonic chains can be tailored across the visible spectrum by using magnetic particles of different sizes. We also demonstrate that by controlling the timing of magnetic exposure, the separation between neighboring Fe_3O_4 particles can be tuned, yielding a diffraction peak shift up to ~80 nm. The chain length can also be conveniently controlled from two to tens of micrometers by adjusting the duration of applied magnetic field. The convenient control over the chain structure, fast on/off switching of the diffraction state in response to external fields, tolerance to environmental variances, and excellent mechanical and optical stability make the current system promising for many potential applications such as bio- and chemical sensors, labeling, and energy efficient color displays.

3.5 References

(1) J. D. Joannopoulos, R. D. Meade, J. N. Winn, *Photonic Crystals*, Princeton University Press, Princeton, **1995**.
(2) D. J. Norris, *Nat. Mater.*, 2007, **6**,177.
(3) F. Fleischhaker, A. C. Arsenault, Z. Wang, V. Kitaev, F. C. Peiris, G. von Freymann, I. Manners, R. Zentel, G. A. Ozin, *Adv. Mater.*, 2005, **17**,2455.
(4) Z. Z. Gu, A. Fujishima, O. Sato, *J. Am. Chem. Soc.*, 2000, **122**,12387.
(5) O. D. Velev, A. M. Lenhoff, E. W. Kaler, *Science*, 2000, **287**,2240.
(6) R. A. Barry, P. Wiltzius, *Langmuir*, 2006, **22**,1369.
(7) F. Fleischhaker, A. C. Arsenault, V. Kitaev, F. C. Peiris, G. von Freymann, I. Manners, R. Zentel, G. A. Ozin, *J. Am. Chem. Soc.*, 2005, **127**,9318.
(8) S. A. Asher, V. L. Alexeev, A. V. Goponenko, A. C. Sharma, I. K. Lednev, C. S. Wilcox, D. N. Finegold, *J. Am. Chem. Soc.*, 2003, **125**,3322.
(9) J. Ge, Y. Yin, *J. Mater. Chem.*, 2008, **18**,5041.
(10) J. Ge, Y. Hu, T. Zhang, T. Huynh, Y. Yin, *Langmuir*, 2008, **24**,3671.
(11) J. Ge, Y. Hu, M. Biasini, W. P. Beyermann, Y. Yin, *Angew. Chem. Int. Ed.*, 2007, **46**,4342.
(12) J. Ge, Y. Hu, Y. Yin, *Angew. Chem. Int. Ed.*, 2007, **46**,7428.
(13) J. Ge, Y. Yin, *Angew. Chem. Int. Ed.*, 2010,in press (invited review article).

(14) J. Ge, S. Kwon, Y. Yin, *J. Mater. Chem.*, 2010, **20**,5777.
(15) J. Ge, H. Lee, L. He, J. Kim, Z. Lu, H. Kim, J. Goebl, S. Kwon, Y. Yin, *J. Am. Chem. Soc.*, 2009, **131**,15687.
(16) A.-H. Lu, E. L. Salabas, F. Schüth, *Angew. Chem. Int. Ed.*, 2007, **46**,1222.
(17) M. Ye, Q. Zhang, Y. Hu, J. Ge, Z. Lu, L. He, Z. Chen, Y. Yin, *Chem. Eur. J.*, 2010, **16**,6243.
(18) R. Weissleder, H. C. Cheng, A. Bogdanova, A. Bogdanov, *J. Magn. Reson. Imaging* 1997, **7**,258.
(19) C. E. Reese, S. A. Asher, *Analytical Chemistry*, 2003, **75**,3915.
(20) J. Ge, Y. Yin, *Adv. Mater.*, 2008, **20**,3485.
(21) J. Z. Wang, A. Sugawara, A. Shimojima, T. Okubo, *Langmuir*, 2010, **26**,18491.
(22) A. Vincent, S. Babu, E. Brinley, A. Karakoti, S. Deshpande, S. Seal, *J. Phys. Chem. C*, 2007, **111**,8291.

Chapter 4

Control over the Permeation of Silica Nanoshells by Water-Based Etching

4.1 Introduction

We have made a remarkable progress in fabricating magnetic-responsive photonic crystal structures through a one-dimensional assembly of SPM iron oxide (Fe_3O_4) nanocrystal clusters (CNCs) in the presence of an external magnetic field.[1-5] The magnetically responsive photonic crystals exhibit effective control over photonic properties of the assembled structures with improved spectral tunability and response rate by using external magnetic fields. However, the stability of the previous system in long term has been troublesome in the practical application because the assembled structures and correspondingly the photonic properties can change as the repulsive forces vary over time by the gradual detachment of polyelectrolyte molecules from the surface.[2]

To stabilized the polyelectrolyte and achieve high stability of our photonic crystals, a thin porous protecting layer coated the charged Fe_3O_4 particles can fulfill this purpose. The porous can prevent the polyelectrolyte from detaching from the particles and at the same time allow the polyelectrolyte to ionize and produce strong electrostatic interactions among particles. Silica is chosen as the protecting layer due to its convenient sol-gel based coating procedure, low processing temperature, and the well-developed silylation chemistry for further surface functionalization.[6-12] However, it remains a great challenge to achieve control over the pore size and at the same time prevent the isolation of pores from each other within a thin silica layer.[13-15] Though silica shell with

mesoporous channel pores can be formed by self-assembly of block copolymers during the coating process, the complexity of the self-assembly process and the limited variety of block-copolymer templates make it inconvenient to continuously tune the pore size in a relatively wide range.[16, 17] In addition, the defect-rejecting nature of the self-assembly process makes encapsulation of nanoparticles with mesoporous shells difficult to achieve. In the very few cases where porous coating has been successfully realized, the orientations of the pore channels were often found parallel to the core surface, making mass transfer through the channels to the core still difficult.[18] Also, the "surface-protected etching" approach that we developed for convenient conversion of dense silica[15, 19] and titania colloids[20] into mesoporous structures with controllable porosities has been troublesome to be applied to create mesopores in very thin silica shells.[21, 22]

Therefore, a milder etchant which can dissolve colloidal silica in a more controllable manner is required. It is known that silica colloids prepared by a sol-gel process usually involves incomplete hydrolysis and polycondensation of a precursor such as tetraethyl orthosilicate (TEOS), which lead to the formation of amorphous structures because the interconnection of Si-O-Si bonds is highly disordered and discontinuous.[23] These colloidal silica particles, when dispersed as a diluted solution in water, can be re-dissolved in the form of monomeric form $Si(OH)_4$ until the solubility-equilibrium can be established.[12, 24] Due to the highly disordered structure, amorphous silica appears to be more soluble than crystalline silica (quartz), showing a solubility that significantly increases with temperature.[25, 26]

On the basis of these prior studies, we demonstrate in this chapter that water can be used as a mild etchant for producing mesoporous and hollow structures from both pure colloidal silica particles and various silica-coated nanostructures with diameters ranging from several hundred nanometers to tens of nanometers. The etching can be easily performed by heating the dispersion containing silica colloids in water at 95 ^{o}C at normal pressure for a few hours with or without the presence of surface protecting ligands such as PVP. This process is simple, effective, scalable, and able to produce monodisperse porous or hollow samples.

4.2 Experimental Section

4.2.1 Materials

Ethanol (denatured), isopropanol, ammonium hydroxide aqueous solution (28%), and potassium carbonate were purchased from Fisher Scientific. Ethylene glycol (EG, 99+%) was obtained from Acros Organics. PVP (M_w = ~10,000) was obtained from Fluka. Silver nitrate, chloroauric acid, sodium borohydride, PVP (M_w = ~50,000), 3-Bromo-1-propanol (97%) and TEOS (98%) were obtained from Sigma-Aldrich. Deionized (DI) water was used throughout all the experiments. All chemicals were used as received without further purification.

4.2.2 Synthesis

Synthesis of porous silica spheres. Solid silica spheres ~360 nm in diameter were prepared using a sol-gel procedure originally described by Stöber *et al*.[36] A mixture of TEOS (4.5 mL) and ethanol (45.5 mL) was added into a mixture of water (24.75 mL), NH_3•H_2O (9.0 mL) and ethanol (16.25 mL) at room temperature under magnetic stirring.

After reacting for 1 h, solid silica spheres were collected by centrifugation and cleaned with ethanol and water three times, respectively. The silica spheres were then re-dispersed in 30 mL water. Silica spheres with different porosities were prepared by simply heating the dispersion of solid silica spheres in water at 95 ^{o}C for various amounts of time. Aliquots (0.5 mL) were extracted after different reaction periods and cleaned several times with water and ethanol, and finally dispersed in ethanol.

Synthesis of Ag@SiO$_2$ core-shell colloids. Ag nanocrystals (NCs) ~20 nm in diameter were prepared by reducing $AgNO_3$ (0.1 g) with EG (3 mL) at 120 ^{o}C in the presence of PVP (5.0 g, M_w = 10,000) in a one-pot polyol synthesis process. The as-synthesized Ag NCs were collected after 1 h and cleaned with ethanol once. Ag@SiO_2 core-shell colloids were then prepared through a modified Stöber process. Typically, a solution of NH_3•H_2O (4 mL) was injected into the ethanol solution containing Ag NCs (140 mL) under vigorous stirring. After ~30 s, TEOS (0.75 mL) was added. Another 0.75 mL TEOS was added after 30 min. The dispersion was stirred for additional 30 min, and then the resulting colloids with ~25 nm thick silica shells were collected by centrifugation and washed three times with ethanol and water, respectively, to remove excess NH_3•H_2O.

Synthesis of Ag@SiO$_2$ colloids with porous SiO$_2$ shells. In a typical synthesis, the as-obtained Ag@SiO_2 core-shell colloids were heated in water (30 mL) at 95 ^{o}C for 2 h in the presence of PVP (0.4 g, M_w = ~ 10,000). Aliquots (0.5 mL) were extracted at different reaction times, cleaned several times with water and ethanol, and were finally dispersed in ethanol.

Etching Ag core. The solution containing $Ag@SiO_2$ colloids with porous SiO_2 shells (25 μL) was added to a quartz cuvette together with a mixture of isopropanol (2 mL) and 3-bromo-1-propanol (200 μL). UV-Vis absorption spectra were recorded at regular intervals to monitor the etching progress of the Ag core.

Synthesis of $Au@SiO_2$ core-shell colloids. Au NCs were prepared by reducing $HAuCl_4$ with $NaBH_4$. $HAuCl_4$ aqueous solution (4%, 375 μL) was mixed with K_2CO_3 (500 μL, 0.2 M) aqueous solution and water (100 mL) in a round-bottom flask cooled with an ice-water bath. Then a $NaBH_4$ aqueous solution (5 mL, 0.5 mg/mL) was added into the mixture under rapid stirring. Au NCs with diameter of ~5 nm were obtained after stirring for 5 min. $Au@SiO_2$ core-shell colloids were then prepared through a modified Stöber process. The surface of Au NCs was first modified with PVP by refluxing as-prepared Au NCs solution (10 mL) in the presence of PVP (0.2 g) for 6 h. Then PVP modified Au NCs solution (4 mL) was mixed with ethanol (40 mL). Later, $NH_3•H_2O$ (0.8 mL) was injected into the mixture under vigorous stirring and then TEOS (0.75 mL) was added after 30 s. The resulting $Au@SiO_2$ core-shell colloids were collected after 30 min and washed three times with ethanol and water, respectively.

Synthesis of $Au@SiO_2$ yolk-shell colloids. The as-obtained $Au@SiO_2$ colloids and PVP (0.4 g, M_w = ~ 50,000) were added into water (30 mL) and the mixture was heated at 95 ^oC for 2 h. Aliquots (0.5 mL) were extracted at different reaction times, cleaned several times by centrifugation and water redispersion, and finally dispersed in ethanol.

4.2.3 Characterization

The morphology of the obtained products was characterized using a Tecnai T12 transmission electron microscope (TEM). The TEM samples were prepared by transferring one drop of sample dispersion in ethanol onto a carbon-coated copper grid and then drying in air. The UV-Vis spectra measured by a probe-type Ocean Optics HR2000CG-UV-Vis spectrophotometer were used to monitor the etching process of the pure silica and composite silica samples. The integration time was 300 ms.

4.3 Results and Discussion

4.3.1 Porous Silica Nanospheres by Water Based Etching

The heat treatment of colloidal silica in water at around 95 ^{o}C was accompanied by gradual decrease in the turbidity of the solution, which can be clearly monitored using UV-Vis spectroscopy. The change in turbidity was more apparent after the particles being transferred into ethanol. As shown in Figure 4.1A, the transmittance of the SiO_2 colloids solution in ethanol at 400 nm increased from 0% to 95% with a nonlinear dependence on the reaction time over a period of 8 h. No significant change in transmittance can be observed with prolonged reaction time. The decrease in the transmittance suggests the removal of the solid materials from the SiO_2 colloids, which leads to the reduction of their effective refractive index. When dispersed in ethanol which has a slightly higher refractive index (1.361) than water, the etched colloidal SiO_2 spheres become almost transparent to the naked eye due to the close refractive index matching between the particles and the solvent. Figure4.1B and C compare the appearance of the unetched and etched samples when they are dispersed in ethanol. Because the dependence of transmittance on etching time was very consistent for

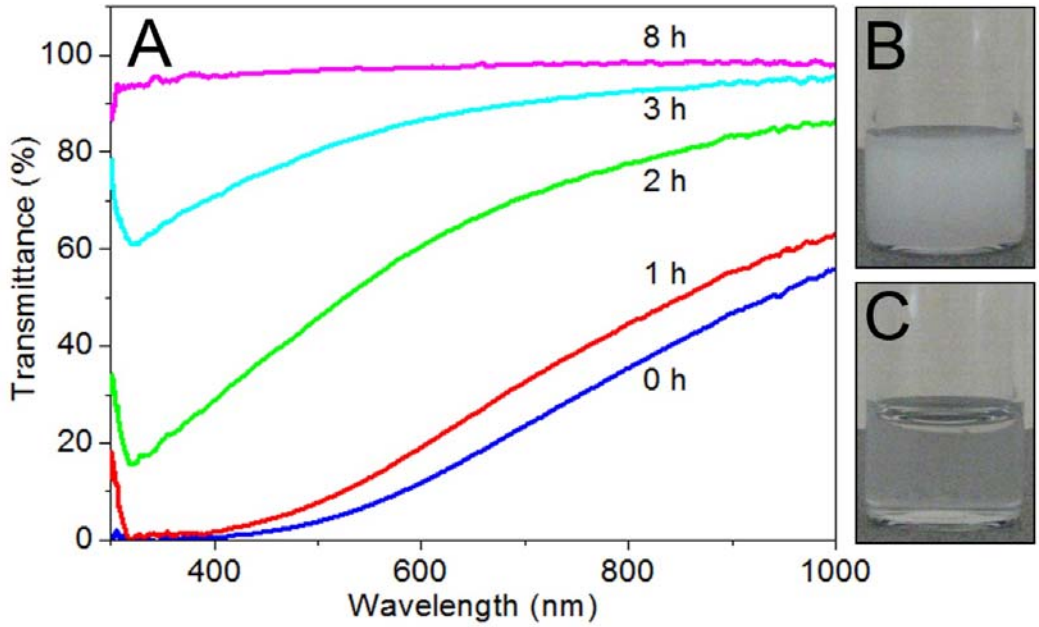

Figure 4.1 (A) Transmittance spectra of SiO_2 spheres (~360 nm in diameter) in ethanol after they are heated in water at 95 ^oC for various periods. (B, C) Digital photos of unetched (B) and etched (C) silica spheres dispersed in ethanol. The etched colloidal SiO_2 spheres become almost transparent due to the close matching of their refractive index with the solvent.

particles with a specific size, we have been able to use the change in transmittance to estimate the progress of etching. It is also worth noting that the time needed to reach the maximum porosity increases for larger SiO_2 particles.

TEM was employed to determine the change in the SiO_2 spheres after water etching. As shown in Figure 4.2, the size and shape of the SiO_2 spheres remained nearly unchanged after heat treatment. The major difference lies in the lower contrast of the etched samples, as shown in the high magnification image in Figure 4.2D, which again suggests a porous structure. In our previous studies, SiO_2 colloidal spheres were found to be rapidly etched in alkaline solution.[27, 28] In order to protect the SiO_2 surface from complete removal, we developed a "surface protected etching" process by introducing a layer of polymers such as PVP to temporally stabilize the surface layer of oxide. Because the alkaline solutions are strong etchants, a large portion of SiO_2 can be dissolved from each colloid, resulting in many pores with sizes typically larger than several nanometers. As a result, after extensive etching with alkaline solutions, the colloids show a noticeably lower contrast during TEM imaging. Unlike these prior systems, the water etching of such large SiO_2 spheres seems to effectively stop after a certain period, thus only producing pores with small average size and limited total volume as evidenced by the relatively small reduction in the TEM contrast of the etched particles. Prior studies suggest that the dissolution of colloidal silica in water proceeds by breaking the Si-O-Si network structures and producing mainly monosilicic acid $Si(OH)_4$.[12, 24] It is therefore expected that the etching efficiency is directly related to the degree of condensation of the silica network. This has been confirmed by our experimental observations: freshly

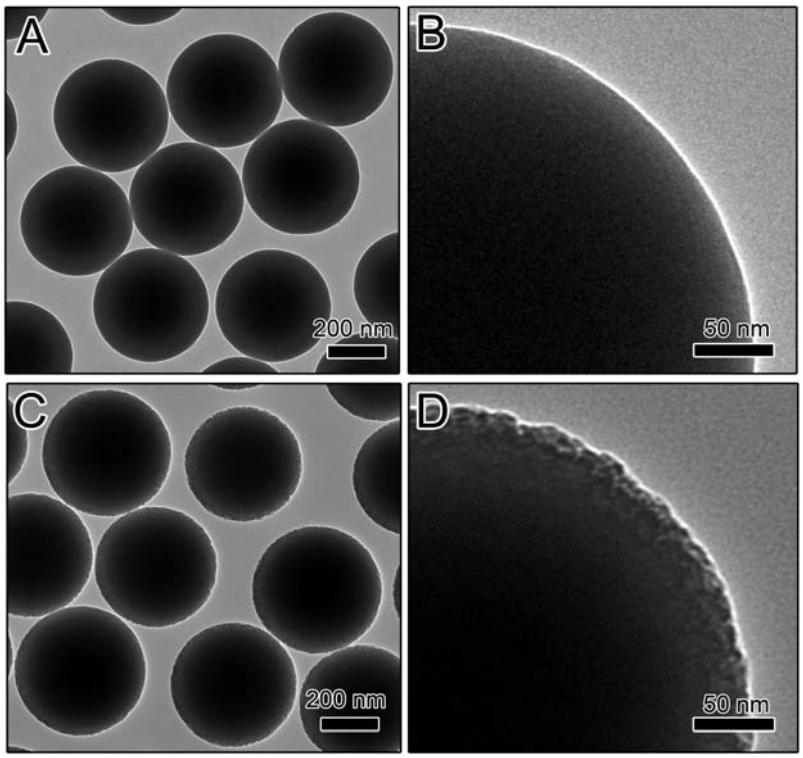

Figure4.2 (A, C) TEM images of 360 nm colloidal SiO_2 spheres (A) before and (C) after heat treatment in water at 95 ^{o}C for 8 h; (B, D) High magnification TEM images of the silica spheres (B) before and (D) after heat treatment in water.

prepared Stöber silica particles can be etched relative quickly due to the poor condensation of the silica network, while the samples that have been aged at room temperature for a few weeks showed dramatically lower etching rates due to the enhanced condensation within the Si-O-Si network. This is also consistent with the fact that crystalline silica (quartz) has a much lower solubility in water than amorphous silica.[12, 25, 26] It is well known that sol-gel derived colloidal SiO_2 is the result of coagulation of many oligomeric silicates, therefore the degree of condensation within each particle is inhomogeneous.[23] While regions with perfect Si-O-Si networks are more resistant to water etching, those with highly discontinuous networks can be dissolved quickly, thus producing mesoscale pores after controlled water etching. Compared with the alkaline solutions, water is a very mild etchant for silica so that the main framework of silica spheres remains relatively stable during water etching, even with heat treatment. This is why there is no absolute need for the surface protection of polymeric ligands to maintain the size and shape of colloidal particles during water etching. Interestingly, we noticed that Giersig et al. reported earlier that boiling Au@SiO_2 colloids caused silica densification which rendered the particles almost impervious to cyanide.[29] As no sufficient description and discussion can be found in their report, we are not able to directly compare the two systems and find out the cause for the dramatically different conclusions.

4.3.2 Porous Silica Nanoshells by Water Based Etching

This simple and mild etching process is in fact complementary to the "surface-protected etching" process that we have developed for converting solid oxide particles

into mesoporous permeable shells that can allow efficient mass transfer. In particular, water etching can be applied to small sized core-shell particles with a very thin silica shell, where surface-protected etching becomes very difficult to avoid overetching due to the use of more aggressive etchants. We demonstrate here that monodisperse $Ag@SiO_2$ core-shell nanostructures with overall size of tens of nanometers can be prepared with controlled shell permeability through this water etching process. Although surface protecting agent PVP is not critical in this process, we found that its presence during etching can still better maintain the shell structure and prevent the aggregation of these small particles. Figure 4.3A-E show that after heat treatment in water, the size and shape of the $Ag@SiO_2$ core-shell colloids together with the thickness of the silica layer remained nearly unchanged except that the silica coating gradually became more porous with prolonged treatment time. As the silica shell was only about ten nanometers in thickness, the etching of the silica layer reached its maximum after ~2 h of reaction time. In this case, PVP with a low molecular weight (M_w = ~10,000) was used so that they can gradually diffuse into the porous structure of the shell during the reaction and protect it from further etching.

We used UV-Vis spectroscopy to study the reaction kinetics of the etching of the $Ag@SiO_2$ core-shell colloids with water. As shown in Figure 4.3F, with heat treatment in water, the characteristic absorption at 420 nm due to the surface plasmon resonance (SPR) of Ag nanoparticles increased quickly in the first 30 min, then slowed down, and finally stabilized after ~1.5-2 h. The increase in the absorption of the Ag particles was caused by the gradual removal of silica which led to a reduced average refractive index of

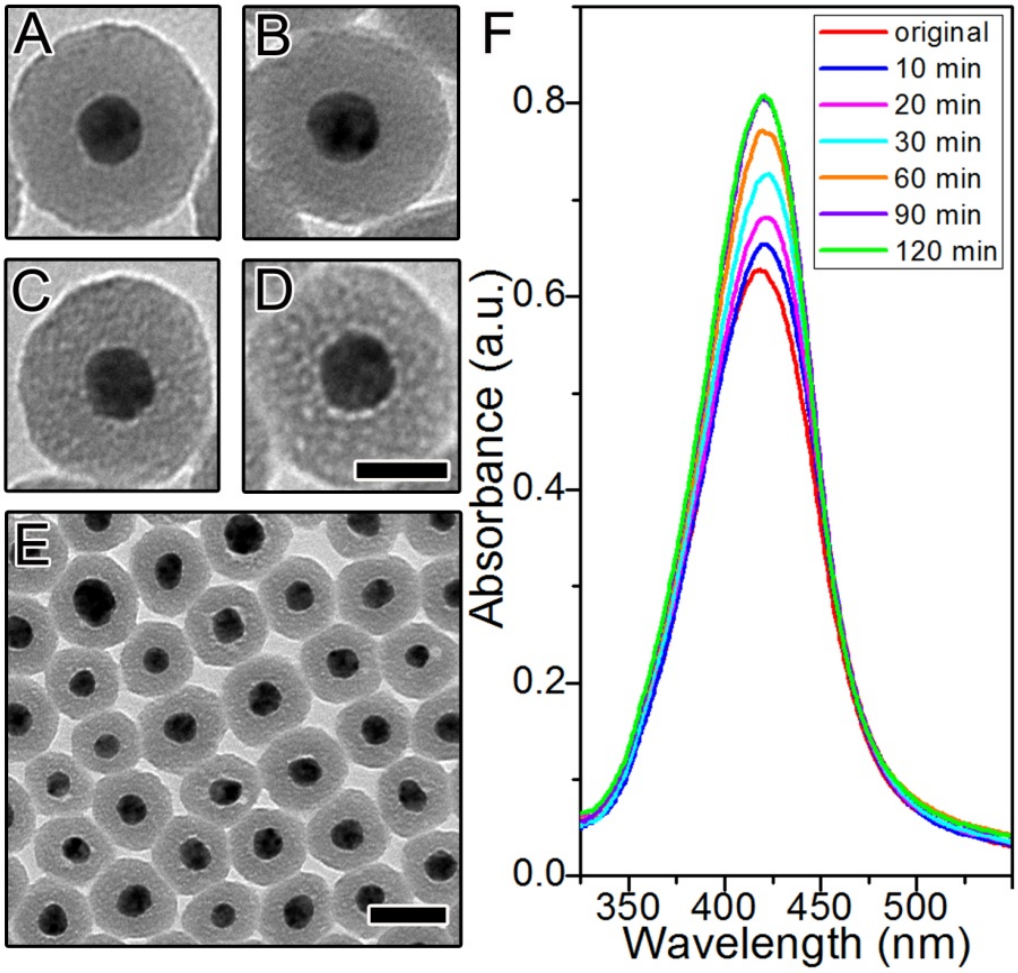

Figure 4.3 (A-D) High-magnification TEM images of the Ag@SiO_2 core-shell colloids after heat treatment in water for 0 min, 10 min, 30 min, and 120 min. (E) The corresponding low-magnification TEM survey image for the sample shown in D. (F) UV-Vis absorption spectra of Ag@SiO_2 core-shell colloids in ethanol after heat treatment in water at 95 °C for various times. The scale bars are 20 nm in A to D and 50 nm in E.

the shell. The better refractive index matching between the shell and the solvent resulted in less scattering of the shell, and eventually enhanced the contribution of absorption from the Ag cores.

4.3.3 Controlled Permeation of Silica Nanoshells

We further demonstrate here that etching by heat treatment in water allows for convenient control over the permeation of molecules through the shells. The catalytic destruction and mineralization reaction of a halocarbon, 3-bromo-1-propanol, with Ag nanoparticles by forming AgBr was chosen as a model system. The intensity change of the characteristic SPR peak of Ag nanoparticles at 420 nm was used for determining the dissolution of Ag nanoparticles encapsulated in silica shells during the model reaction. When a trace amount of 3-bromo-1-propanol was introduced into the Ag@SiO_2 colloidal solution, the absorption at 420 nm decreased gradually (Figure 4.4A), indicating the oxidation of Ag cores into AgBr. The complete consumption of Ag cores can also be visually observed by a gradual change from the originally bright-yellow solution into a colorless one (Inset in Figure 4.4A). TEM images in Figure 4.5A-C further verify the gradual dissolution of Ag cores encapsulated inside the silica shell by 3-bromo-1-propanol. The size of the cavities formed due to the removal of Ag cores matches well with that of the original Ag cores. As shown in Figure 4.4 B, the etching process by heat treatment in water allows the precise control of the pore size of the silica shells, and therefore the permeability of reagents through the shells and the kinetics of the catalytic reactions. Untreated silica shells are almost impenetrable to 3-bromo-1-propanol as only

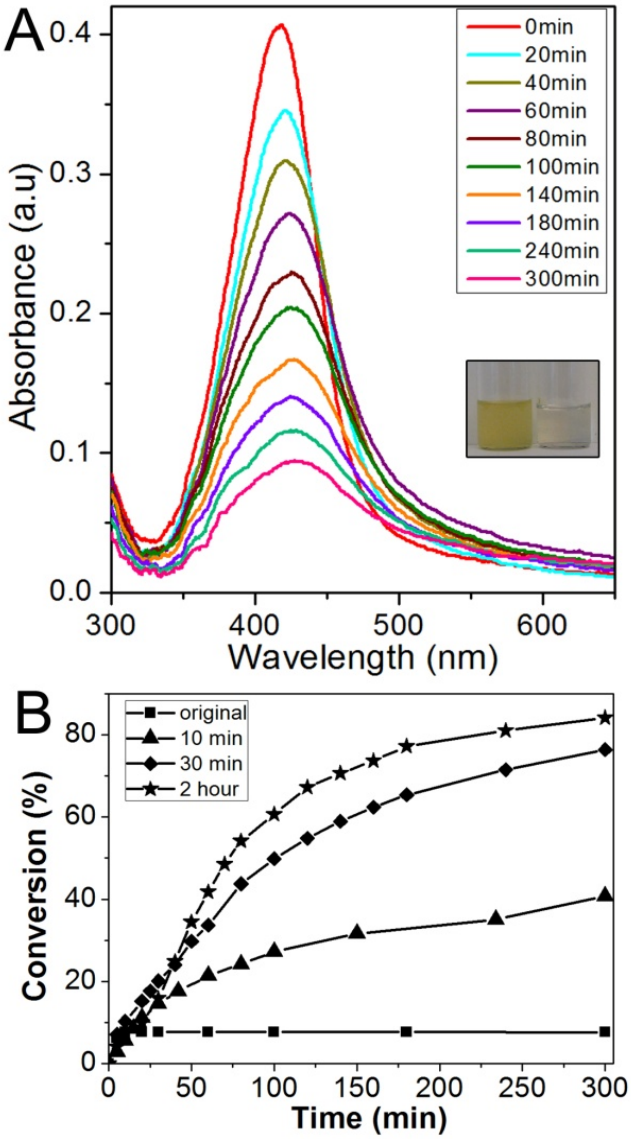

Figure 4.4 (A) UV-Vis spectra showing gradual etching of Ag nanoparticles in Ag@SiO_2 core-shell colloids by halocarbon. The Ag@SiO_2 core-shell colloids have been pre-treated with water at 95 °C for 2 h. The inset is a digital photo of Ag@SiO_2 core/shell colloids dispersed in isopropanol before (left) and after (right) reaction with halocarbon; (B) Percent conversion of Ag nanoparticles in Ag@SiO_2 core-shell colloids which have been treated with water at 95 °C for various periods.

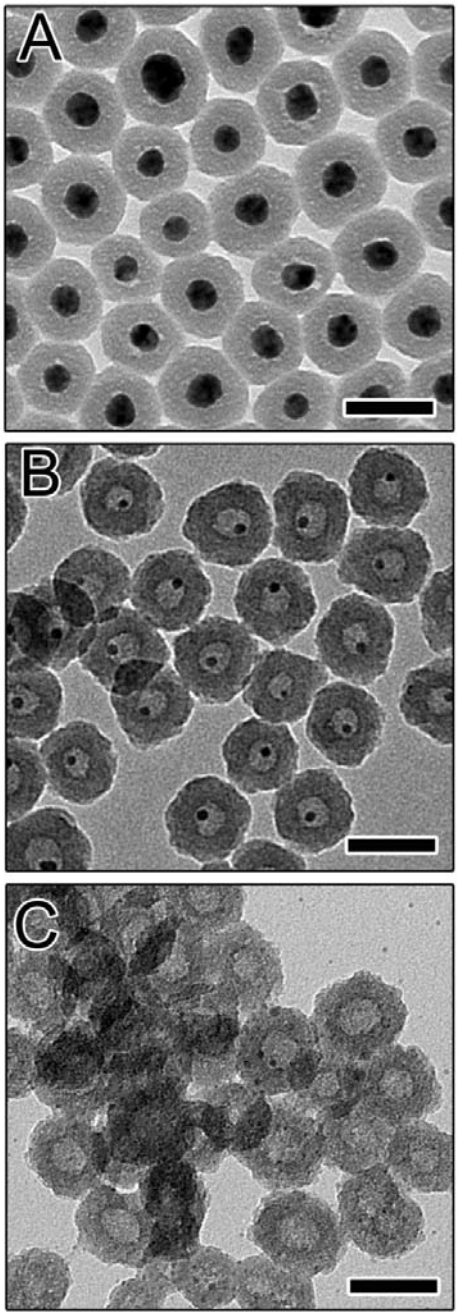

Figure 4.5 TEM images of $Ag@SiO_2$ core-shell colloids have been etched by halocarbon for various times: (A) 0 h, (B) 4 h (C) 14 h. Prior to the halocarbon etching, the samples have been treated with water at 95 °C for 2 h. All scale bars are 50 nm.

a minimal conversion of Ag (~8% estimated from the absorption spectra) can be detected over the duration of 5 h.

This is because the very small pores formed in the original SiO_2 shells greatly limited the permeation of 3-bromo-1-propanol through the porous channels to react with Ag. Due to their extremely small size, the micropores might also possibly be blocked by the AgBr precipitations produced from the initial reaction. A sample pre-heated in water for 10 min showed a faster conversion of Ag nanoparticles, indicating a more porous silica shell. The conversion reached ~41% after 5 h and completed within 1 day. The conversion rate of Ag nanoparticles increased consistently for samples with more extensive water etching: the conversion at 5 h reached ~82% for the sample pre-treated for 2 h, demonstrating that the control over the permeability of the shell is achievable by this mild etching process. The etching rates during the first 30 min for the three water-etched samples are similar, but they differ significantly when the reaction continues.

4.3.4 Hollow Silica Nanoparticles by Water Based Etching

By establishing a sufficient contrast of etching rates between the surface and the inner region of silica layer, extensive water etching can lead to the production of small hollow silica particles. This follows the same concept of surface-protected etching that we have developed for large (>100 nm) hollow silica particles.[30] In this case, we use PVP with a relative high molecular weight (M_w = ~50,000) as the protecting agent because they cannot fully penetrate into the shell but only adsorb at the near surface region, primarily enhancing the stability of the outer surface layer against etching. Without the protection inside, the interior silica network breaks down gradually upon

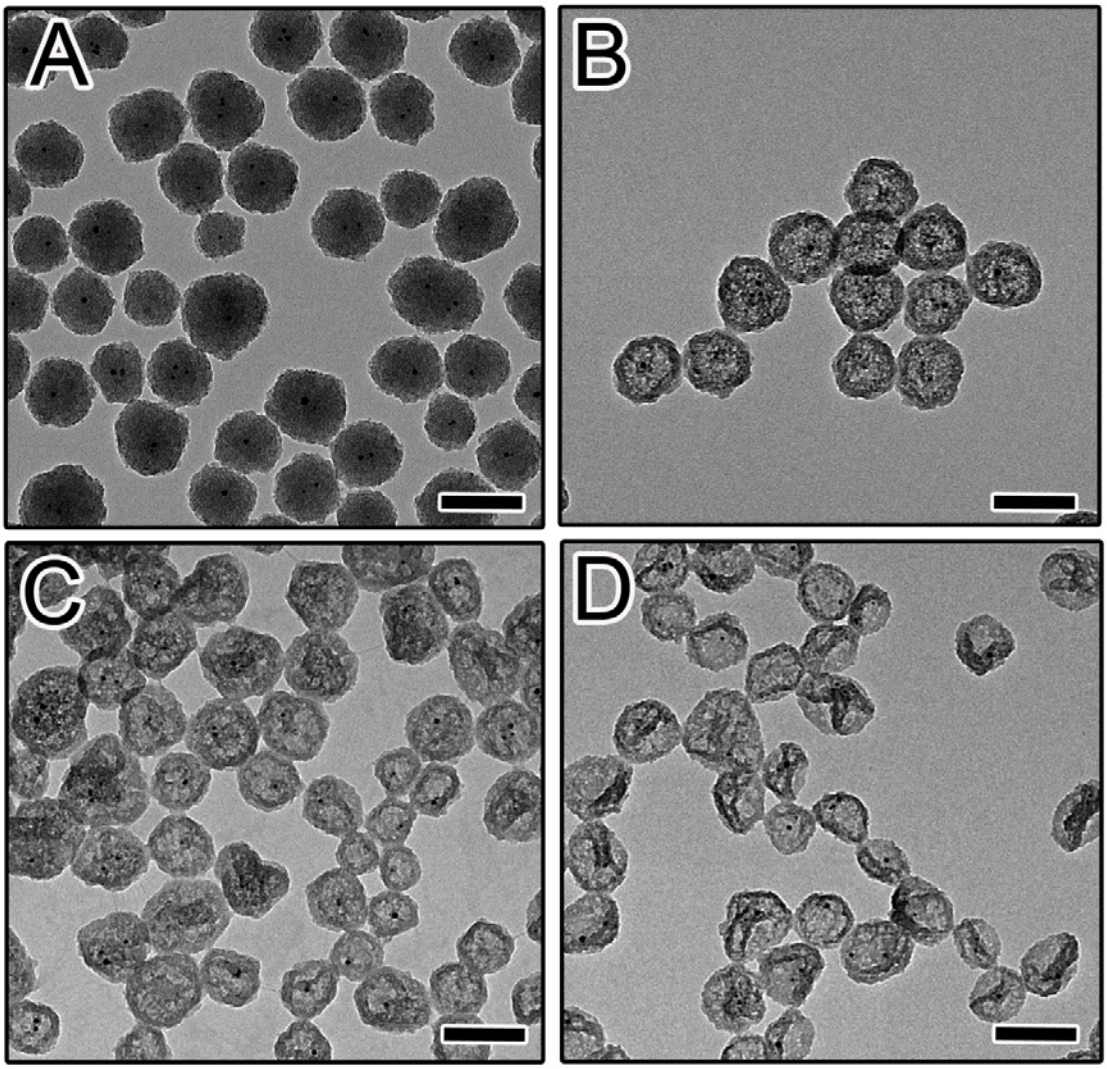

Figure 4.6 TEM images of Au@SiO_2 core-shell colloids after heat treatment with water at 95 °C for various time: (A) 0 min, (B) 30 min, (C) 60 min, (D) 120 min. All scale bars are 100 nm.

extensive etching, and eventually leads to the formation of hollow shells. As a demonstration, we show here the production of $Au@SiO_2$ yolk-shell nanostructures with diameter of ~60 nm by using the surface-protected water etching process. It is worth control due to the high reaction rate. In order to prepare uniform SiO_2 nanospheres, we used Au nanoparticles of a few nanometers as seeds and yielded solid $Au@SiO_2$ core-shell spheres, as shown in Figure 4.6A. Upon heat treatment in water at 95 °C for a short time in the presence of PVP, the solid $Au@SiO_2$ core-shell spheres slowly became porous and hollow but the size and shape of the spheres barely changed (Figure 4.6B). It is shown in Figure 4.6C and D that with the reaction continued, the composite silica particles displayed more apparent hollowness and the silica shells became thinner and softer.[31] This is because PVP can only temporarily stabilize the silica surface, which can still be removed gradually by water if the reaction time is long enough. The displacement of the Au cores from the central position indicates that they are movable inside the cavities.

4.4 Conclusions

In summary, we have demonstrated a water-based etching strategy for converting solid silica shells into porous ones with controllable permeability. The mild etching around the boiling point of water makes it suitable for treating small silica particles or core-shell particles with very thin silica shells for which the other etching method has been difficult to control. The process is simple, inherently scalable, and easy to carry out. It is expected that this method can be conveniently extended to the production of porous silica shells containing various sensitive materials whose diffusion to outside and/or

reaction with outside species can be precisely controlled. PVP as a surfactant and protecting ligand plays a very critical role during the etching: it can not only prevent the aggregation of silica particles but also stabilize the silica network structure. By using PVP with different molecular weights, porous or hollow silica structures can be achieved. Considering its great advantages, we believe that the strategy described here can be utilized for fabricating the protective porous silica layer on the Fe_3O_4 SPM colloids to improve the stability and also find other applications in many fields, especially in the synthesis of novel composite nanostructures, catalysis, and bio-sensing and detection.

4.5 References:

(1) J. Ge, Y. Hu, Y. Yin, *Angew. Chem. Int. Ed.*, 2007, **46**,7428.
(2) J. Ge, Y. Hu, T. Zhang, T. Huynh, Y. Yin, *Langmuir*, 2008, **24**,3671.
(3) J. Ge, L. He, J. Goebl, Y. Yin, *J. Am. Chem. Soc.*, 2009, **131**,3484.
(4) J. Ge, S. Kwon, Y. Yin, *J. Mater. Chem.*, 2010, **20**,5777.
(5) J. Ge, Y. Yin, *J. Mater. Chem.*, 2008, **18**,5041.
(6) Y. Lu, Y. D. Yin, Z. Y. Li, Y. A. Xia, *Nano Lett.*, 2002, **2**,785.
(7) A. K. Van Helden, J. W. Jansen, A. Vrij, *J. Colloid Interface Sci.*, 1981, **81**,354.
(8) K. Yoshinaga, J. Shimada, T. Kobayashi, in *Surfactant Science Series, Vol. 131 (Colloidal Silica)* (Eds.: H. E. Bergna, W. O. Roberts), **2006**, pp. 229.
(9) K. Yoshinaga, M. Teramoto, *Bull. Chem. Soc. Jpn.*, 1996, **69**,2667.
(10) K. N. Pham, D. Fullston, K. Sagoe-Crentsil, *Journal of Colloid and Interface Science*, 2007, **315**,123.
(11) P. K. Jal, S. Patel, B. K. Mishra, *Talanta*, 2004, **62**,1005.
(12) G. B. Alexander, W. M. Heston, R. K. Iler, *J. Phys. Chem.*, 1954, **58**,453.
(13) Y. Hu, Q. Zhang, J. Goebl, T. Zhang, Y. Yin, *Phys. Chem. Chem. Phys.*, 2010, **12**,11836.
(14) J. Ge, Q. Zhang, T. Zhang, Y. Yin, *Angew. Chem. Int. Ed.*, 2008, **47**,8924.
(15) Q. Zhang, T. Zhang, J. Ge, Y. Yin, *Nano Lett.*, 2008, **8**,2867.
(16) G. Buchel, K. K. Unger, A. Matsumoto, K. Tsutsumi, *Adv. Mater.*, 1998, **10**,1036.
(17) B. Tan, S. E. Rankin, *Langmuir*, 2005, **21**,8180.
(18) Y. Frere, P. Gramain, *React. Polym.*, 1992, **16**,137.
(19) Q. Zhang, J. Ge, J. Goebl, Y. Hu, Z. Lu, Y. Yin, *Nano Res.*, 2009, **2**,583.
(20) Y. Hu, J. Ge, Y. Sun, T. Zhang, Y. Yin, *Nano Lett.*, 2007, **7**,1832
(21) R. A. Caruso, M. Antonietti, *Chem. Mater.*, 2001, **13**,3272.

(22) F. Caruso, *Nano-Surface Chemistry*, 2002,505.
(23) L. L. Hench, J. K. West, *Chem. Rev. (Washington, DC, U. S.)*, 1990, **90**,33.
(24) K. Kato, Y. Kitano, *Journal of the Oceanographical Society of Japan*, 1968, **24**,147.
(25) G. W. Morey, J. J. Rowe, R. O. Fournier, *Journal of Geophysical Research*, 1964, **69**,1995.
(26) R. O. Fournier, J. J. Rowe, *Am. Mineral.*, 1977, **62**,1052.
(27) H. J. Hah, J. I. Um, S. H. Han, S. M. Koo, *Chem. Commun. (Cambridge, U. K.)*, 2004, **8**,1012.
(28) T. R. Zhang, J. P. Ge, Y. X. Hu, Q. Zhang, S. Aloni, Y. D. Yin, *Angewandte Chemie-International Edition*, 2008, **47**,5806.
(29) M. Giersig, T. Ung, L. M. LizMarzan, P. Mulvaney, *Adv. Mater.*, 1997, **9**,570.
(30) Q. Zhang, T. R. Zhang, J. P. Ge, Y. D. Yin, *Nano Lett.*, 2008, **8**,2867.
(31) Y. X. Hu, J. P. Ge, Y. G. Sun, T. R. Zhang, Y. D. Yin, *Nano Lett.*, 2007, **7**,1832.

Chapter 5

Magnetically Tunable Photonic Crystals with Long Term Stability

5.1 Introduction

As discussed in previous chapters, the incorporation of superparamagnetic (SPM) components into colloidal building blocks allows for effective magnetic field assisted self-assembly, precise control over photonic properties, improved diffraction tunability and response rate by using external magnetic fields.[1-6] Driven by the great need for developing a simple and flexible process that allows the instantaneous creation of high quality photonic crystal structures with tailored photonic properties, [7-9] we have made remarkable progress in fabricating magnetic-responsive photonic crystal structures through a one-dimensional assembly of SPM iron oxide (Fe_3O_4) nanocrystal clusters (CNCs) in the presence of an external magnetic field.[10-13] The key to assemble magnetic colloids into ordered structures is to establish competing attractive and repulsive forces between colloids. High magnetic content in SPM Fe_3O_4 particles induces strong and stable interparticle dipole attractions which can be controlled by external magnetic field. The creation of long-range strong repulsions between SPM particles is highly demanded to balance the magnetic dipole attractions, and achieve long-term stabilized magnetically responsive photonic structures with improved quality in terms of enhancing the structure ordering, and broadening the tunability as well as the corresponding diffraction colors. In previous cases, strong electrostatic repulsions can be built up by a layer of highly charged polyelectrolyte covered on the colloidal surface. However, the assembled structures and

correspondingly the photonic properties can change as the repulsive forces vary over time, for example, by the gradual detachment of polyelectrolyte molecules from the surface, which might limit their practical applications.

The stability of the optical performance has been improved in the cases where the assembled ordered chains were fixed by a polymer matrix or silica, but the tunability of that can be greatly hampered.[14, 15] Also modifying CNCs surface with a layer of silica did help in stabilization of the polyelectrolyte,[16] but the electrostatic repulsions as a dominant contributor to balance the magnetic attractions was largely diminished. Thus the tuning range of the diffraction from the photonic chains was narrowed a lot.[13] Up till now, it remains a great challenge to develop high quality magnetically responsive photonic structures with widely tunable optical properties and long-term stability. The crucial issue is to establish strong and stable long-range interparticle repulsive interactions.

In fact, high stability can be achieved by coating the charged Fe_3O_4 particles with a thin porous protecting layer which can prevent the polyelectrolyte from detaching from the particles and at the same time allow the polyelectrolyte to ionize and produce strong electrostatic interactions among particles. Silica is chosen as the protecting layer due to its convenient sol-gel based coating procedure, low processing temperature, and the well-developed silylation chemistry for further surface functionalization.[17-21] A porous thin silica shell on the Fe_3O_4 particles' surface can be easily created by a water-based mild etching method that has been developed and discussed in chapter 4. The water-based etching is selected to create porosity because it overcomes the challenges of the alkaline-

based surface-protected etching process that we previously developed and effectively creates controllable permeability within a thin layer of silica.[22-24]

In this chapter, we present an effective process to enhance the charge stability and maintain the long-range repulsion, allowing for the self-assembly of photonic structures with widely tunable optical properties and long-term stability. A two-step strategy is utilized for the creation of a porous protecting layer by coating the surface-charged Fe_3O_4 particles with a layer of solid protecting layer which are then post-treated to produce micropores and mesoscale pores. The porous structure in thin silica layer facilitates effective ionization of PAA on the particle surface and the resulting high charge density guarantees the strong repulsive force. Besides, additional hydroxyl groups from water-based etching provide extra negative charges in the porous silica networks, contributing to the enhanced repulsive interactions. By taking advantage of the unique features of the post-treatment strategy, high quality magnetic responsive photonic crystals with long stability can be achieved. It is considered to be widely applicable in the fabrication of novel optical components, sensors, and color display units.

5.2 Experimental Section

5.2.1 Materials

Ethanol (denatured), anhydrous iron(III) chloride ($FeCl_3$), ammonium hydroxide solution (Fluka), tetraethyl orthosilicate (TEOS, 98%, Acros Organics) and sodium hydroxide (NaOH) were purchased from Fisher Scientific. Polyacrylic acid (PAA, MW = 1800) and Diethylene glycol (DEG) were obtained from Sigma-Aldrich. Distilled

water was used throughout all the experiments. All chemicals were used as received without further treatment.

5.2.2 Synthesis

Synthesis of Fe_3O_4/SiO_2 core/shell colloids. Superparamagnetic iron oxide nanocrystal clusters (~130 nm in diameter) in water were synthesized according to a high-temperature hydrolysis reaction reported previously.[25] Fe_3O_4@SiO_2 core/shell colloids were prepared through a modified Stöber process.[26] Typically, an aqueous solution (3 mL) containing Fe_3O_4 CNCs (ca. 25 mg) was mixed with ammonium hydroxide (28%, 1 mL) aqueous solution and sonicated for 3 minutes. Ethyl alcohol (20 mL) was then added into the mixture under strong sonication, which was further sonicated for 5 minutes. TEOS (120 μL) was injected to the solution after it was transferred into a 100 mL flask with vigorous stirring using mechanical stirrer. After 20 min, the Fe_3O_4/SiO_2 core/shell colloids were collected by centrifugation, washed with ethanol and water two times respectively and finally dispersed in distilled water (20 mL).

Synthesis of Fe_3O_4/p-SiO_2 core/shell colloids. Fe_3O_4/SiO_2 colloids in 20 mL distilled water were aged for 24 hours before treated with boiling water.[22] First, the Fe_3O_4/SiO_2 colloidal solution was transferred to a 100 mL three-neck flask under magnetic stirring at 800 rpm after it was sonicated for 5 min. Then the solution was heated to and kept at ~95 ^{o}C while reflux water was running to keep water from evaporation throughout the boiling process. Heating was stopped when the color of the solution started to turn from dark brown to brown-yellowish. The Fe_3O_4/p-SiO_2

core/shell colloids were cleaned several times with distilled water, and finally dispersed in distilled water (3 mL).

5.2.3 Characterization

The morphology of the obtained products was characterized using a Tecnai T12 transmission electron microscope (TEM). The TEM samples were prepared by transferring one drop of sample dispersion in water onto a carbon-coated copper grid and then drying in air. Zeta potentials were measured by a Brookhaven Instruments Zeta Potential Analyzer at a scattering angle of 90° and a temperature of 25 °C. The UV-Vis spectra were measured by a probe-type Ocean Optics HR2000CG-UV-Vis spectrophotometer in reflection mode. The integration time was 300 ms.

5.3 Results and Discussion

5.3.1 Two–step Strategy for Enhanced Stability

The purpose of our strategy is to stabilize the charges on the SPM Fe_3O_4 colloids and subsequently enhance the electrostatic repulsion by coating a porous protective layer on the colloidal surface to facilitate the ionization of PAA salt underneath. Scheme in Figure 5.1 illustrates the process to realize the stabilization and enhancement of the repulsive interactions between SPM particles. First, a thin layer of silica is deposited to the charged SPM particle surface through a modified sol-gel process.[26] Then the coated particles are etched with a mild etchant -- water to produce controlled porosity in the silica layer during the post-treatment process.[22] The resulted porous structure allows the diffusion of water molecules and hydrated ions to accelerate the ionization of PAA salt beneath the silica layer while the additional hydroxyl groups in the porous silica networks

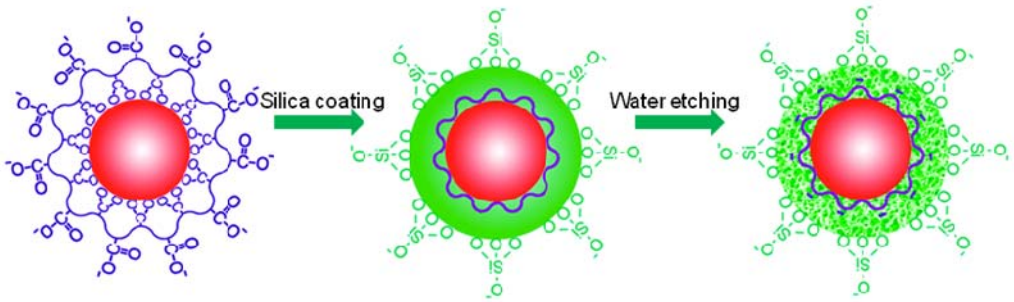

Figure 5.1 Scheme that illustrating a two-step strategy to fabricate SPM Fe_3O_4/p-SiO_2 colloids with high negative charge densities on the colloidal surface.

provide extra negative charges. This post-treatment process renders the surface of porous silica coated CNCs' (Fe_3O_4/p-SiO_2) a layer of relative higher density of negative charges than that on the original Fe_3O_4 colloids. The stronger electrostatic repulsions between Fe_3O_4/p-SiO_2 colloids are then built up and allow the self-assembly of magnetite colloids into more ordered structures in solution, resulting in broader tuning range and higher diffraction intensities.

Etching in hot water bath can effectively create controllable permeability within a thin layer of silica. TEM images in Figure 5.2 demonstrate the evolution process of effective creation of pores in the silica layer during the water-based etching process. At the beginning, the Fe_3O_4 colloids are well coated with a uniform thin layer of SiO_2 (ca. 20 nm) using a modified sol-gel method. The core-shell structure can be appreciated in Figure 5.2A in which the Fe_3O_4 cores and the smooth silica coating can be identified by the contrast between the core and the shell. After a post treatment of the Fe_3O_4/SiO_2 colloids in water at around 95 ^oC for 20 minutes, the size and shape of the colloids remain nearly unchanged (Figure 5.2B). The major difference lies in the lower contrast of the shell in the etched samples, as shown in the high magnification image in Figure 5.2B inset, which suggests a porous structure created in the SiO_2 layer. This is because the incomplete hydrolysis and polycondensation of the precursor--tetraethyl orthosilicate (TEOS) in the coating process lead to the formation of amorphous structures in SiO_2 layer with highly disordered and discontinuous interconnection of Si-O-Si bonds. When Fe_3O_4/SiO_2 colloids are dispersed as a diluted solution in water at an elevated temperature, water etching partially breaks the imperfectly condensed SiO_2 network and

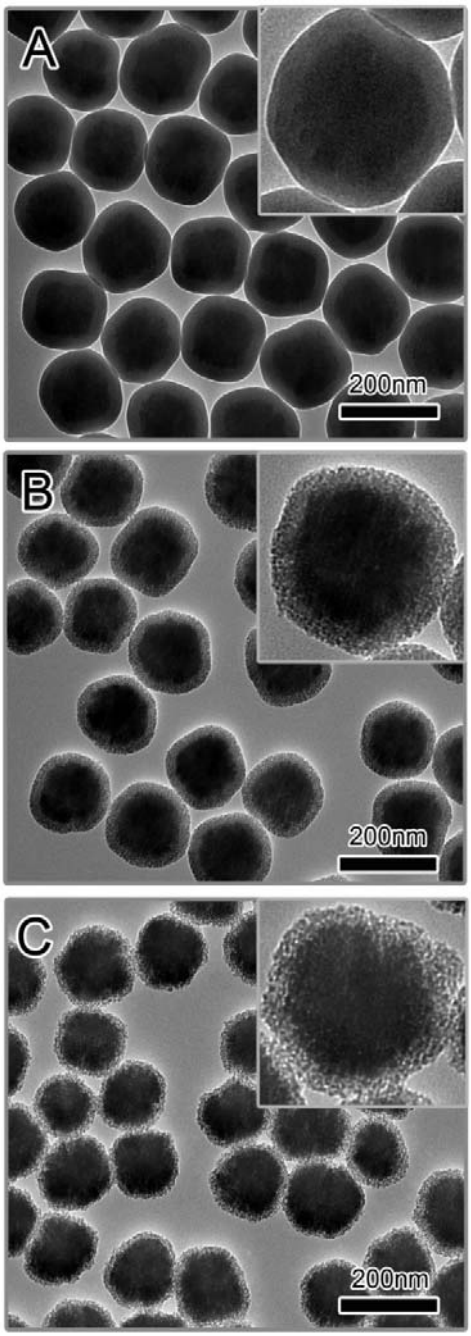

Figure 5.2 TEM images of Fe_3O_4/SiO_2 etched with water for A) 0 min, B) 20min, C) 60 min, respectively. Inset in each TEM shows a corresponding high magnification image of the resulting particle.

forms soluble monosilicic acid, eventually producing mesoscale pores in silica shell and additional hydroxyl groups in the porous network.[22] Benefiting from the mild etchant of water, a controlled larger portion of SiO_2 can be dissolved when prolonging the etching period, resulting in bigger pores with size of a few nanometers. As a result, after extensive etching for 60 minutes, the shell of the etched particles shows enlarged pores from a noticeably lower contrast during TEM imaging (figure 5.2C inset). In addition, the thickness of the SiO_2 shell is decreased when the outer shell is subjected to excessive etching, resulting in a decreased overall size of the colloids.

5.3.2 Enhanced Charge Density on CNCs

The porous protective layer on the CNCs surface accelerates the ionization of PAA salt underneath the silica layer by enhancing the diffusion of water molecules and hydrated ions in/out of this porous protective layer. Before the post-treatment process, the conventional base-catalyzed sol-gel route has resulted in the formation of microporous structures inside the amorphous silica protective layer with micropore size less than 1 nm.[27, 28] As a result, the ionization of PAA salt is limited owing to the lower effective diffusion rates of water molecules and hydrated ions restricted by the pore.[16] Previous experimental and simulation studies show that water molecules confined in nanoscale geometries exhibit strong water-silica hydrogen bonding when the hydroxylated silica surfaces are in small separation, typically less than ~ 1 nm apart.[29, 30] Thus the water molecules, confined in micropores strongly adjacent to the silica surface, form layered structure that greatly hampers their effective diffusion rate. Additionally, the hydrated metal ions are bound to the silica micropore surface in complete registry,

which also limits the ionization of PAA salt underneath the silica shell. However, central bulklike regions of free water start to present with enlarged pores (> 1 nm), which allows the improved effective diffusion of water molecules together with the hydrated salt ions.[31] Thus, an enhanced negative charge density on colloidal surface from ionization of PAA salt can be achieved by taking advantage of the increased porosity and pore size created in the silica framework after a water-based etching process.

We have monitored the change of the ζ potential during the etching process of the silica layer to demonstrate the enhanced surface charge of the Fe_3O_4/p-SiO_2 colloids (Figure 5.3A). Before etching, the silica-coated Fe_3O_4 colloids displayed a ζ potential of ~-38.5 mV, suggesting a high density of silanol groups on the surface after the sol-gel based coating process. This value was consistent with that measured for silica colloids freshly prepared through sol-gel processes.[32] However, this value was much lower than that of bare Fe_3O_4 particles with a ζ potential of ~-49.0 mV, which indicates that the ionization of the PAA salt underneath the silica layer cannot be fully achieved. At the initial stage of etching for ~60 min, the ζ potential rapidly increased to ~-56.5 mV due to the enhanced ionization of PAA salt underneath the silica layer with an improved effective diffusion rate through the gradually porous framework. At the same time, the formation of extra hydroxyl groups during the breakdown of Si-O-Si networks introduced a relatively high density of hydroxyl groups so that the particle surface obtained additional negative charges. The ζ potential gradually increased, and eventually stabilized at ~-57.3 mV after the etching was carried out for 2 hours. Further etching would not affect the ζ potential too much due to the balanced ionization of PAA salt and

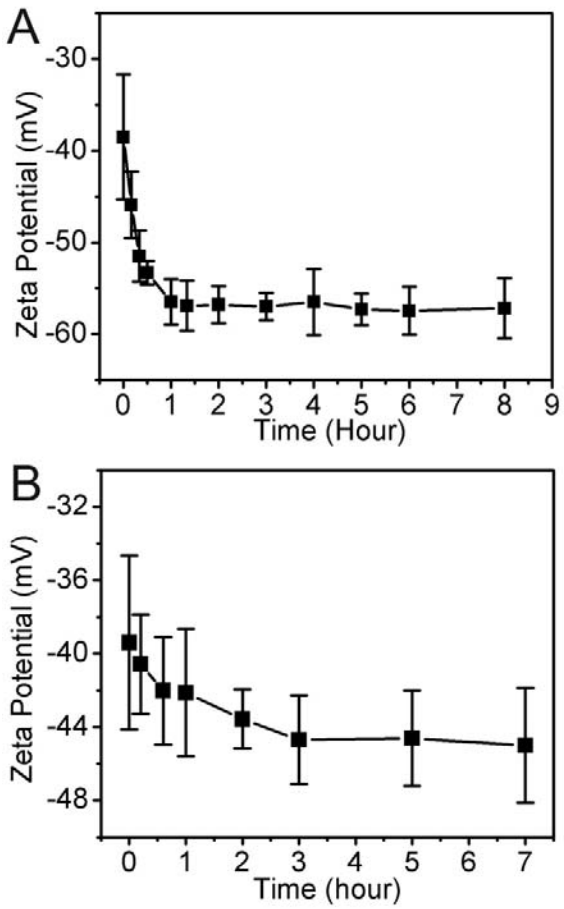

Figure 5.3 Plots of the ζ potential change of A) Fe_3O_4/SiO_2 and B) pure SiO_2 spheres during the water-based etching process.

the stabilized silica porous framework after fully condensation. For comparison, we have also measured the ζ potentials variation during the water-based etching of SiO_2 solid nanoparticles with similar size prepared by sol-gel process, which only gave values slightly changing from -39.4 to -45.0 mV in 7 hours' etching (figure 5.3B). The apparent difference of the ζ potential change between the etched core/shell particles and etched silica solid spheres demonstrates that the major source for the excessive negative charges on the Fe_3O_4/p-SiO_2 colloids is the ionization of PAA salt. It is therefore believed that the etching process not only introduces additional hydroxyl groups on the SiO_2 framework but also facilitates the ionization of PAA salt underneath to enhance the charge density once the pore size in silica shell has been increased.

5.3.3 Magnetically Tunable PCs with Greatly Improved Quality

The enhanced negatively charged surface renders the Fe_3O_4/p-SiO_2 colloids stronger repulsive force inbetween to achieve high quality tunable photonic crystals. In principle, stronger electrostatic repulsion between Fe_3O_4/p-SiO_2 colloids will increase the interparticle distance in a magnetic field with fixed strength. Thus when a stronger magnetic field is applied to balance the increased electrostatic repulsion, the colloids are organized with improved long-range order and increased diffraction intensity. In our strategy, immediately following the water-based etching, the charge density on the particles surface has been greatly increased, which can significantly enhance the electrostatic repulsive interactions and therefore the overall diffraction intensities. Figure 5.4 compares the typical reflection spectra of an aqueous solution of 128 nm Fe_3O_4 particles and an aqueous solution of 131 nm (overall diameter, with 106 nm core size and

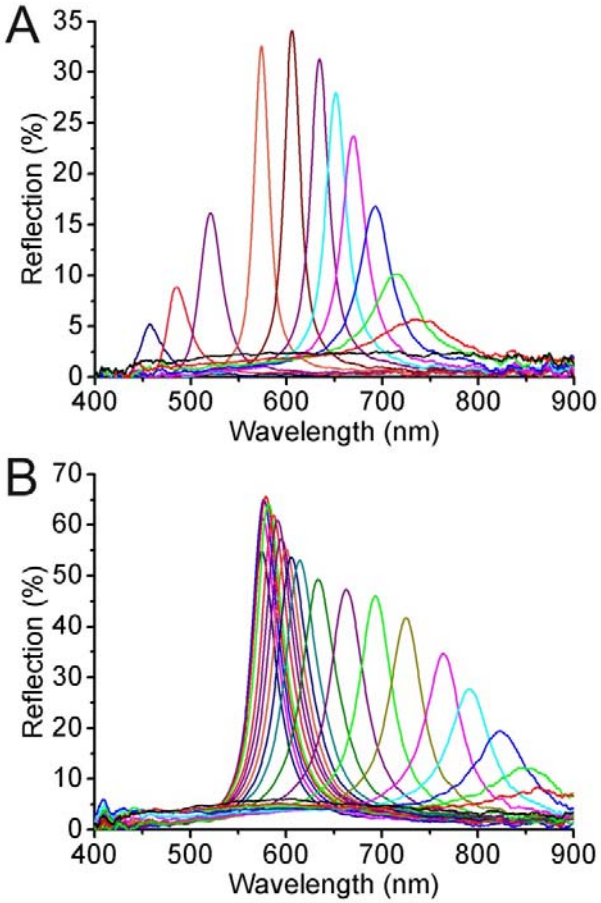

Figure 5.4 Reflection spectra of A) Fe_3O_4 CNCs aqueous solution and B) Fe_3O_4/p-SiO_2 aqueous solution in response to an external magnetic field with varying strength, achieved by changing the magnet-sample distance. The diffraction peak blue-shifts as the distance decreases from 4.8 to 3.9cm for (A) and 3.8 to 0 cm for (B), with step size of 0.2 cm.

12.5 nm shell thickness) Fe_3O_4/p-SiO_2 particles as a function of the external magnetic field strength. For Fe_3O_4 particles in water, the reflection spectra present a typical symmetric profile (Figure 5.4A): the intensity of the diffraction peak first increases, and then decreases after reaching the maximum as the magnetic field increases gradually. Simultaneously, the diffraction peaks shift to shorter wavelengths at the same time. However, for an aqueous solution of Fe_3O_4/p-SiO_2 particles, the diffraction intensity increases steadily with increasing external field strength until reaching a saturation value. Further increasing the strength of the magnetic field does not significantly change the peak position and the peak intensity, indicating a strong electrostatic repulsive force with a fixed average interparticle spacing (Figure 5.4B). The contour of the peaks therefore shows a skewed profile, which is similar with that of Fe_3O_4/SiO_2 ethanol system.[26] But contribution from ‘‘solvation force’’ in the repulsions can be ignored in Fe_3O_4/p-SiO_2 aqueous system because the solvation layers of two nearby particles cannot overlap in a relative larger interparticle separation. In addition, the diffraction intensities are much higher in Fe_3O_4/p-SiO_2 aqueous system than that in bare aqueous Fe_3O_4 system or Fe_3O_4/SiO_2 ethanol system, resulting from the significantly enhanced charge density on the particles’ surface.

The distinct optical responses to vairous magnetic field strength in ordering Fe_3O_4/p-SiO_2 in water and Fe_3O_4 in water are due to the differences between the strength of the electro-repulsive forces involved in the two cases. In aqueous systems, for both charged Fe_3O_4/p-SiO_2 and Fe_3O_4 particles, the electrostatic force dominates the particle interactions and determines the periodicity of the assembled structures by countering the

induced magnetic attraction, based on Derjaguin–Landau–Verwey–Overbeek (DLVO) theory.[10] The long-range electrostatic repulsion allows the particles to assemble at a large separation distance (ca. 144 nm for Fe_3O_4 and ca. 193 nm for Fe_3O_4/p-SiO_2), keeping the adjacent particles in ‘‘soft contact’’ with each other. For the Fe_3O_4 aqueous dispersions, the packing force is the main factor of disturbing the long-range order inside the particle chains and diminishing the diffracted intensity within several minutes when the magnet-sample distance is small enough.[11] For the Fe_3O_4/p-SiO_2 aqueous dispersions, the significantly increased high surface charge density leads to stronger repulsive interactions together with an increase of the interparticle distance in a magnetic field with fixed strength, therefore red-shifting the diffraction peak at low magnetic field strength. While the strength of magnetic field increases, the enhanced electrostatic force still dominate the interparticle repulsions at smaller separations, making it capable of countering the induced magnetic attractive dipole force and packing force. The resulting balance between the stronger magnetic attractions and the increased electrostatic repulsions assemble the particles into improved ordered structures with higher diffraction intensity. Moving the magnet even closer (~ 0 mm) can effectively increase the magnetic packing force, but the ordered assembly of the particles ($D_{s\text{-}s}$ = 86 nm) can be kept against coagulation and precipitation in dispersion within a period of tens of minutes. By taking advantages of the significantly enhanced surface charge density, the increased repulsive forces render the Fe_3O_4/p-SiO_2 aqueous system greatly improved diffraction intensities and tuning range of the diffraction to the changes in the strength of magnetic field.

5.3.4 Magnetically Tunable PCs with Long-term Stability

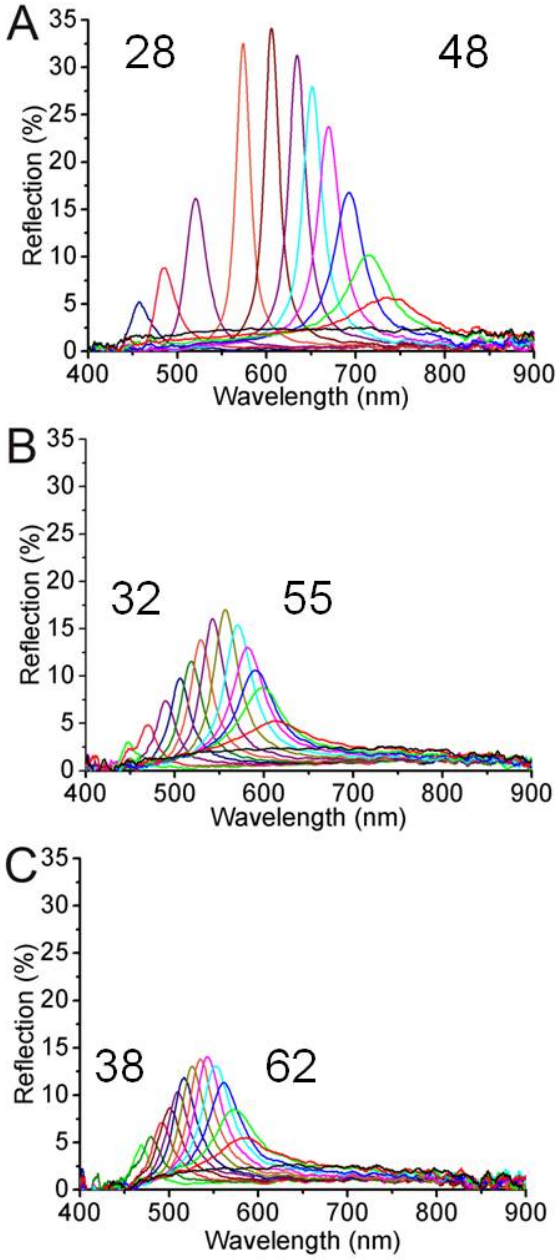

Figure 5.5 Reflection spectra of Fe_3O_4 CNCs aqueous solution in response to an external magnetic field with varying strength, achieved by changing the magnet-sample distance, after preparation for: A) 1 day; B) 2 days; C) 4 days. The two numbers showed in each image indicates the tuning range of magnet-sample distance with diffraction peak observable.

The long-term stability of the magnetically tunable photonic crystal system has been remarkably improved, resulting from the stabilization of the repulsive forces by a layer of porous protecting silica shell. In previous aqueous Fe_3O_4 system, the stability against long-term storage suffers from the PAA salt detachment and the ionic strength variation induced by dissolution of extra ions from the storage vial.[11] As a result, the diffraction peaks greatly blue shift and the tuning range of peak position shrink a lot. The diffraction intensity decreases monotonically and fades away in storage of ~ 3 days (Figure 5.5). To demonstrate the long term stability of the designed system, we have monitored the optical performance of the prepared Fe_3O_4/p-SiO_2 aqueous dispersions by reflection spectra over 3 weeks. Figure 5.6 in supporting information shows the variation of magnetically induced reflection spectra of a Fe_3O_4/p-SiO_2 with storage time. Generally, the system needs a short period of time to reach a stabilized stage right after it is post-treated with water-based etching. During the initial 3 days, at a fixed low magnetic strength, the diffraction peaks consistently blue-shifted with an increased storage time. It indicates a mild decrease of repulsive electrostatic interactions as the hydroxyl groups in the porous silica framework continue with condensation, gradually reducing the negative charges from silica layer. The slight decrease of charge density on the particles can also be proven by the decreased diffraction intensities at short wavelength when strong magnetic fields with high gradient are applied. However, the overall performance in weaker magnetic fields stays the same because the negative charges from the ionization of PAA salt are relatively stable. Only the diminishment of the hydroxyl groups on porous silica layer leads to a gradual evolution from a skewed

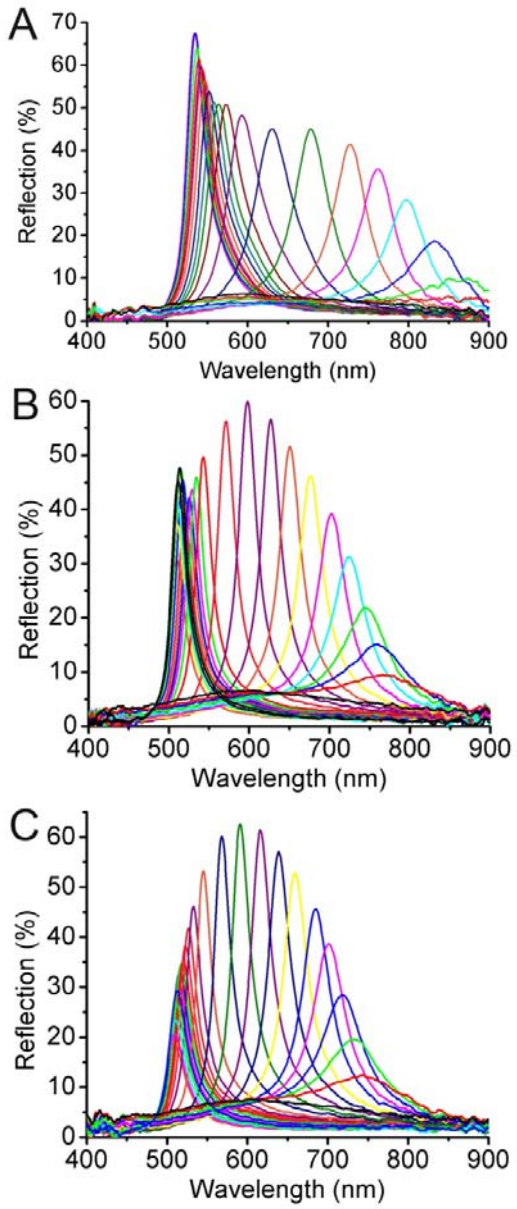

Figure 5.6 Reflection spectra of Fe_3O_4 /p-SiO_2 aqueous solution in response to an external magnetic field with varying strength, achieved by changing the magnet-sample distance, after preparation for: A) 1 day; B) 2 days; C) 3 days. The two numbers showed in each image indicates the tuning range of magnet-sample distance with diffraction peak observable.

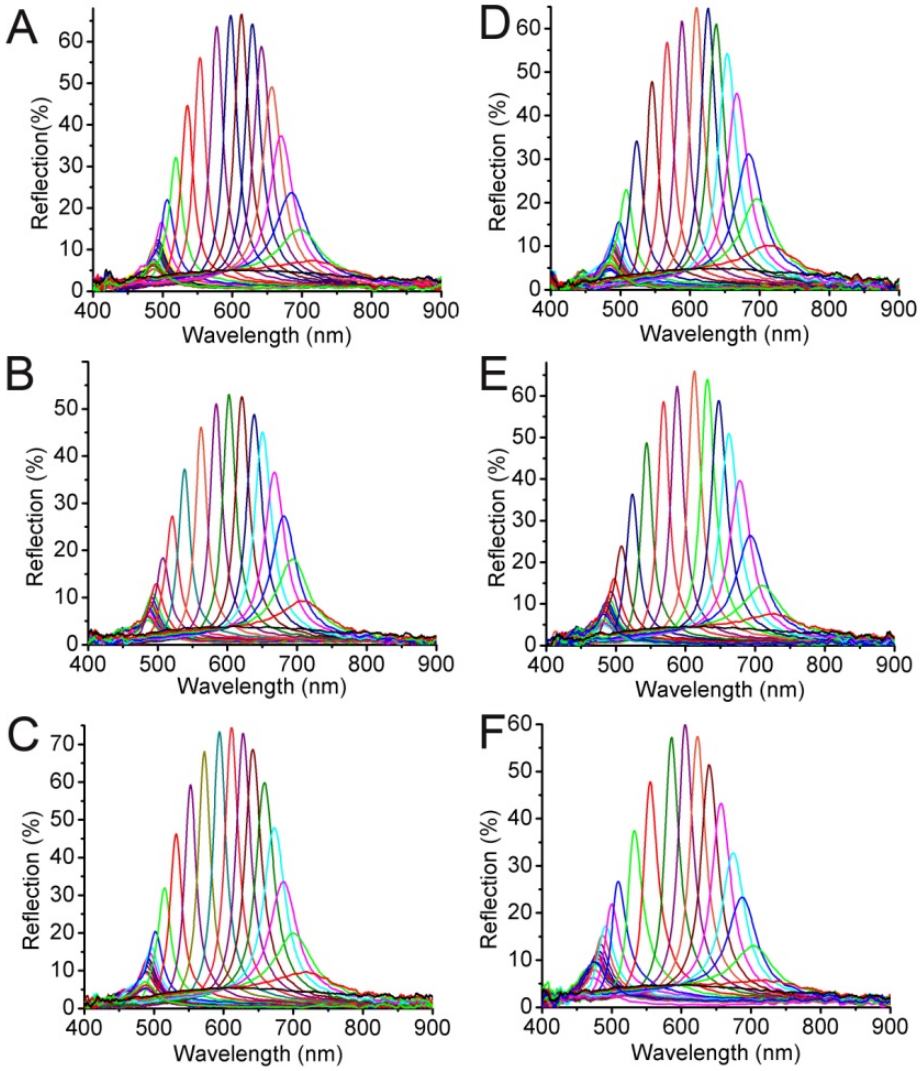

Figure 5.7 Reflection spectra of Fe_3O_4 /p-SiO_2 aqueous solution in response to an external magnetic field with varying strength after preparation for: A) 1 day; B) 3 days; C) 7 days; D) 11 days; E) 15 days; F) 21 days.

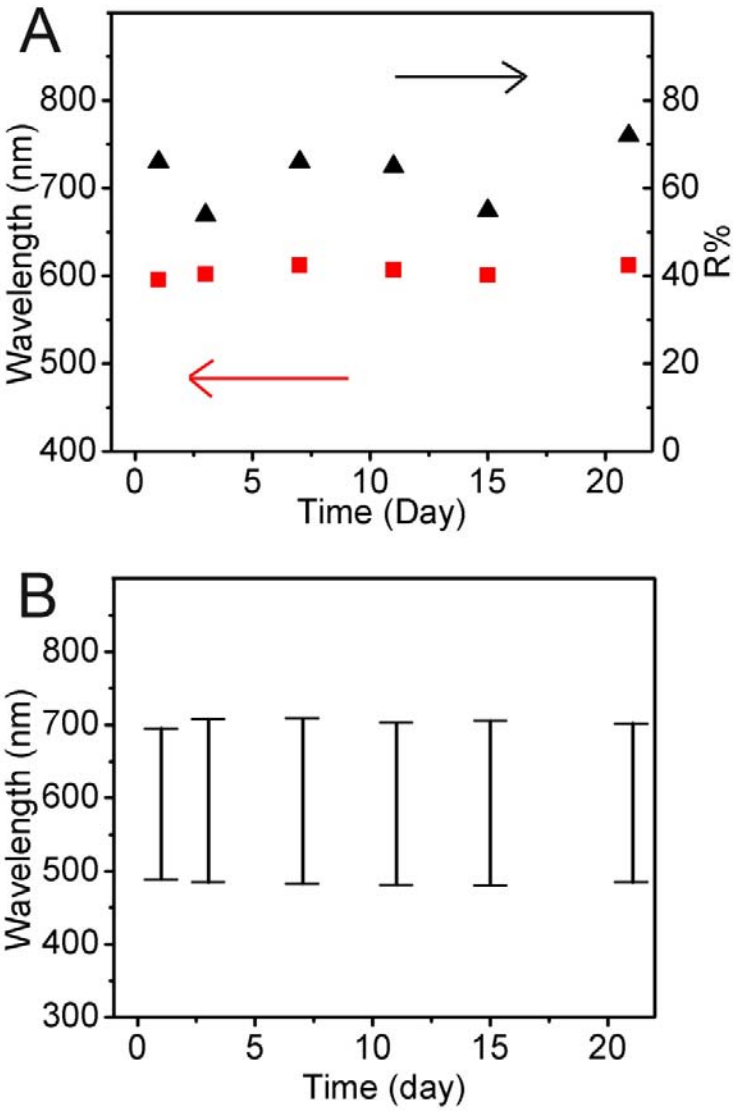

Figure 5.8 A) Plots of the change in peak position (red square) and diffraction intensity (black triangle) of a Fe_3O_4/p-SiO_2 aqueous solution with varying storage time at fixed magnetic field strength of ca.131G. B) A plot of the diffraction peak tuning ranges in variable magnetic field with storage time.

diffraction profile to a symmetric profile. The resulting symmetric diffraction profile is similar with that of a PAA coated Fe_3O_4 aqueous system, indicating the effective negative charges are from ionization of PAA salt underneath the porous shell once it is stabilized after condensation.

After an initial stabilization period, the photonic performance becomes very stable without peak shift and intensity variation. The photonic performance has been monitored over 3 weeks and the diffraction spectra were shown in Figure 5.7. The change in peak position and diffraction intensity of a cleaned Fe_3O_4/p-SiO_2 solution have been summarized in Figure 5.8 A as functions of storage time at fixed magnetic field strength of ~ 131G. During the storage, the peak position kept almost the same at 605 nm with slight fluctuations in diffraction intensity, which can be ascribed to the instrument errors. The diffraction intensity reached as high as more than 60%, which was hard to achieve in Fe_3O_4 aqueous system. The tuning ranges of the diffraction peak did not change too much over 3 weeks but kept in the range from 700 nm to 480nm. The steady photonic performance of this system indicates the stability of the charges on the surface of Fe_3O_4/p-SiO_2 from the ionization of PAA salt. All the results demonstrate the successful protection of the ionized PAA salt by the porous silica shell, which helps enhancing the long-term stability of the photonic properties.

5.4 Conclusion

In summary, a two-step strategy is developed to fabricate high quality magnetically tunable photonic structures with long-term stability: stabilize the charges on Fe_3O_4 CNCs particles by modifying the surface with a porous protecting silica layer to

prevent the detachment of PAA from CNCs surface, which caused the charge instability in the original CNCs aqueous system. Meanwhile, the porous structure of the silica shell in Fe_3O_4@p-SiO_2 allows the ionization of PAA salt underneath it. Both the ionization of PAA salt and the addition of hydroxyl group on the porous silica framework contribute to the increase of negative charges on the Fe_3O_4/p-SiO_2 particles, making them the ideal building blocks to create high quality magnetically responsive photonic crystals with widely and reversibly tunable structural colors, enhanced diffraction intensity and long term stability. The enhanced electrostatic repulsive forces also stabilize the dynamic chaining structures against aggregation induced by magnetic packing force in a magnetic field with high gradient. The system reported here shows important features such as high stability, a fast, reversible, and tunable optical response to external magnetic fields. The ability to stabilize the photonic performance allows the practical applications in displays or sensors. It is worth noting that the porous silica surface can be further modified with a large variety of functional groups through silane chemistry to further broaden the application.

5.5 References

(1) J. Ge, Y. Yin, *Angewandte Chemie International Edition*, 2011, **50**,1492.
(2) S. A. Asher, V. L. Alexeev, A. V. Goponenko, A. C. Sharma, I. K. Lednev, C. S. Wilcox, D. N. Finegold, *J. Am. Chem. Soc.*, 2003, **125**,3322.
(3) M. Ben-Moshe, V. L. Alexeev, S. A. Asher, *Anal. Chem.*, 2006, **78**,5149.
(4) U. Jeong, Y. Xia, *Angew. Chem. Int. Ed.*, 2005, **44**,3099.
(5) S.-L. Kuai, G. Bader, P. V. Ashrit, *Appl. Phys. Lett.*, 2005, **86**,221110.
(6) Y. J. Lee, P. V. Braun, *Adv. Mater.*, 2003, **15**,563.
(7) B. Gates, Y. Xia, *Adv. Mater.*, 2001, **13**,1605.
(8) X. Xu, G. Friedman, K. D. Humfeld, S. A. Majetich, S. A. Asher, *Adv. Mater.*, 2001, **13**,1681.
(9) C. Lopez, *Adv. Mater.*, 2003, **15**,1679.
(10) J. Ge, Y. Hu, Y. Yin, *Angew. Chem. Int. Ed.*, 2007, **46**,7428.

(11) J. Ge, Y. Hu, T. Zhang, T. Huynh, Y. Yin, *Langmuir*, 2008, **24**,3671.
(12) J. Ge, S. Kwon, Y. Yin, *J. Mater. Chem.*, 2010, **20**,5777.
(13) J. Ge, Y. Yin, *J. Mater. Chem.*, 2008, **18**,5041.
(14) J. Ge, H. Lee, L. He, J. Kim, Z. Lu, H. Kim, J. Goebl, S. Kwon, Y. Yin, *J. Am. Chem. Soc.*, 2009, **131**,15687.
(15) Y. Hu, L. He, Y. Yin, *Angewandte Chemie International Edition*, 2011, **50**,3747.
(16) J. Kunetz, L. Hench, *J. Am. Ceram. Soc*, 1998, **81**,877–884.
(17) Y. Yin, Y. Lu, Y. Sun, Y. Xia, *Nano Lett.*, 2002, **2**,427.
(18) P. M. Johnson, C. M. vanKats, A. vanBlaaderen, *Langmuir*, 2005, **21**,11510.
(19) K. Yoshinaga, J. Shimada, T. Kobayashi, in *Surfactant Science Series, Vol. 131 (Colloidal Silica)* (Eds.: H. E. Bergna, W. O. Roberts), **2006**, pp. 229.
(20) K. N. Pham, D. Fullston, K. Sagoe-Crentsil, *Journal of Colloid and Interface Science*, 2007, **315**,123.
(21) R. K. Iler, *The Chemistry of Silica*, Wiley, New York, **1979**.
(22) Y. Hu, Q. Zhang, J. Goebl, T. Zhang, Y. Yin, *Phys. Chem. Chem. Phys.*, 2010, **12**,11836.
(23) Q. Zhang, T. Zhang, J. Ge, Y. Yin, *Nano Lett.*, 2008, **8**,2867.
(24) Q. Zhang, J. Ge, J. Goebl, Y. Hu, Z. Lu, Y. Yin, *Nano Res.*, 2009, **2**,583.
(25) J. Ge, Y. Hu, M. Biasini, W. P. Beyermann, Y. Yin, *Angew. Chem. Int. Ed.*, 2007, **46**,4342.
(26) J. Ge, Y. Yin, *Adv. Mater.*, 2008, **20**,3485.
(27) W. Fahrenholtz, D. Smith, D. Hua, *J. Non-Cryst. Solids*, 1992, **144**,45.
(28) G. Frenzer, W. Maier, *Annu. Rev. Mater. Res.*, 2006, **36**,281–331.
(29) A. Malani, K. G. Ayappa, S. Murad, *The Journal of Physical Chemistry B*, 2009, **113**,13825–13839.
(30) A. Burneaub, J. Lepage, G. Mauricea, *J. Non-Cryst. Solids*, 1997, **217**,1.
(31) S. Kerisit, C. Liu, *Environ. Sci. Technol.*, 2009, **43**,777–782.
(32) Z. Lu, J. Duan, L. He, Y. Hu, Y. Yin, *Anal. Chem.*, 2010, **82**,7249–7258.

Chapter 6

Agarose Assisted Magnetically Tunable Photonic Film with Remarkable Stability

6.1 Introduction

There has been increasing interest in developing responsive photonic materials owing to their broad applications that are relevant to the controlling of colors.[1-3] Previously, we developed a magnetically tunable photonic crystal system by assembling highly charged superparamagnetic Fe_3O_4 colloidal nanocrystal clusters (CNCs) in aqueous solutions.[4-6] Stabilized by the balance of attractive (magnetic) and repulsive (electrostatic) forces, the colloids form ordered structures along the direction of the external magnetic field with a regular interparticle spacing on the order of hundreds of nanometers. As a result, the solutions strongly diffract visible light. By changing the strength of the external field, one can conveniently tune the diffraction wavelength throughout the entire visible spectrum. Further surface modification with a silica layer followed by a mild water etching (Fe_3O_4@p-SiO_2) helps in preventing the detachment of PAA molecules from the surface, enhances the stability during storage and improves the dispersity in various solvents such as alkanol solutions.[6, 7] Magnetically responsive photonic structures with significantly reduced dimensions can also be realized by fixing individual magnetic particle chains with silica coating.[8]

However, in a magnetic field with large gradient, the magnetic packing force Fm = $\nabla(\mu B)$, with μ being the induced magnetic moment and B being the strength of the external field, is effectively exerted on every particle and attracts them toward the

maximum of local magnetic gradient.[9] As a result, either the dynamic ordered assemblies of Fe_3O_4@p-SiO_2 or the fixed nanochains suffer from chain coagulation and precipitation induced by magnetic packing force, gradually ruining their photonic performance.[5] The stability of the system in a high gradient magnetic field acts as a big barrier in the practical applications. In fact, a uniform magnetic field without gradient can stabilize the photonic structures but is hard to achieve. An alternative way to enhance the stability against magnetic packing force as well as retain the tunability of the photonic structures is to employ a polymer matrix with steric block strong enough to prevent the chain aggregation. An effective polymer matrix should be optical clear, compatible with Fe_3O_4@p-SiO_2 colloids, and porous enough to allow the tunability of the periodic structures.

Herein, we present a strategy by utilizing agarose gel as a polymer matrix to stabilize the photonic structures embedded inside to counter the packing force in a magnetic field. Agarose is a well-known hydrogel-forming material that is commonly used in our daily life and scientific research.[10, 11] It is a linear polymer, made up of the repeating monomeric unit of saccharide with abundant exterior hydroxyl groups.[12] Agarose gel is able to consist up to 99.5% of water and the gel network is stabilized by the presence of water molecules bound inside the cavity. As a hydrogel, the porosity of agarose matrix is directly related to the percentage of agarose in the system.[13, 14] Gels made from purified agarose with low percentage have a relatively large pore size,[15] leaving enough space for the magnetic assembly of Fe_3O_4@p-SiO_2 colloids with preserved tunability. By taking advantage of the steric block of agarose network, the

dynamic chains of Fe_3O_4@p-SiO_2 colloids are able to counter the packing force in high gradient magnetic field against coagulation. In addition, the hydroxyl groups possessed by agarose network function as flexible anchors for the Fe_3O_4@p-SiO_2 colloids by hydrogen bonding to provide additional resistance against aggregation. The neutral charge and lower degree of chemical complexity of agarose make it less likely to influence the ionic strength in the system and interfere with the photonic performance; therefore agarose has become a preferred matrix to assist the stability of the photonic structure of Fe_3O_4@p-SiO_2 colloids. The periodic structure can be kept in a high gradient magnetic field for days without obvious decay in diffraction. The outstanding long-term stability in a magnetic field, the fast, fully reversible optical response, the compatibility with environment and the low cost suggest great potential of the agarose matrix assisted magnetically tunable photonic structures for uses in color displays, sensors or optical switches.

6.2 Experimental Section

6.2.1 Materials

Ethanol (denatured), anhydrous iron(III) chloride ($FeCl_3$), ammonium hydroxide solution (Fluka), tetraethyl orthosilicate (TEOS, 98%, Acros Organics), agarose (genetic analysis grade) and sodium hydroxide (NaOH) were purchased from Fisher Scientific. Polyacrylic acid (PAA, MW = 1800) and Diethylene glycol (DEG) were obtained from Sigma-Aldrich. Distilled water was used throughout all the experiments. All chemicals were used as received without further treatment.

6.2.2 Synthesis

Synthesis of Fe_3O_4@p-SiO_2 core/shell colloids. Superparamagnetic iron oxide nanocrystal clusters (~130 nm in diameter) in water were synthesized according to a high-temperature hydrolysis reaction reported previously.[16] Fe_3O_4@SiO_2 core/shell colloids were prepared through a modified Stöber process.[7] Typically, an aqueous solution (3 mL) containing Fe_3O_4 CNCs (ca. 25 mg) was mixed with ammonium hydroxide (28%, 1 mL) aqueous solution and sonicated for 3 minutes. Ethyl alcohol (20 mL) was then added into the mixture under strong sonication, which was further sonicated for 5 minutes. TEOS (120 μL) was injected to the solution after it was transferred into a 100 mL flask with vigorous stirring using mechanical stirrer. After 20 min, the Fe_3O_4@SiO_2 colloids were collected by centrifugation, washed with ethanol and water two times respectively and finally dispersed in distilled water (20 mL). Later, the Fe_3O_4@SiO_2 colloidal solution was heated to and kept at ~95 ^{o}C while reflux water was running to keep water from evaporation throughout the boiling process.[17] Stopped boiling after 20 minutes and the Fe_3O_4@SiO_2 colloids were cleaned several times with distilled water, and finally dispersed in distilled water (1 mL).

Synthesis of agarose assisted magnetically tunable photonic film. An aqueous agarose stock solution was prepared by dissolving agarose (0.05 g) in distilled water (10 mL) by boiling for 10 min, cooled, and kept at 70 ^{o}C. First, hot aqueous agarose solution (30 μL) was immediately added into a pre-warmed Fe_3O_4@p-SiO_2 colloidal solution (120 μL) and mixed into homogeneous solution by a short-time vortex. Then the mixture of Fe_3O_4@p-SiO_2 colloids and agarose solution was quickly transferred to a glass vessel (1cm x 4cm x 1mm) and cooled to room temperature. The sample was kept still for 30

minutes to complete the gelation of agarose solution and gradually formed a uniform magnetically tunable composite agarose film. The as-prepared agarose film showed a brown color, which was a typical color of Fe_3O_4@p-SiO_2 colloids.

6.2.3 Characterization

The UV-Vis spectra were measured by a probe-type Ocean Optics HR2000CG-UV-Vis spectrophotometer in reflection mode. The integration time was 300 ms. A Zeiss AXIO Imager optical microscope was used to observe the visible-range diffraction and the in-situ assembly of Fe_3O_4@p-SiO_2 colloids in an agarose film or in an aqueous solution under a magnetic field. The sample was sandwiched between two thin 3/4" x 3/4" cover glass slides into a thin film and then transferred onto the stage of an optical microscope for in situ observation. A NdFeB magnet was placed on another stage beneath the sample stage and could be manually moved vertically to change the magnet-sample distance. A digital SLR camera (Canon EOS Rebel T2i) was also used to record the visible-range diffraction of the agarose assisted magnetic photonic film under a magnetic field. The morphology of the obtained Fe_3O_4/p-SiO_2 colloids was characterized using a Tecnai T12 transmission electron microscope (TEM). The TEM samples were prepared by transferring one drop of sample dispersion onto a carbon-coated copper grid and then drying in air.

6.3 Results and discussion

6.3.1 Fabrication Strategy

Figure 6.1A demonstrates the fabrication process for agarose assisted magnetically

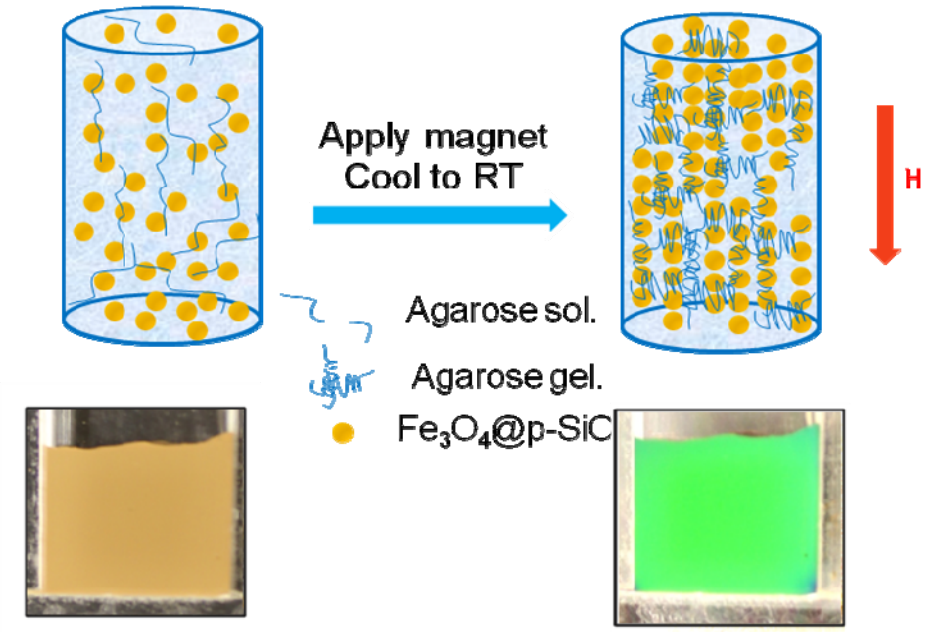

Figure 6.1 Scheme the fabrication process for agarose assisted magnetically responsive photonic hydrogel film

tunable photonic hydrogel film. Typically, agarose stock solution (0.1%) was prepared in advance and kept at 70 ^{o}C that was higher than its transitional temperature (~ 60 ^{o}C) to maintain the solution phase.[18, 19] Then a certain amount of hot aqueous agarose solution was immediately mixed with pre-warmed Fe_3O_4@p-SiO_2 aqueous solution to ensure a homogeneous span of agarose across the whole aqueous volume before it starts gelation. After transferred into a glass vessel, the mixture was naturally cooled to room temperature. During the cooling process, the internal network structure formed by hydrogen bonding inbetween the linear polymer chains and Fe_3O_4@p-SiO_2 colloids were confined inside the polymer matrix. The resulting agarose film showed a typically brown color of the Fe_3O_4@p-SiO_2 colloids embedded inside, as demonstrated by the digital photo in Figure 1B. The Fe_3O_4@p-SiO_2 particles were able to self-assembly into periodic structures inside the agarose network upon a magnetic field; thus retained their photonic properties. Bright visible light can be diffracted by the photonic structures in the agarose film and a brilliant green color across the whole film can be appreciated from digital photo in Figure 1C when a proper magnetic field strength was applied.

6.3.2 Retained Magnetically Tunable Photonic Properties

Since the addition of agarose neither affects the electrostatic repulsions inbetween colloids nor hampers their assembly within the pores of the network, a tunable optical response can be obtained from the agarose assisted magnetic photonic film in the presence of a controllable external magnetic field. Figure 2A and B compares the typical reflection spectra of an aqueous solution of 132 nm (overall diameter, with 106 nm core size and 13 nm shell thickness) Fe_3O_4@p-SiO_2 and an agarose film with the same

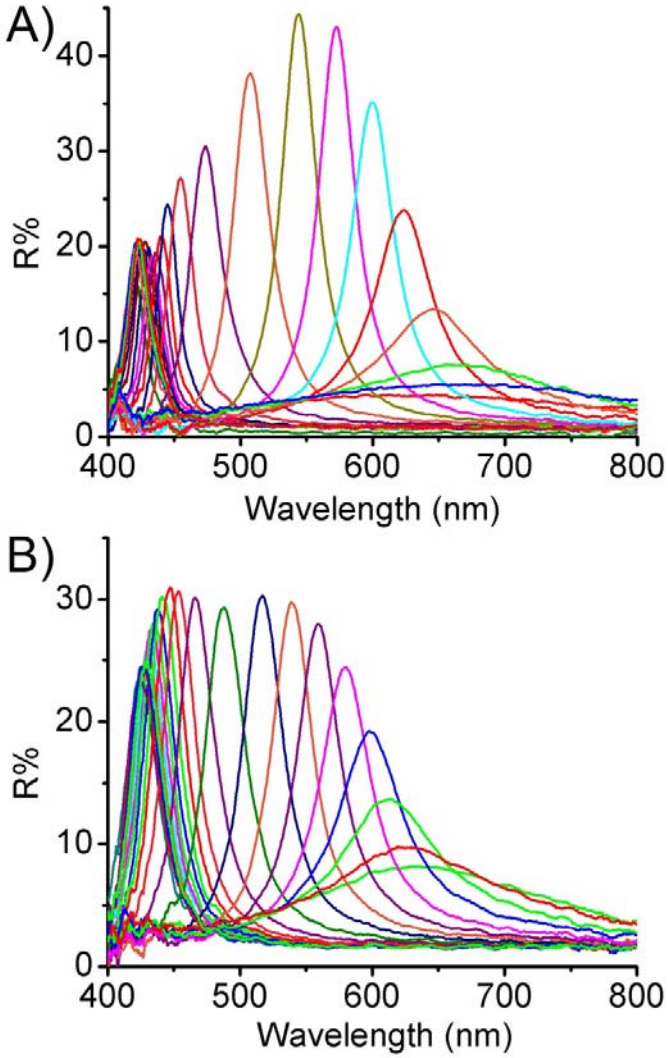

Figure 6.2 The reflection spectra of the magnetic photonic crystals on the distance of the sample from the magnet. A) in water; B) in agarose gel. Diffraction peaks blue-shift (from right to left) as the distance decreases from 4.2 to 0 cm with step size of 0.2 cm.

particles incorporated as a function of the external magnetic field strength. The optical diffraction which results from the formation of periodically ordered structures in the agarose network is similar to that in aqueous solution when in a relative weaker magnetic field. The diffraction of the magnetic agarose film shows a steady increase and blue shift in a gradual strengthened magnetic field at initial stage, suggesting that the agarose polymer chains do not affect the chaining of the colloids within the pores of the network. The diffraction intensity in agarose system drops only a little after reaching a saturation value and the peak position slightly blue-shifts with further increased magnetic field strength (Figure 6.2B), but the intensity of diffraction in aqueous system decreases after reaching the maximum and finally stays at a value much lower than the maximum intensity (Figure 6.2A). The much more stabilized intensities in agarose system when subjected in strong magnetic fields with high gradient indicate that the chain aggregation has been successfully prevented by the steric confinement from the polymer network.[20] From the reflection spectra, one can estimate an average value for interparticle spacings using Bragg's law, $\lambda=2nd\sin\theta$, as well as a surface-to-surface distance, $d_{s\text{-}s}$, by subtracting the colloid diameter.[9] It should be noted that the Fe_3O_4@p-SiO_2 colloids start to assemble at $d_{s\text{-}s}\approx 106$ nm in agarose system and reaches its maximum diffraction intensity at a spacing of ca. 37 nm while the Fe_3O_4@p-SiO_2 aqueous system starts to form ordered structures when $d_{s\text{-}s}\approx 130$ nm, and achieves its maximum diffraction intensity as $d_{s\text{-}s}$ decreases to ca. 73 nm under a steadily rising magnetic field. The respectively smaller interparticle spacing in agarose system than that in aqueous system demonstrates that stronger attractions in agarose system are needed as compensation to the additional

confinement from polymer chains in order to initiate the periodic assembly of the colloids and achieve the most ordered structure. In both cases, the colloids within a chain stop moving closer at the same $d_{s\text{-}s} \approx 29$ nm even when magnetic field is as high as ca. 4700G with gradient of 2590 G/cm, indicating that the electro repulsive forces in the two system are similar and have not been affected by the agarose polymer chain.

Differences between the repulsive forces involved in ordering Fe_3O_4@p-SiO_2 in agarose film and in water should be responsible for their dissimilar optical responses as a function of magnetic field strength. Based on Derjaguin–Landau–Verwey–Overbeek (DLVO) theory,[21] the electrostatic repulsion is the main repulsive forces in both systems, in which water is the continuous phase and the colloids are highly charged. At low magnetic field strength, the long-range electrostatic repulsion dominates the particle interactions and determines the periodicity of the assembled structures by countering the induced magnetic attraction in both cases.[7] At high magnetic field with large gradient, the assembled chain-like structures in aqueous solution are forced to coagulate by the magnetic packing force which attracts them toward the maximum of local magnetic gradient, resulting in the decrease of diffraction intensity.[5] For the Fe_3O_4@p-SiO_2 colloids in agarose film, additional repulsive forces such as steric hindrance introduced by polymer network as well as strong hydrogen bonding between the hydroxyl groups on agarose network[20] and the Fe_3O_4@p-SiO_2 surface can function as confinement against aggregation. Thus, chains are prevent from coming together once a strong magnetic field with high gradient is applied, at which the confinement from polymer network in addition to the electrostatic force are able to balance the strengthened magnetic attractions

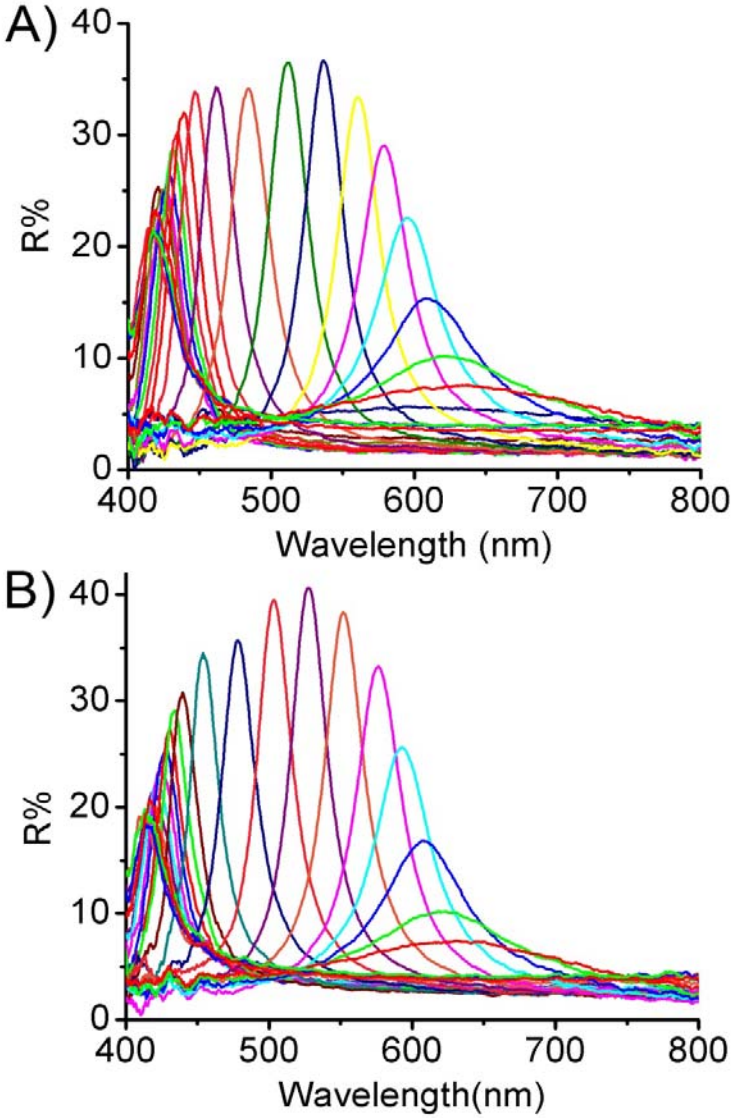

Figure 6.3 Reversible optical response of colloidal photonic crystals to varying external magnetic field. Diffraction peaks blueshift (A) as the magnet-sample distance decreases from 4.4 to 0 cm, and red shift (B) as the distance increase from 0 to 4.4 cm in step sizes of 0.2 cm in both cases.

between chains. As a result, the ordered structures in agarose film can be well preserved against the magnetic packing force, as demonstrated by the invariable peak position and the slightly reduced intensity at short wavelengths. Even when the field is further strengthened, the diffraction intensity keeps unchangeable. By comparison of the two systems, the overall maximum intensity of the diffraction peak in agarose film is reduced a little and the peak tuning rage is slightly blue-shift, due to the relative short assembled particle chains and physical confinement from the polymer network. The successful assembly of the magnetic particles in agarose film as well as the improved stability against magnetic packing force has demonstrated the possibility of incorporating such tunable photonic systems in a hydrogel network as long as additional repulsive interactions can be introduced such as steric forces or hydrogen bonding.

6.3.3 Fully Reversible Optical Response

The optical response of the agarose assisted magnetic photonic crystals to the changes in external magnetic field is fully reversible and stable. Figure 6.3A shows the blue shift of the diffraction peak of a photonic agarose film in response to an increasing magnetic field induced by reducing the distance between the magnet and the sample. The reverse process by moving the magnet away from the sample is able to red-shift the diffraction peak back to the original position (Figure 6.3B). Summarization from diffraction spectra comparison shows that the diffraction peak intensity and position can be well reproduced at a fixed sample-magnet distance with little hysteresis in either the forward or reverse direction of motion of the magnet. The slight mismatches observed in intensities and peak positions for a few points can be ascribed to inaccurate manual

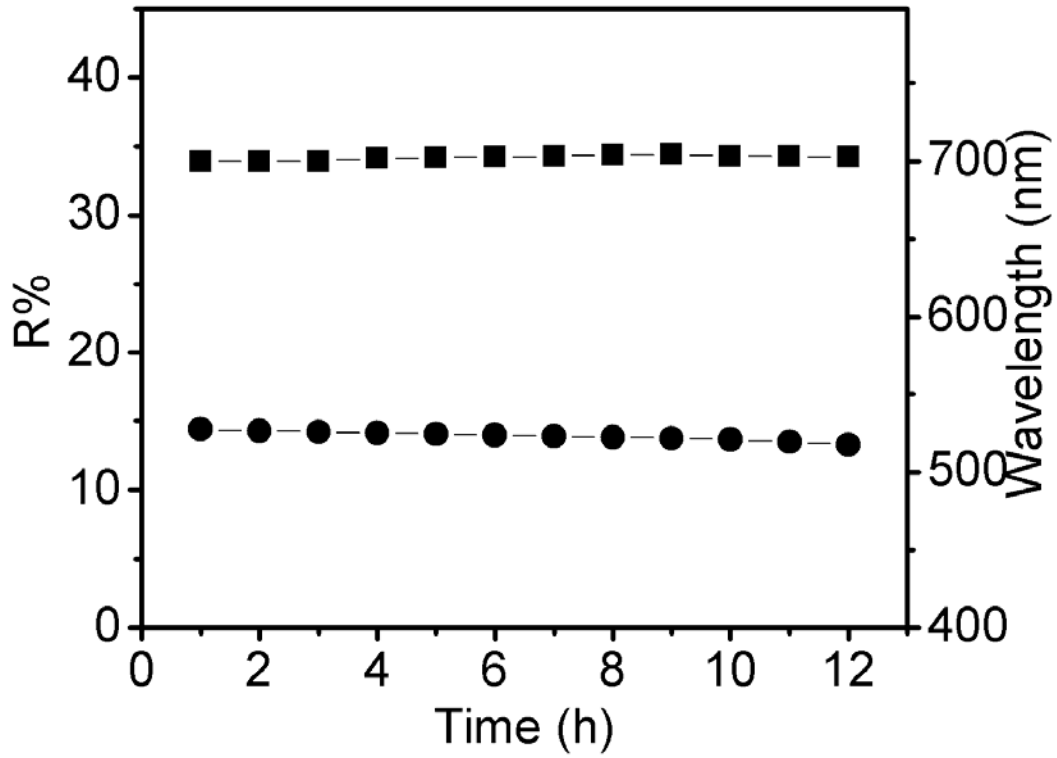

Figure 6.4 Plot of Reflectance intensity (■) and peak position (●) of agarose assisted magnetically tunable photonic film with time in an external magnetic field of 360 G with gradient of 115G/cm.

placement of the magnet, as small errors in distance will alter the magnetic field strength applied to the colloidal sample. The photonic structures are very stable and no precipitation of the CNCs can be observed after multiple tests of reversibility.

6.3.4 Ultra-high Stability in High Gradient Magnetic Field

One remarkable improvement in the agarose assisted photonic system is the excellent stability achieved while applying a magnetic field with high gradient. In aqueous system, the assembled dynamic chains will concentrate at a place with higher magnetic gradient and gradually coagulate and precipitate from solution while in agarose assisted system, the steric hindrance and hydrogen bonding introduced by the polymer network counter the packing force and retain the ordered structures with stable photonic properties.[22] As a demonstration, an agarose assisted film with Fe_3O_4@p-SiO_2 incorporated was subjected in a magnetic field with strength of 360G and 115G/cm in gradient and the corresponding photonic performance was monitored over 12 hours. The diffraction intensities and the peak positions were plotted according to the variation of time and summarized in Figure 6.4, both of which were invariable with only slight fluctuations due to the instability of the spectrometer. The dramatically improved stability in magnetic field ensures the potential of the agarose assisted tunable photonic structures for the practical applications.

6.3.5 Ultra-high Stability Studied By Optical Microscope

The significantly enhanced stability of the photonic structures against chain coagulation with the assistant of agarose gel can also been confirmed by the optical microscope study. Figure 6.5 shows the self-assembly process of Fe_3O_4@p-SiO_2 colloids

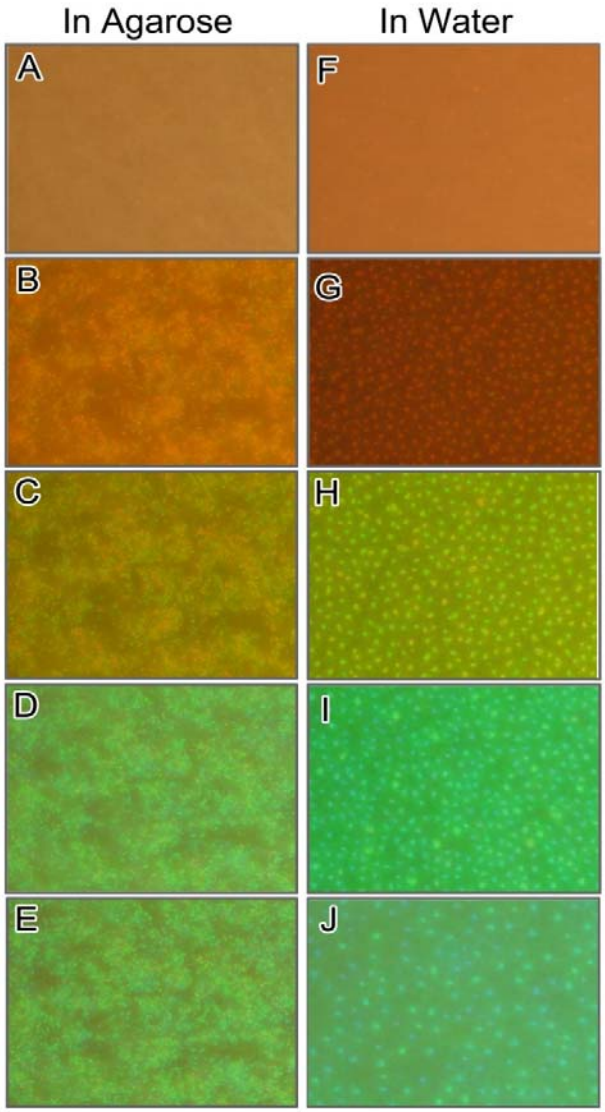

Figure 6.5 The dark-field optical microscopy images showing the self-assembly process of Fe_3O_4@SiO_2 colloids in agarose gel and in water respectively in response to varying external magnetic field strength: A,F) 141 G; B,G) 288 G; C,H) 378 G; D,E,I,J) 967 G. E, J are corresponding images of D, I after applying a magnetic field of 967 G to the samples for 5 minutes, respectively.

in agarose gel and in water, respectively, in response to varying external magnetic field strength. Samples are formed by sandwiched between two cover glasses, and then mounted on the sample stage of the microscope. A magnet is placed on another stage underneath the sample and can be moved vertically for convenient control of the sample-magnet distance. Microscopic images of Figure 6.5A-D reveal the photonic structure assembly process in agarose gel while Figure 6.5F-I show that in an aqueous system. Particles in both cases exhibit similar assembly behavior: when a weak magnetic field is vertically applied at the beginning, it is difficult to capture a clear image of the particles due to their Brownian motion.[5] When the magnetic field is gradually strengthened, the movement of particles slows down and bright red spots start to appear as chains of particles are lined up along the magnetic field. With further increase of magnetic field, the diffraction color in both systems turns from red to green, indicating a decrease in the interparticle separations. By comparing the dark-field optical microscopy images in both cases, the bright spots are not uniformly distributed in agarose gel as in water because the local concentrations of agarose across the gel are variable with different amount of particles confined inside. However, if the samples are kept in a high magnetic field, for example at ~ 967 G for 5 minutes, the bright green spots appear thicker in aqueous solution and the number density decreases gradually after a careful inspection (Figure 6.5J). The color of the bright spots changes from green to blue, indicating the formation of 3-dimensional photonic domains by the coagulation of particle chains. But for the sample in agarose gel, the distribution of the bright spots and their diffraction color are identical after applying a high magnetic field for 5 min (Figure 6.5E), indicating that the

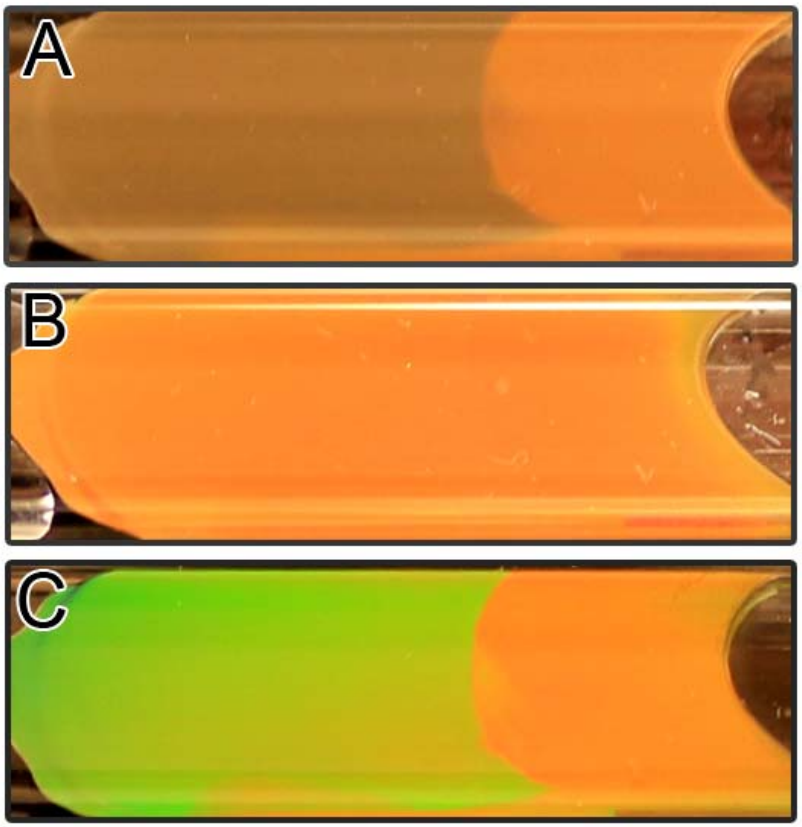

Figure 6.6 Digital images that show different diffraction colors of a patterned film under different magnetic field: A) 0 G; B) 162 G; C) 500 G.

assembled chain structures are stabilized by the agarose matrix against chain coagulations. No obvious change of the assembled structures can be observed in agarose gel even after prolonging the magnetic field application time, suggesting a great improvement in the stabilization of the photonic structures by agarose gel.

6.3.6 Potential Application as Display Unit

To further illustrate the excellent stabilization of photonic chain structures by agarose matrix, we demonstrate a simple display unit by placing two composite agarose films in contact with each other. Contrast is achieved by using Fe_3O_4@p-SiO_2 colloids of two different sizes. The patterned film is fabricated by sequentially forming the green colored film and the orange colored film using agarose solution containing Fe_3O_4@p-SiO_2 colloids of ca. 128 nm and 142 nm, respectively. If no magnetic field is applied, a low contrast can be observed from the various scattering of different sized particles (Figure 6.6A). Interestingly, the display unit is able to reach a state without any contrast across the film in a low magnetic field (~ ca. 162G) when both parts of agarose film diffract red color (Figure 6.6B). Contrast starts to appear in a stronger magnetic field and a maximum contrast between two parts can be realized by applying a magnetic field as strong as 570 G to achieve the saturation of diffraction intensity from both sets of particles (Figure 6.6C). Film with a striking green/orange contrast can thus be observed.

The diffraction of the composite film has been monitored in a magnetic field of ca. 570G with gradient of ca. 198G/cm over 18 hours. No obvious change can be detected by comparison of the digital photos in Figure 6.7: the boundary between green and orange agarose film remains clear and its position does not shift; the bright

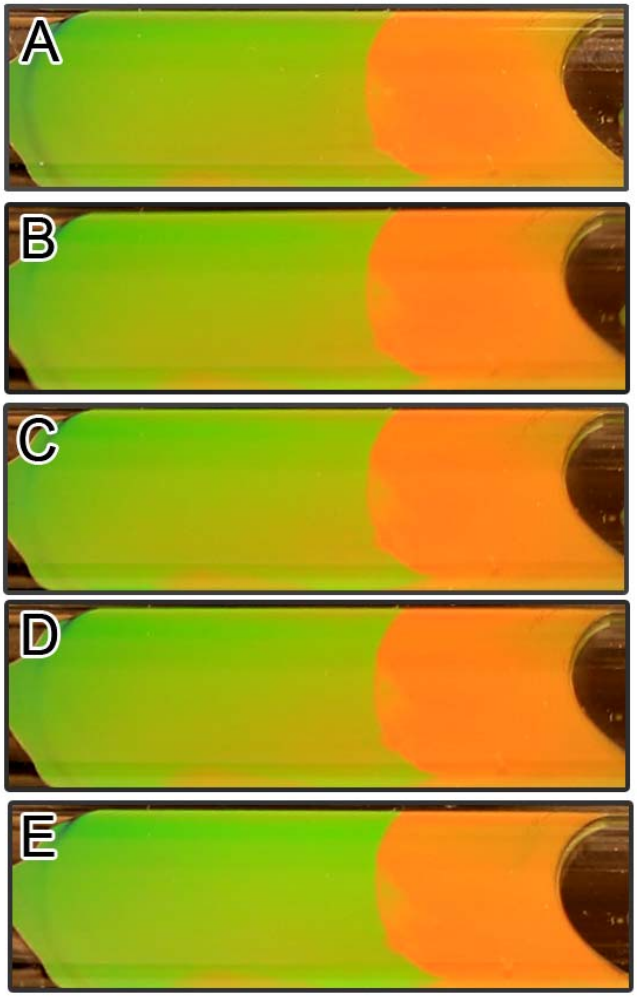

Figure 6.7 Digital images of the patterned photonic agarose film under a magnetic field of 570 G with gradient of 198 G/cm with different periods: A) 0 hour; B) 0.5 hour; C) 1 hour; D) 1.5 hours; E) 18 hours.

diffraction color in each film keep the same without fading indicating no effective migration of different sized particles inbetween different part of agarose matrix. Thus it proves that a limited diffusion of assembled particle chains in the agarose film can be achieved, which indirectly demonstrated the improved stabilization of the assembled photonic chains in magnetic field by the agarose network.

6.3.7 Effect of Agarose Concentration on Optical Performance

Although the agarose network has been proved to be able to stabilize the ordered chain-like structures in a magnetic field, the degree of confinement from the network is crucial to influence the optical performance of the agarose assisted magnetically tunable photonic film. An important parameter that affects the confinement is its pore size in the agarose gel, which is dependent on the percentage of agarose.[13, 14] The intensity and the tuning range of diffraction peaks are strongly related to the locally available free space which determines the number of periodical units within an assembled chain and the adjustable interparticle spacing. The pore size presented in the agarose gel can be increased by decreasing the percentage of agarose in the gel which can lower the steric confinement from the polymer network.[23] In contrary, the higher percentage of agarose in the system, the denser the polymer network spanned across the gel, which results in smaller pore size and limited adjustable space. The increased confinement from the agarose polymer network lowers the diffraction intensity of the photonic assemblies with a relative narrower tuning range of the diffraction peak. For example, the diffraction intensities are lowered by half in a 0.5% agarose gel (Figure 6.8D) than that in a 0.1% agarose gel (Figure 6.8A), with corresponding peak tuning range shrunk to 1/8 of that in

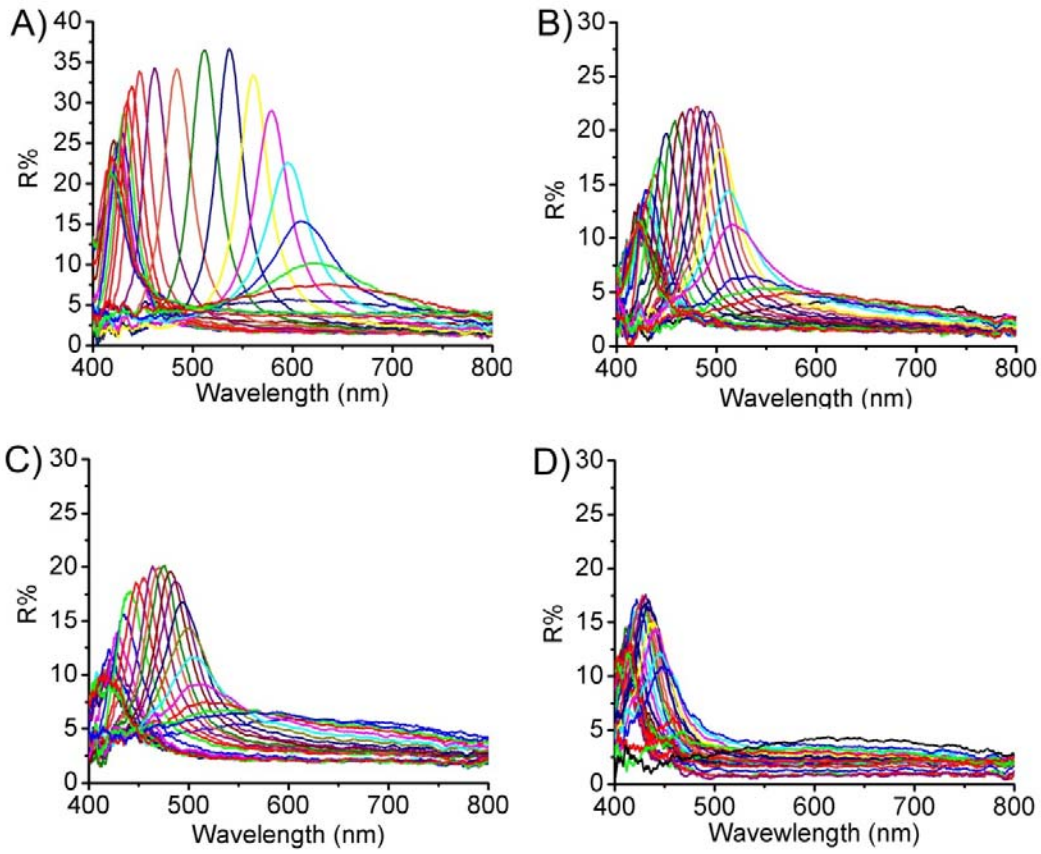

Figure 6.8 The reflection spectra of the photonic crystals in varying magnetic fields incorporated in agarose film with different agarose percentage: A) 0.1%; B) 0.2%; C) 0.3%; D) 0.5%.

0.1% agarose gel after large blue-shifts. Further increasing the percentage of agarose to larger than 0.5% will diminish the diffraction intensity since not enough effective diffraction units can be assembled in a dense agarose matrix. Up till now, the optimal percentage of agarose in assisting the photonic structure is 0.1%, lower than which the confinement by the polymer network is not enough to effectively keep chains from aggregation and the mechanic strength of the gel is too weak.

6.4 Conclusion

In summary, agarose assisted magnetically tunable photonic film have been fabricated by assembling Fe_3O_4@p-SiO_2 colloids in agarose hydrogel. Water confined in agarose networks allows good dispersion of Fe_3O_4@p-SiO_2 colloids across the film. The electrostatic repulsions from charged surface, the steric hindrance together with hydrogen bonding from the agarose network contribute to the interparticle repulsion, which can effectively counter the magnetically induced attractive force and packing force during the assembly of Fe_3O_4@p-SiO_2 colloids in agarose gel. The system reported here shows a remarkable stability against an external magnetic field with high gradient, which has not been realized before. Other features such as a fast, reversible, and tunable optical response to external magnetic fields can also be demonstrated in this system. The ability to stabilize the assemblies of the magnetic particles by a hydrogel matrix in long-term period allows the fabrication of field-responsive polymer composite films for potential applications as color displays or sensors. It is worth noting that the nontoxic agarose is a kind of temperature sensitive phase transition material which later can be utilized in temperature controlled magnetic responsive color display.

6.5 References

(1) J. Ge, Y. Yin, *Angewandte Chemie International Edition*, 2011, **50**,1492.
(2) K. Matsubara, M. Watanabe, Y. Takeoka, *Angewandte Chemie-International Edition*, 2007, **46**,1688.
(3) M. K. Maurer, I. K. Lednev, S. A. Asher, *Adv. Funct. Mater.*, 2005, **15**,1401.
(4) J. Ge, Y. Hu, Y. Yin, *Angew. Chem. Int. Ed.*, 2007, **46**,7428.
(5) J. Ge, Y. Hu, T. Zhang, T. Huynh, Y. Yin, *Langmuir*, 2008, **24**,3671.
(6) J. Ge, Y. Yin, *J. Mater. Chem.*, 2008, **18**,5041.
(7) J. Ge, Y. Yin, *Adv. Mater.*, 2008, **20**,3485.
(8) Y. Hu, L. He, Y. Yin, *Angewandte Chemie International Edition*, 2011, **50**,3747.
(9) X. Xu, G. Friedman, K. D. Humfeld, S. A. Majetich, S. A. Asher, *Chem. Mater.*, 2002, **14**,1249.
(10) S. Aront, A. Fulmer, W. E. Scott, *J. Mol. Biol.*, 1974, **90**,269.
(11) J. R. Brody, S. E. Kern, *Anal. Biochem.*, 2004, **333**,1.
(12) M. Djabourov, A. H. Clark, D. W. Rowlands, S. B. Ross-Murphy, *Macromolecules*, 1989, **22**,180.
(13) N. Pernodet, M. Maaloum, B. Tinland, *Electrophoresis*, 1997, **18**,55.
(14) M. Maaloum, N. Pernodet, B. Tinland, *Electrophoresis*, 1998, **19**,1606.
(15) J. Xiong, J. Narayanan, X. Liu, T. Chong, S. Chen, T. Chung, *J. Phys. Chem. B*, 2005, **109**,5638–5643.
(16) J. Ge, Y. Hu, M. Biasini, W. P. Beyermann, Y. Yin, *Angew. Chem. Int. Ed.*, 2007, **46**,4342.
(17) Y. Hu, Q. Zhang, J. Goebl, T. Zhang, Y. Yin, *Phys. Chem. Chem. Phys.*, 2010, **12**,11836.
(18) J. Narayanan, J. Xiong, X. Liu, *Journal of Physics: Conference Series*, 2006, **28**,83.
(19) G. A. Griess, K. B. Guiseley, P. Serwer, *Biophys. J.*, 1993, **65**,138.
(20) E. M. Johnson, D. A. Berk, R. K. Jain, W. M. Deen, *Biophys. J.*, 1996, **70**,1017.
(21) Y. Xia, B. Gates, Y. Yin, Y. Lu, *Adv. Mater.*, 2000, **12**,693.
(22) R. J. Phillips, W. M. Deen, J. F. Brady, *J. Colloid. Interface Sci.*, 1990, **139**,363.
(23) V. Yamakov, A. Milchev, *Phys. Rev. E: Stat., Nonlinear, Soft Matter Phys.*, 1997, **55**,1704.

Chapter 7

Bistable Magnetically Tunable Photonic Film

7.1 Introduction

The responsive photonic crystals have attracted broad interest for many potential applications, such as displays, chemical and biochemical sensors, decoration and optoelectronic devices.[1-4] Particularly interesting is the reversible color transformations in a material due to external chemical or physical influences like variations in temperature,[5] electrical field,[6] magnetic field,[7] PH[8], or etc. On the basis of the special behavior, photonic paper[9-11] and color displays[12] that are based on photonic crystals have shown their own advantages over the commercialized technologies in display: One benefit from photonic papers/displays is that they are brilliant and free of glare in sunlight, which is superior to the other display technologies for outdoor usage.[9] For example, each pixel in E Ink display[12, 13] is limited to a single primary color, which makes the color images inconvenient to generate and lack of intensity. Another advantage is that the structural colors of photonic paper are usually more durable than traditional pigments and dyes.[13-15]

In order to achieve practical application, two major obstacles need to be overcome. First, it requires samples over large length scales free from defects and easy to make. However, most self-assembly photonic crystal systems suffer from point defects and grain boundaries.[16] The methods developed to combat these disorders involve a slow and complicated process which typically requires state-of-the-art nanofabrication techniques that are expensive and not scalable or still produce a large number of intrinsic defects.[10,

[17, 18] The newly developed M Ink solves the above-mentioned problem and can obtain high-resolution patterning of multiple structural colors within seconds, but the color is not allowed to change once the structure is fixed.[19] Second, application in displays rely on materials whose color states are bistable in which the image they hold requires no energy to maintain but needs energy to change.[20] However, this cannot be achieved through conventional self-assembly methods alone. In fact, extra stimulus is utilized to initiate the switch between the bistable states, such as an external electrical field,[21] temperature,[22] or solvent ink[23]. For example, the color displayed in the photonic papers is usually controlled by volatile solvent or salt ink which is applied to swell the polymer matrix, change the periodicity of the photonic structure, and eventually the color of inked region.[9, 10] The color can disappear when the solvent evaporates which makes the state not bistable and the responsive time to reach the equilibrium state is relative long. Since displays rely on materials whose color states are bistable it is preferable to utilize a single material to give all the necessary colors for a display while keeping its bistability under the control of an external stimulus.

In chapter 6, we have discussed a strategy to stabilize magnetic responsive photonic structures without sacrificing their tunability and photonic intensities by utilizing agarose gel as a polymer matrix.[24] These magnetic particles confined in the agarose pores undergo an instantaneous process in an external field and self-assemble into periodic arrays to diffract light. This process allows their rapid assembly into large-area photonic film with brilliant diffraction color. The range of the diffraction color can be controlled by the external field strength and cover the whole visible range. Benefiting

from the steric barrier from the agarose network, long term stability can be obtained as the chainlike structures embedded inside agarose network are stabilized from aggregation induced by magnetic packing force.[25, 26] Thus it provides a possibility to form a state that can display color and require no energy to maintain. Since a mixture of magnetic and non-magnetic colloids can undergo phase separation in an external magnetic field by packing force,[27] it is possible that a similar concentration gradient can be built up between magnetic and non-magnetic colloids in agarose solution before its gelation. With the assistance of agarose after its gelation from solution, the concentrated magnetic colloids can be confined in localized layer, and still exhibit the magnetic tunable photonic properties. In addition to being an excellent hydrogel matrix for stabilization, agarose has a special property with its sol/gel transition point at 60 ^{o}C which provides the potential in the construction of bistable states in a composite photonic agarose film.[28]

In this chapter, we demonstrate a reliable and rapid approach for the fabrication of a bistable magnetic tunable photonic film with bilayered structure that exhibits two stable states at room temperature. We show that by taking advantage of agarose gel as a stabilizing polymer host and active matrix, the film is allowed to switch between colored photonic state ("on" state) and white background state ("off" state), wherein an external alternating magnetic field enables us to precisely and conveniently manipulate the diffraction color in "on' state. Generally, the agarose matrix facilitates the phase separation of Fe_3O_4/p-SiO_2 and PS colloids in an external magnetic field as well as maintains the tunable photonic properties in the corresponding magnetic layer. The layer with Fe_3O_4/p-SiO_2 accumulated is used as the color generated photonic layer while the

layer with PS colloids enriched is used as a blank background. In an "on" state, tunable diffracted visible light can be obtained from the top view. The diffracted color is precisely and conveniently manipulated by the external magnetic field when in "on" state. If temperature of the film is increased to dissolve the agarose gel into solution, the magnetic colloids can be switched to the bottom layer upon the application of an opposite magnetic field. Thus only pure white color can be observed in the "off" state as the PS colloids gathering at the top layer can screen the diffraction from the bottom magnetic photonic layer. This bilayered magnetic tunable photonic film exhibits excellent bistability and cycle stability, which shows great potential in an energy-efficient display with convenient color control, and can be utilized in the applications in outdoor advertising billboards, or color displays in e-book products.

7.2 Experimental Section

7.2.1 Materials

Ethanol (denatured), anhydrous iron (III) chloride ($FeCl_3$), ammonium hydroxide solution (Fluka), tetraethyl orthosilicate (TEOS, 98%, Acros Organics), agarose (genetic analysis grade) and sodium hydroxide (NaOH) were purchased from Fisher Scientific. Polyacrylic acid (PAA, MW = 1800), acrylic acid (99%), diethylene glycol (DEG), styrene (Reagent Plus grade), methyl methacrylate (99%) and ammonium persulfate (A. C. S. reagent grade) were obtained from Sigma-Aldrich. Distilled water was used throughout all the experiments. All chemicals were used as received without further treatment.

7.2.2 Synthesis

Synthesis of Fe_3O_4/p-SiO_2 core/shell colloids. Superparamagnetic iron oxide nanocrystal clusters (~130 nm in diameter) in water were synthesized according to a high-temperature hydrolysis reaction reported previously.[29] Fe_3O_4/SiO_2 core/shell colloids were prepared through a modified Stöber process.[30] Typically, an aqueous solution (3 mL) containing Fe_3O_4 CNCs (ca. 25 mg) was mixed with ammonium hydroxide (28%, 1 mL) aqueous solution and sonicated for 3 minutes. Ethyl alcohol (20 mL) was then added into the mixture under strong sonication, which was further sonicated for 5 minutes. TEOS (120 μL) was injected to the solution after it was transferred into a 100 mL flask with vigorous stirring using mechanical stirrer. After 20 min, the Fe_3O_4/SiO_2 core/shell colloids were collected by centrifugation, washed with ethanol and water two times respectively and dispersed in distilled water (20 mL). Later the Fe_3O_4/SiO_2 core/shell colloidal solution was boiled in water at 95 °C for 20 minutes and washed with water two times and finally dispersed in distilled water (2 mL).

Synthesis of Polystyrene (PS) colloids. Monodisperse Polystyrene spheres with size of 350 nm were synthesized through an emulsion polymerization method.[27] Distilled water (50 mL) was degassed with Nitrogen for 30 min at first. Styrene (3.3 mL), methyl methacrylate (0.5mL) and Acrylic acid (0.5 mL) were then injected into the above water. The mixture solution was further degassed with nitrogen for 30 min and heated to 70 °C later. Ammonium persulfate (0.5 g) in distilled water (1 mL) was injected to initiate the polymerization. The reaction mixture was kept stirring at 70 °C for 7 h before cooled down to room temperature. The as-obtained polymer spheres were washed with DI water

several times and finally dispersed in DI water. The volume fraction of polymer spheres was about 5%.

Synthesis of agarose assisted bi-stable magnetically tunable photonic film. An aqueous agarose stock solution was prepared by dissolving agarose (0.05 g) in distilled water (10 mL); this colorless mixture was heated at 90^{o}C in a hot water bath for 20 min, cooled, and kept at 70 ^{o}C. First, hot aqueous agarose solution (30 μL) was immediately added into a pre-warmed mixture of Fe_3O_4/p-SiO_2 colloidal solution (110 μL) and PS colloidal solution (10 μL), and mixed into homogeneous solution by a short-time vortex. Then the as-prepared mixture was quickly transferred to a glass vessel (1cm x 4cm x 1mm) and cooled to room temperature with a cubic magnet (2"× 2" × 0.5") right on the top of the vessel. The sample was kept still for 30 minutes to complete the gelation of agarose solution and gradually formed a uniform two layered composite film with a white PS-agarose layer at the bottom and a magnetically tunable agarose layer on the top. The color of the magnetic layer can be tuned by an external magnetic field strength. This state is defined as "ON" state.

Switch between the bi-stable states of magnetically tunable photonic film. To switch the magnetically tunable layer from the bottom to the top of the composite film, the glass vessel with the sample film inside was heated in a water bath of 80 °C. After the composite agarose gel become solution, the vessel was cooled to room temperature with a cubic magnet beneath. The magnetic colloids were pulled to the bottom by the magnetic force and the PS colloids were driven to the top, resulting in a two-layered composite agarose film. This state is defined as "Off" state. The composite film can be

switched between “on” and “off” states by reheating and change the direction of external magnetic field.

Fabrication of a Patterned Bistable Composite Film. PS colloids were separated from water (1.5 mL) and redispersed into EG (0.25 mL) under sonication. Their EG solution was mixed with silicone elastomer prepolymer (4 g, Sylgard 184) and curing agent (0.4 g) by mechanical stirring (300 rpm). A two-step process was used to prepare patterned PDMS composite film. First, steel templates of letters were placed in the Petri dish, and PDMS precursor 1 (containing PS colloids in EG) was added to fill the Petri dish around the template. After curing, the template was removed and PDMS precursor (containing PS and Fe_3O_4/p-SiO_2 colloids) was added to fill the cavity left by the template. The film was finally cured overnight at room temperature.

7.2.3 Characterization

The morphology of the obtained Fe_3O_4/p-SiO_2 colloids and PS were characterized using a Tecnai T12 transmission electron microscope (TEM). The TEM samples were prepared by transferring one drop of sample dispersion in water onto a carbon-coated copper grid and then drying in air. The UV-Vis spectra were measured by a probe-type Ocean Optics HR2000CG-UV-Vis spectrophotometer in reflection mode. The integration time was 300 ms. A digital SLR camera (Canon EOS Rebel T2i) was used to record the visible-range diffraction of the agarose assisted bi-stable magnetic photonic film under a magnetic field.

7.3 Results and discussion

7.3.1 Fabrication Strategy

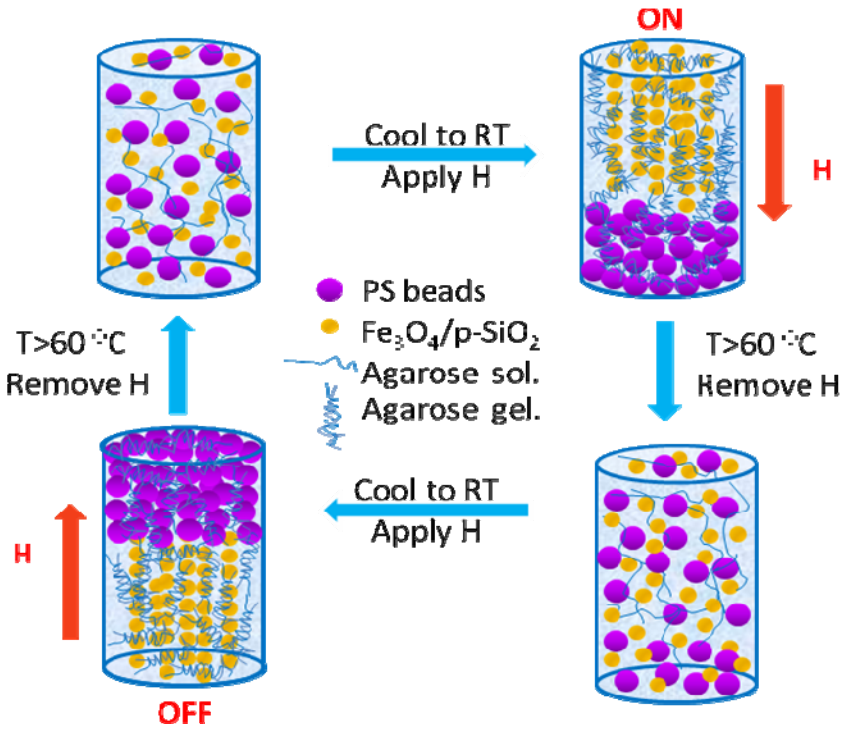

Figure 7.1 Scheme for fabrication of the bistable magnetic tunable photonic film and the switch between "on" and "off" states.

In this chapter, we present a new type of bistable magnetically tunable photonic film with layered structure, in which switchable color information can be turned "on" or "off" by controlling the component in the corresponding layers and the color of the film in the "on" state is able to be tuned by the external magnetic field. As illustrated in Figure 7.1, the basic idea is to create a bilayered film with bistable states available by embedding magnetic Fe_3O_4/p-SiO_2 colloids and nonmagnetic PS colloids into a hydrogel polymer matrix. The component in the surface and bottom layer of the film can be switched between magnetic photonic structures and nonmagnetic PS colloids with the assistant of an external magnetic field. Before the polymer matrix is gelated, the mixed colloids of PS and Fe_3O_4/p-SiO_2 can be separated by an induced magnetic packing force. Once the gelation is completed, the external magnetic field can no longer alter the component of the layered film but only change the color in the Fe_3O_4/p-SiO_2 concentrated layer. Thus in an "on" state, as a magnetic field is applied to the top of the film before the hydrogel gelation, magnetic particles are drawn to the top layer and driven the PS colloids to concentrate at the bottom layer. After gelation of the hydrogel matrix, concentrated magnetic colloids confined in the top layer can diffract tunable visible light in a magnetic field as can be visually seen from a top view. If the polymer matrix is dissolved back into solution, the magnetic colloids can be switched to the bottom layer when applying an opposite magnetic field. At the same time, PS colloids are pushed to the top with only white color to be observed and the diffraction from the bottom magnetic photonic layer can be fully screened, as in an "off" state. The bistable film is allowed to be switched between "on" and "off" states discretionally. Agarose here

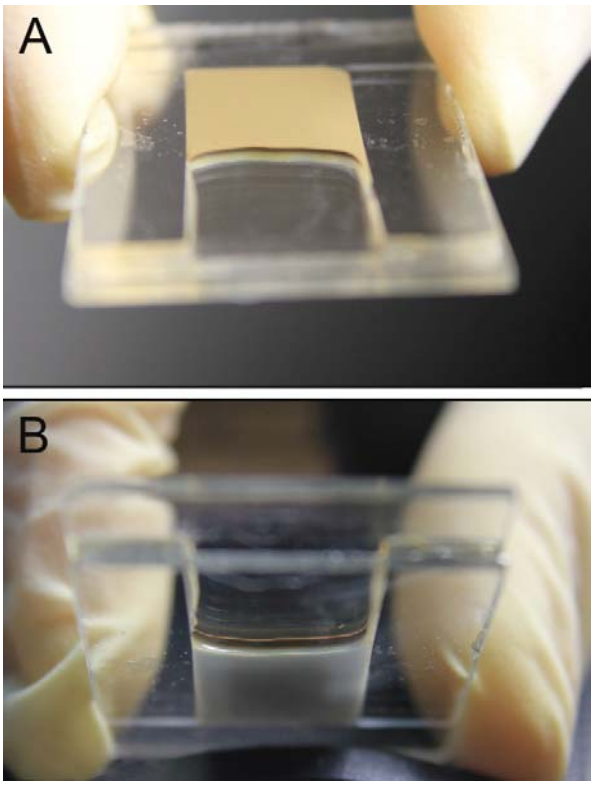

Figure 7.2 Digital photos of a bistable photonic film with well separated layered structure in a vessel: A) top view; B) bottom view.

is chosen as the hydrogel matrix for the bistable film because it has been previously demonstrated to be an excellent compatible polymer matrix to enhance the stabilization of the photonic structures embedded inside without impairing the photonic intensities and tunability.[24] In addition to the mentioned properties, agarose is selected because of its proper sol/gel phase transition point around 60 °C. When heated, the agarose matrix dissolves, allowing the switch of the colloidal component in the bilayer structure directed by an external magnetic field. Therefore a temperature activated magnetic directed bilayered film with switchable color information can be simply fabricated and tunable color in the "on" state is available by control of the magnetic field strength.

The bistable photonic film is fabricated through the fast magnetic packing force induced phase separation of magnetic Fe_3O_4/p-SiO_2 colloids and non-magnetic PS colloids in agarose solution, followed by a cooling process to fix the bilayer structures within the agarose gel matrix. Since the gradient of the magnetic field induces a packing force $F_m = \nabla(\mu B)$, where B is the strength of magnetic field, it drives magnetic particles to move toward regions of maximum magnetic field and nonmagnetic particles toward regions of minimum magnetic field, resulting in concentration gradients in mixed magnetic (Fe_3O_4/p-SiO_2) and nonmagnetic (PS) colloidal suspensions.[27] Thus, bilayered film with Fe_3O_4/p-SiO_2 and PS colloids separated from each other can be obtained after the gelation of agarose solution with fixed components in each layer. As shown in Figure 7.2, the two layers are uniformly separated which can be appreciated by the distinct boundary. The brown colored layer represents the Fe_3O_4/p-SiO_2 embedded layer while the white one indicates the PS inside.

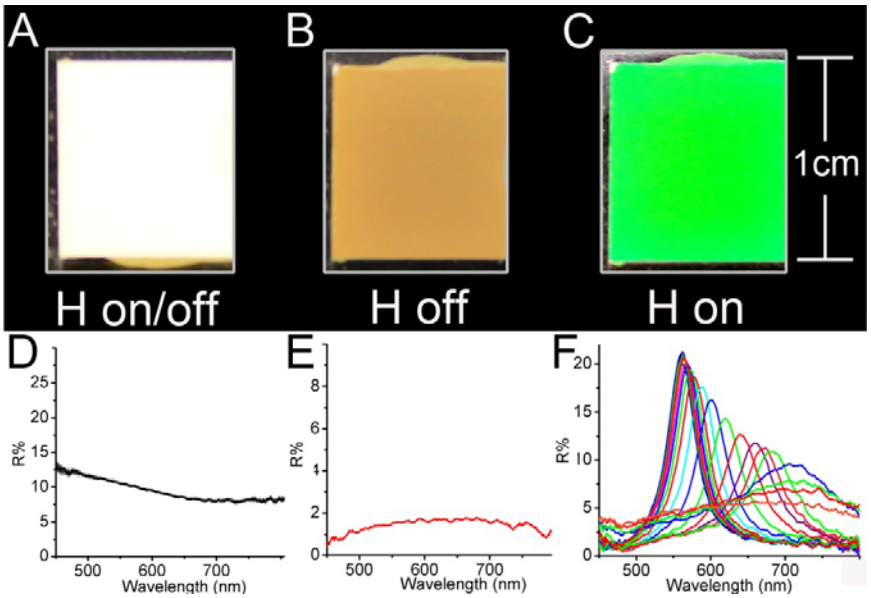

Figure 7.3 Digital photos of the as-prepared bistable photonic film in "ON" state: A) bottom view of the film with or without an external magnetic field applied; B) top view of the film without a magnetic field applied; C) top view of the film with a magnetic field. The corresponding reflection spectra: D) none diffraction peaks from bottom layer of the film with or without an external magnetic field applied; E) none diffraction peaks from top layer of the film when magnetic field is absent and F) diffraction peaks from top layer of the film when magnetic field is applied.

7.3.2 Distinct Optical Properties between "on" and "off" States

When the PS colloids are at the top, which is the "off" state, only pure white color can be obtained from the diffraction of PS colloids no matter the external magnetic field is on or off (Figure 7.3A). The corresponding reflection spectra in Figure 7.3D demonstrate that no obvious reflection peak but a relative strong broad reflection across the whole spectrum is observed as a function of the external magnetic field strength in "OFF" state. As the magnetic colloids are switched onto the top layer of the film, which is defined as the "on" state, strongly diffracted visible light can be observed when an external magnetic field is applied (Figure 7.3C). It is because the Fe_3O_4/p-SiO_2 colloids trapped in agarose matrix are able to form chainlike structures with tunable regular interparticle spacing of a few hundred nanometers along the external magnetic field. The tunability is well preserved due to the relative large pore size in the agarose matrix, allowing the change of the interparticle spacing, as demonstrated by the reflection spectrum in Figure 7.3F. The diffraction intensity increases steadily with increasing external field strength until reaching a saturation value. Further increasing the strength of the magnetic field slightly blue-shifts the peak position and the peak intensity drops only a little, which is comparable to that in the pure Fe_3O_4/p-SiO_2 colloids embedded agarose film. However, the color of the film in the "ON" state is brown without external magnetic field, resulting from the original of Fe_3O_4/p-SiO_2 colloids (Figure 7.3B). The corresponding reflection spectrum is recorded in Figure 7.3E, in which a very low and broad reflection is obtained across the visible range. Thanks to this recent discovery of agarose as the switchable matrix and the magnetically tunable assembly techniques, the

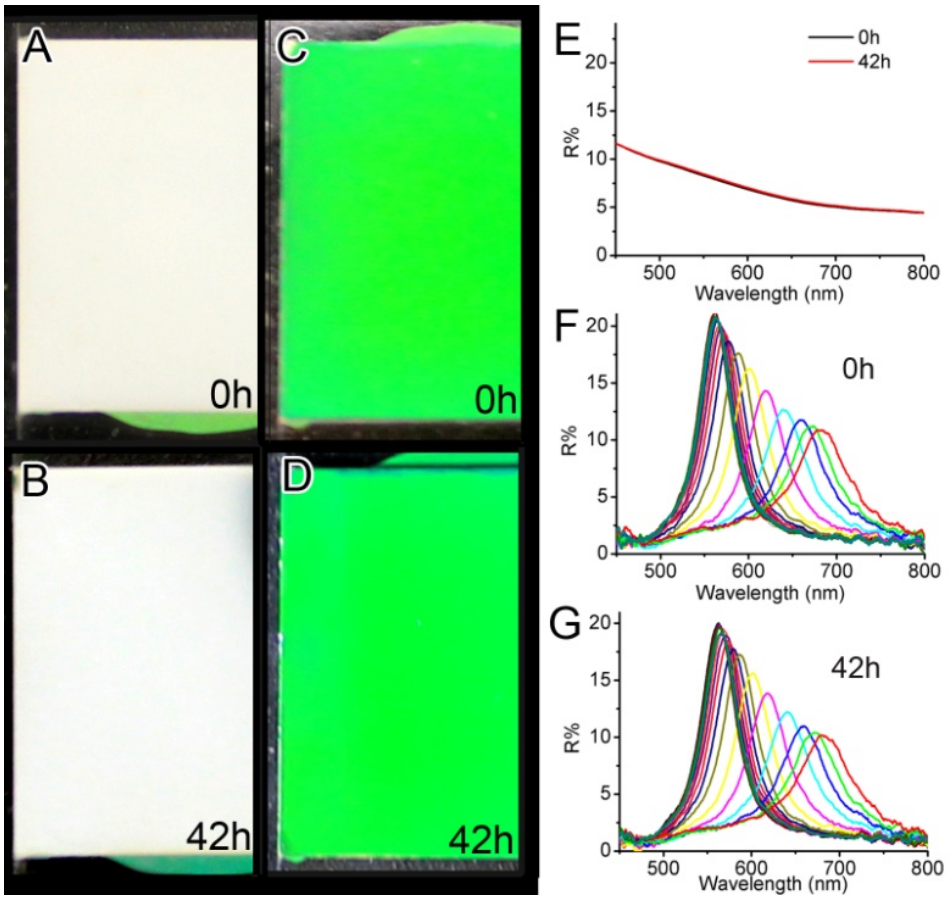

Figure 7.4 Digital photos and reflection spectra of a bistable photonic film in 1.0 × 0.5 × 0.1 cm^3 glass cells in an external magnetic field with strength of 350 G: A) in "off" state at 0 h; B) in "off" state at 42 h; C) in "on" state at 0 h; D) in "on" state at 42 h. The corresponding reflection spectra: E) display non diffraction peaks in "off" state before and after 42 h, F) display diffraction peaks at 0h and G) at 42 h in the "on" state.

tunability of the diffraction color in this bistable photonic film is well-preserved while the color information of the film can be switched. This process is easier to make large area photonic film than the conventional assembly processes which involve the close packing of colloids, the infiltration of monomers, photopolymerization. In addition, it has better control in precisely tuning the color of the film by simply using a magnet, which is hard to achieve by the conventional methods using a swelling and deswelling process.

7.3.3 Excellent Bistability in External Magnetic Field

For the potential application in display, stability of the bistable states is one of the most important parameters for evaluating photonic films.[14] Owing to the utilization of agarose gel as a stabilizing polymer matrix, the bistable magnetically tunable photonic film has achieved superior stability in the presence of an external magnetic field.[24] When the bistable film is switched to the "on" state, Fe_3O_4/p-SiO_2 colloids are confined in the top layer of the agarose matrix and a bright diffraction color can be obtained from the top view when a proper magnetic field is applied. By monitoring the diffraction of the photonic layer as well as the bottom PS layer during a period of time, the stability of the film in their bistable states can be tested. Figure 7.4 compares the time evolution of the diffractions in a magnetic field for the top layer as well as the bottom of the film respectively. The diffraction of a bilayered photonic film with the size of 1 cm × 0.7 cm in a magnetic field strength of 350 G was monitored in the "on" state through a period of 42 hours. By comparison of the digital photos of the top or the bottom layer of the film before and after the monitoring period, no observable change can be detected. Figure 7.4A and B verify that the PS colloids confined in the bottom layer of the film are

stabilized without any Fe_3O_4/p-SiO_2 colloid diffused in because only pure white color other than mixed brown color can be observed visually. The reflection spectra of the PS concentrated layer were also compared, and the similar diffraction pattern (Figure 7.4E) further demonstrated that pure PS colloids were the main component in the bottom layer. The same brilliant green color from figure 7.4 C and D also verifies that the diffusion of PS colloids from the bottom to the top layer of the film was limited and the ordered assemblies of the Fe_3O_4/p-SiO_2 colloids trapped inside the agarose networks were well preserved. The similar diffraction peak and tuning range from the reflection spectra (Figure 7.4F) also prove the excellent stabilities of the as-fabricated film in the presence of an external magnetic field. The slight fluctuations observed in intensities and peak positions might be due to inaccurate manual placement of the magnet, as small errors in distance will alter the magnetic field strength felt by the sample. It turns out that a film fabricated by this approach has excellent bistability and preserve dynamic tunability in the magnetic photonic layer with the help of steric barriers from agarose networks to trap the assembled particles within the localized pores from migration.

7.3.4 Thermal Erasable Optical Properties

One unique advantage deriving from the bistable tunable photonic film is the ability of switching between “on” and “off” states while keeping a stabilized photonic performance in the magnetic layer in multicycle test. In each cycle to switch the film from “on” to “off”, brief heating in a water bath above 60°C is required to dissolve the agarose gel into solution phase, allowing the driving and aligning of magnetic colloids upside down using magnetic fields. After the system is cooled to room temperature, the

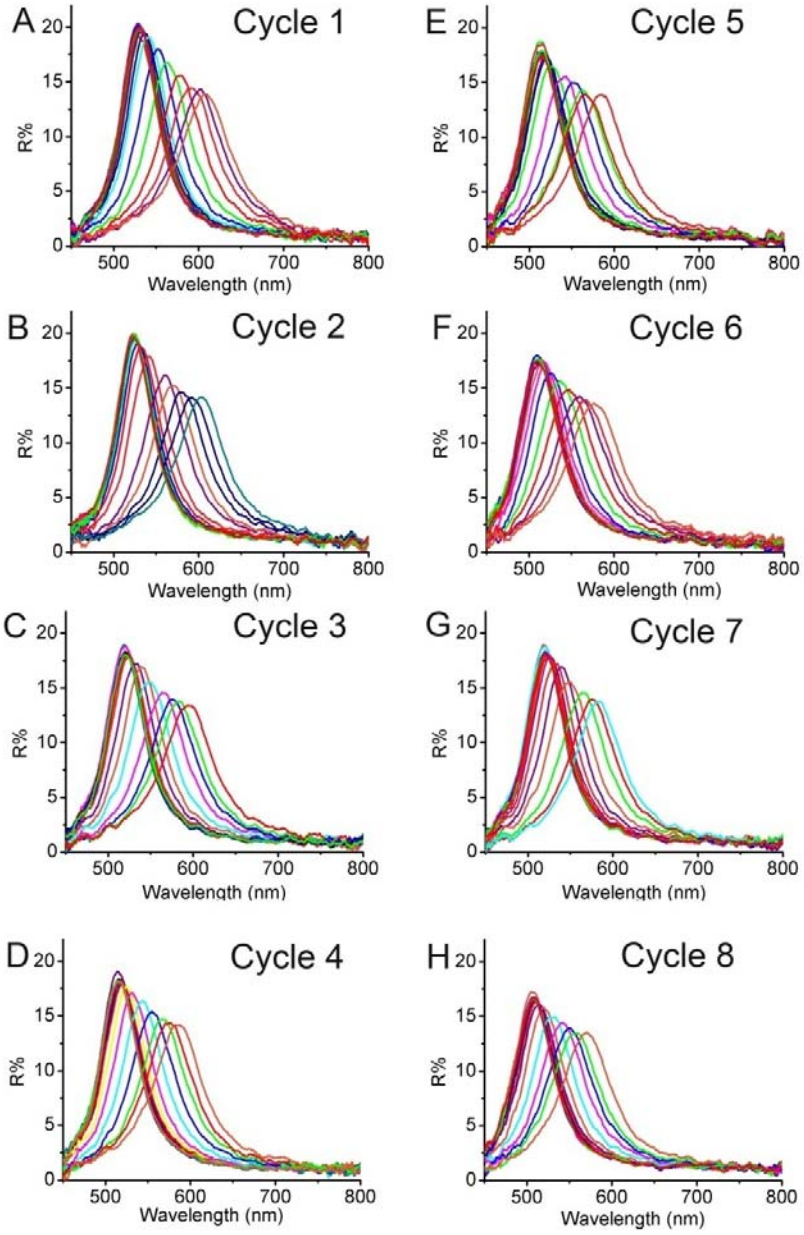

Figure 7.5 The reflection spectra of the bistable magnetic tunable photonic film in "on" state in varying magnetic fields at different cycles test: A) cycle 2; B) cycle 4; C) cycle 6; D) cycle 8; E) cycle 10; F) cycle 12; G)cycle 14; F) cycle 16.

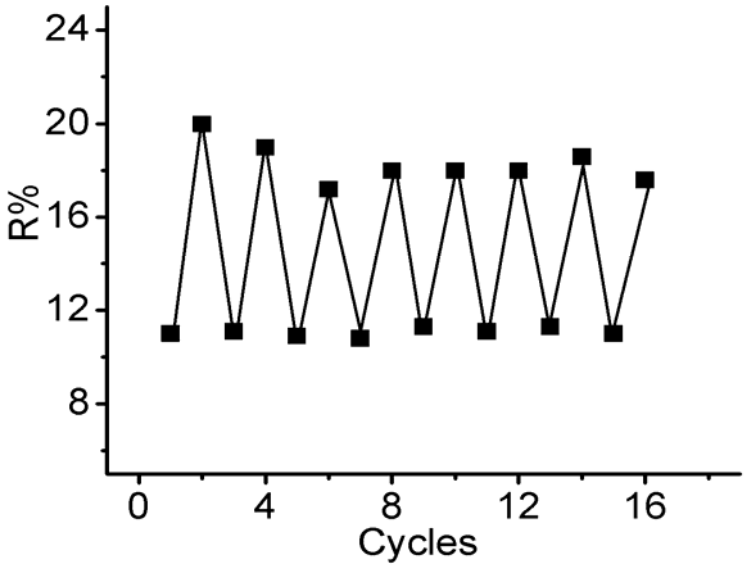

Figure 7.6 Plot of the diffraction peak intensities from the top layer of the bistable photonic film at wavelength of 520 nm against the cycle times.

agarose solution gelates and the component colloids in each layer are locally confined so that magnetic colloids concentrate in the bottom layer while PS colloids accumulate on the top of the film. The color information switches to pure white which screens the tunable diffraction from the bottom photonic layer in an external magnetic field. The state can be held without the need of additional energy other than a magnetic field. Reheating the agarose film and applying a magnetic field in an opposite direction will erase the color information by switching magnetic colloids back to the top layer with colored diffraction in an "on" state again. Figure 7.5 compares the 8 diffraction spectra of the film in the "on" states during a multicycle test of 16 times. The diffraction peaks in response to an increasing magnetic field in each cycle demonstrate that the overall maximum intensity of the diffraction peak is quite consistent with each other: only slight reduce in diffraction intensities and a tiny blue-shift in the peak tuning rage. It can be ascribed to the small variation of the ionic strength in the system because cations such as sodium ions from the vessel can dissolve into the solution during each heating process. The diffraction information during the switchable cycles has been summarized in Figure 7.6, in which the diffraction peak intensities at wavelength of 520 nm have been plotted against the cycle times. The diffraction intensities are able to switch between the "on" and "off" states and the intensities regarding the "off" states keep quite consistent at 10% while the intensities vary slightly around 18% in all the "on" states. The durability of the bistable tunable photonic film in cycles of switch indicates the potential application in erasable color display.

7.3.5 A Simple Demonstration for Color Display

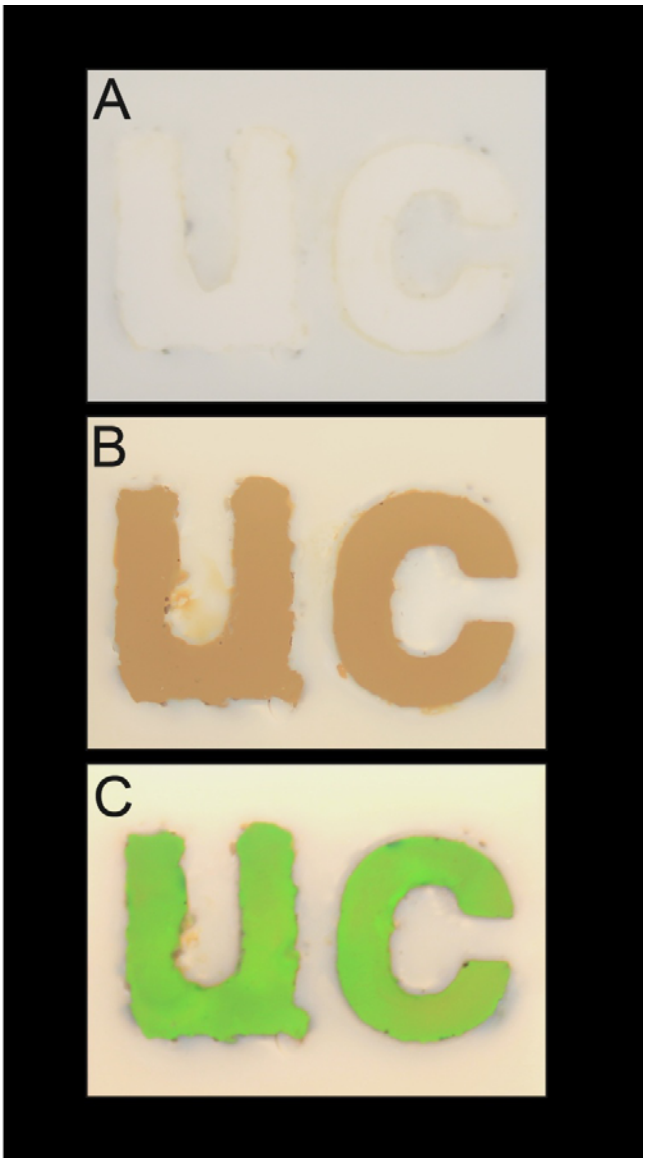

Figure 7.7 Digital photos of a patterned bistable photonic film that can display tunable colored letters in the "on" state upon the application of an external magnetic field: A) "off" state with no contrast all over the uniform white film even in the presence of magnetic field; B) "on" state without magnetic field; C) "on" state with magnetic field.

To further illustrate the potential application of the bistable magnetic responsive composite agarose film, we demonstrated a simple display unit by patterning agarose films through molding. We fabricated a 2×4 cm patterned film by sequentially forming the white background using PS/PDMS mixtures and the letters using agarose containing mixture of PS and Fe_3O_4@SiO_2 colloids. Figure 7.7 shows digital photos of patterned photonic film switched inbetween "on" and "off" states with or without an external magnetic field. When the patterned letters were in "off" states, PS colloids accumulated in the top layer of the letters. No color contrast can be achieved and a uniform white film was observed in figure 7.7A except for the small roughness at the edges of letters caused by the molds. Contrast was achieved by switching the letters to the "on" state: in the absence of external magnetic fields, as shown in Figure 7.7B, the sample showed essentially an obvious contrast between brownish letters and the white background. However, letters with a striking green/ white contrast can be observed when a 2″×2″×0.5″ NdFeB magnet is applied and the color of the letters can be manipulated by an external magnetic field. The maximum contrast between the letters and the background can be realized by applying a magnetic field strong enough to achieve saturation of the diffraction intensity from the magnetic particles (Figure 7.7C). Benefitting from the magnetic assembly, the letters have almost no defects in photonic structure and can be fabricated on a large scale easily. Color displays with desired pattern in large area can easily be obtained if a specially designed electromagnetic field with patterns and parallel field direction throughout is available. It is expected that the use of an IR heating system

with digital designed pattern may be able to uniformly and controllably produce digitally designed color patterns.

7.4 Conclusion

In summary, a bistable color-reflective magnetic tunable photonic film with thermally erasable property can be fabricated through phase separation process induced by an external magnetic field and further stabilized by agarose gel. The fabricated film has bilayered structure in which one layer accumulated with Fe_3O_4/p-SiO_2 colloids while the other concentrated with PS colloids. The diffraction color of the magnetic layer can be controlled by an external magnetic field and cover the whole visible range. The well-known temperature dependent sol/gel phase transition of agarose and the magnetically controllable phase separation enable the composite film to switch inbetween "on" and "off" states, in which tunable colors can be obtained in the "on" state while only white background can be observed in the "off" state. The bistable states have excellent stability at temperatures under the phase transition point of agarose. However, when the heating temperature exceeds phase transition temperature, the bilayered state is disturbed and can be transformed to the other state by directing the external magnetic field. This bistable photonic film exhibits excellent cycling stability and duration over a long period. The simple fabrication process, easy control over the color change, the superior stability over cycling and time, the low cost and energy saving properties allows the potential application in the color-tunable outdoor display with high-contrast, sunlight readability, and low-power performance when a wide temperature range tolerance is necessary.

7.5 References

(1) C. I. Aguirre, E. Reguera, A. Stein, *Adv. Funct. Mater.*, 2010, **20**,2565.
(2) S. A. Asher, V. L. Alexeev, A. V. Goponenko, A. C. Sharma, I. K. Lednev, C. S. Wilcox, D. N. Finegold, *J. Am. Chem. Soc.*, 2003, **125**,3322.
(3) J. Ge, S. Kwon, Y. Yin, *J. Mater. Chem.*, 2010, **20**,5777.
(4) J. D. Joannopoulos, R. D. Meade, J. N. Winn, *Photonic Crystals*, Princeton University Press, Princeton, **1995**.
(5) K. Matsubara, M. Watanabe, Y. Takeoka, *Angewandte Chemie-International Edition*, 2007, **46**,1688.
(6) I. Lee, D. Kim, J. Kal, H. Baek, D. Kwak, D. Go, E. Kim, C. Kang, J. Chung, Y. Jang, S. Ji, J. Joo, Y. Kang, *Adv. Mater.*, 2010, **22**,4973.
(7) J. Ge, Y. Hu, Y. Yin, *Angew. Chem. Int. Ed.*, 2007, **46**,7428.
(8) Y. J. Lee, P. V. Braun, *Adv. Mater.*, 2003, **15**,563.
(9) J. Ge, J. Goebl, L. He, Z. Lu, Y. Yin, *Adv. Mater.*, 2009, **21**,4259.
(10) H. Fudouzi, Y. N. Xia, *Adv. Mater.*, 2003, **15**,892.
(11) H. Fudouzi, Y. Xia, *Langmuir*, 2003, **19**,9653.
(12) A. C. Arsenault, D. P. Puzzo, I. Manners, G. A. Ozin, *Nat. Photonics*, 2007, **1**,468.
(13) S. Kinoshita, S. Yoshioka, *Chemphyschem*, 2005, **6**,1442.
(14) Y. Chen, J. Au, P. Kazlas, A. Ritenour, H. Gates, M. McCreary, *Nature*, 2003, **423**,136.
(15) B. Comiskey, J. D. Albert, H. Yoshizawa, J. Jacobson, *Nature*, 1998, **394**,253.
(16) A. Arsenault, F. Fleischhaker, G. von Freymann, V. Kitaev, H. Miguez, A. Mihi, N. Tétreault, E. Vekris, I. Manners, S. Aitchison, D. Perovic, G. A. Ozin, *Adv. Mater.*, 2006, **18**,2779.
(17) G. A. Ozin, A. C. Arsenault, *Materials Today*, 2008, **11**,44.
(18) A. C. Arsenault, H. Miguez, V. Kitaev, G. A. Ozin, I. Manners, *Macromolecular Symposia*, 2003, **196**,63.
(19) H. Kim, J. Ge, J. Kim, S.-E. Choi, H. Lee, H. Lee, W. Park, Y. Yin, S. Kwon, *Nat. Photonics*, 2009, **3**,534.
(20) C.-J. Tien, C.-Y. Huang, *Mol. Cryst. Liq. Cryst.*, 2009, **511**,231
(21) S.-L. Kuai, G. Bader, P. V. Ashrit, *Appl. Phys. Lett.*, 2005, **86**,221110.
(22) J. M. Weissman, H. B. Sunkara, A. S. Tse, S. A. Asher, *Science*, 1996, **274**,959.
(23) J. A. Lewis, *Adv. Funct. Mater.*, 2006, **16**,2193.
(24) Y. Hu, L. He, Y. Yin, 2011.
(25) A. Pluen, P. A. Netti, R. K. Jain, D. A. Berk, *Biophys. J.*, 1999, **77**,542.
(26) E. M. Johnson, D. A. Berk, R. K. Jain, W. M. Deen, *Biophys. J.*, 1996, **70**,1017.
(27) L. He, Y. Hu, H. Kim, J. Ge, S. Kwon, Yin.Y., *Nano Lett.*, 2010, **10**,4708.
(28) S. Aront, A. Fulmer, W. E. Scott, *J. Mol. Biol.*, 1974, **90**,269.
(29) J. Ge, Y. Hu, M. Biasini, W. P. Beyermann, Y. Yin, *Angew. Chem. Int. Ed.*, 2007, **46**,4342.
(30) J. Ge, Y. Yin, *Adv. Mater.*, 2008, **20**,3485.